

AN EFFICIENT TECHNIQUE FOR STRUCTURAL RELIABILITY WITH
APPLICATIONS

by

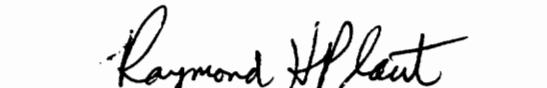
Ibrahim Mustafa Janajreh


Dissertation submitted to the Faculty of the
Virginia Polytechnic Institute and State University
in partial fulfillment of the requirements for the degree of
Doctor of Philosophy
in
Engineering Mechanics

APPROVED:


Dr. Robert A. Heller, Chairman


Dr. Dean T. Mook


Dr. Raymond H. Plaut


Dr. Mahendra P. Singh


Dr. Surot Thangjitham

November, 1992

Blacksburg, Virginia

LD
5655
V856
1992
J363
C.2

AN EFFICIENT TECHNIQUE FOR STRUCTURAL RELIABILITY WITH APPLICATIONS

by

Ibrahim Mustafa Janajreh

Dr. Robert A. Heller, Chairman

Engineering Mechanics

(ABSTRACT)

An efficient reliability technique has been developed based on Response Surface Methodology (RSM) in conjunction with the First Order Second Moment (FOSM) reliability method. The technique is applied when the limit state function cannot be obtained explicitly in terms of the design variables, i.e., when the analysis is performed using numerical techniques such as finite elements. The technique has proven to be efficient because it can handle problems with large numbers of design variables and correlated as well as nonnormal random variables. When compared with analytical results, the method has shown excellent agreement. The technique contains a sensitivity analysis scheme which can be used to reduce the computation time resulting in nearly the same accuracy. This technique allows the extension of most finite element codes to account for probabilistic analysis, where statistical variations can be added to the design variables.

An explicit solution for rocket motors consisting of propellant and steel case under environmental temperature variations is compared to the RSM technique. The method is then used for the analysis of rocket motors subjected to mechanical loads for which the stress analysis is performed using the finite element method. The technique is also applied to study the reliability of a laminated composite plate with geometric nonlinearity subjected to static and time dependent loadings. Different failure modes were considered as well as different meshes. Results have shown that when the relative size of the element is introduced into the probabilistic model, the same reliability value is obtained regardless of the number of elements in the mesh. This is good because it allows the technique to be used for problems where the failure region is unknown.

Dedication

The Author would like to dedicate this work to his parents Nadida and Mustafa Janajreh for their unending support and love, for their sacrifice in all his endeavors and accomplishment academic and otherwise.

Acknowledgements

The author would like to express his sincere appreciation to his advisor Professor Robert A. Heller for his guidance and support during the course of this study. Thanks to Professor S. Thangjitham for his valuable suggestions and ideas. The author also extends his thanks to the members of his committee, Professor R. H. Plaut, Professor M. P. Singh and Professor D. T. Mook; for their constructive comments in reviewing the manuscript.

Special thanks are also to Professor R. H. Myers for his consultation in the area of response surface. The author would like to extend his thanks to his colleges, X. Wang, K. Ganesh, S. Lee and P. Touze; for their constructive discussions and encouragement.

Special thanks and appreciation to the author's wife; Laurie for her love, support and understanding during his good and hard times.

This work was sponsored by the U. S. Army Missile Command (USAMICOM), their financial support is appreciated.

Table of Contents

INTRODUCTION 1

LITERATURE REVIEW 8

THEORY AND APPROACH 16

3.1 Introduction 16

3.2 Response Surface Methodology 17

 3.2.1 Generation of the Polynomial 17

 3.2.2 Central Composite Design 19

 3.2.3 Polynomial Approximation vs. Taylor’s Series Expansion 21

 3.2.4 Sensitivity Analysis 22

3.3 First Order Second Moment Reliability Analysis 24

 3.3.1 Uncorrelated Normally Distributed Variables 26

 3.3.2 Correlated Normally Distributed Variables 26

3.4 Non-Normal Variables 29

 3.4.1 Log Normal Variables 30

 3.4.2 Weibull Distributed Variables 30

 3.4.3 General Strategy for Non-Normal Variables 31

3.5 Progressive Probability of Failure 32

3.6 Weakest Link and Size Effect 33

 3.6.1 Independent Failure Modes 33

 3.6.2 General Strategy for Multi-Independent Failure Modes 35

RELIABILITY OF ROCKET MOTORS UNDER THERMAL LOAD	41
4.1 Introduction	41
4.2 Exact Analysis	42
4.2.1 Thermal Stress Analysis	43
4.2.2 Viscoelastic Properties of the Propellant	45
4.2.3 Cumulative Damage and Aging	47
4.2.4 Results for Exact Analysis	49
4.2.4.1 Evaluation of Stresses	49
4.2.4.2 Evaluation of the Safety Index and the Progressive Probability of Failure	50
4.2.4.2.1 Uncorrelated Non-Normal Variables (aging and cumulative damage included)	50
4.2.4.2.2 Correlated Non-Normal Variables (aging and cumulative damage included)	51
4.3 Approximate Analysis	52
4.3.1 Solution by Approximate Analysis	52
4.3.2 Results for Approximate Analysis	54
4.4 Conclusions	55
 RELIABILITY OF ROCKET MOTORS UNDER MECHANICAL LOAD	 76
5.1 Introduction	76
5.2 Probabilistic Finite Element Program	77
5.3 Rocket Motor Loaded by Static Line Loads	79
5.4 Rocket Motors Loaded by Patch Loads.	80
5.4.1 Static Loads	80
5.4.2 Impact Patch Loads	81
5.4.3 Experimental Impact Loads	81
5.5 Application of Sensitivity Analysis and Correlated Variables	83
5.5.1 Application of Sensitivity Analysis	83
5.5.2 Application of Correlated Variables	84
5.6 Conclusions	85

RELIABILITY OF LAMINATED COMPOSITE PLATES 119

6.1 Introduction 119

6.2 Finite Element Model 120

 6.2.1 Theory and Formulation 120

 6.2.1.1 Kinematics 121

 6.2.1.2 Von Karman Nonlinear Strains 121

 6.2.1.3 Constitutive Relations 122

 6.2.1.4 Equations of Motion 122

 6.2.1.5 Variational formulation 124

 6.2.2 Finite Element Formulation 125

 6.2.2.1 Polynomial Approximation 125

 6.2.2.2 Newmark’s Direct Integration Method for Transient Analysis 126

 6.2.2.3 Newton Raphson Method for Nonlinear Analysis 127

6.3 Probabilistic Model 128

6.4 Applications and Results 128

 6.4.1 Probabilistic Static Analysis (Linear and Nonlinear) 129

 6.4.2 Probabilistic Transient Analysis (Linear and Nonlinear) 130

 6.4.3 Application to Non-Normal Variables 131

 6.4.4 Application to Multi-Failure Modes 131

6.5 Conclusions 133

SUMMARY AND CONCLUSIONS 172

7.1 Introduction 172

7.2 Efficiency and Accuracy of the Developed Technique 173

7.3 Summary of Results and Conclusions 174

7.4 Recommendations for Future Work 177

REFERENCES 181

Vita 187

List of Illustrations

Fig. 3.1	Central composite design for $n=3$	38
Fig. 3.2	A typical performance function.....	39
Fig. 3.3	A performance function obtained by RSM.....	40
Fig. 4.1	Configuration of the solid propellant rocket motor.....	59
Fig. 4.2	The shift function of the core under consideration at different temperatures.....	60
Fig. 4.3	Core modulus, $E(T,w)$, at different temperatures for daily frequency.....	61
Fig. 4.4	Tangential stress, $S(r,t)$, at the bore due to cyclic temperature with time at different locations.....	62
Fig. 4.5	The damage effect, D , on the strength of the core at different locations.....	63
Fig. 4.6	Aging factor, h , with time at different locations.....	64
Fig. 4.7	Core modulus, $E(T,t)$ with time at different locations.....	65
Fig. 4.8	Core strength, R , with time at different locations.....	66
Fig. 4.9	Safety index, b , with time at different locations.....	67
Fig. 4.10	Progressive probability of failure with time at different locations.....	68
Fig. 4.11	Safety index, b , with time for Weibull and Lognormal modulus distributions.....	69
Fig. 4.12	Progressive probability of failure for weibull and Lognormal modulus distributions.....	70
Fig. 4.13	Safety index, b , with time for different levels of correlation.....	71
Fig. 4.14	Progressive probability of failure with time for different levels of correlation.....	72
Fig. 4.15	Comparison between exact and approximate analyses.....	73
Fig. 4.16	The safety index based on exact analysis and polynomial approximation.....	74
Fig. 4.17	progressive probability of failure based on exact analysis and polynomial approximation.....	75
Fig. 5.1	An algorithm for the developed technique.....	93
Fig. 5.2	Motor under two opposite line loads.....	94
Fig. 5.3	Tangential stress at the bore with load.....	95
Fig. 5.4	Response ($R-S$) with load for different mean strength values.....	96
Fig. 5.5	Safety index with load for different mean strength values.....	97

Fig. 5.6	Reliability with load for different mean strength values.....	98
Fig. 5.7	Motor under patch/line loads compination.....	99
Fig. 5.8	Mean and standard deviation of the radial displacement with load at the interface under the load.....	100
Fig. 5.9	Mean and standard deviation of the tangential stress with load at the bore under the load.....	101
Fig. 5.10	Safety index with load for different mean strength values.....	102
Fig. 5.11	Safety index with load for different coefficients of variation.....	103
Fig. 5.12	Probability of failure with load for different coefficients of variation.....	104
Fig. 5.13	Sine wave impact load.....	105
Fig. 5.14	Mean and standard deviation of radial displacement with time at the interface under the load due to sine wave load.....	106
Fig. 5.15	Mean and standard deviation of tangential stress with time at the bore under the load due to sine wave load.....	107
Fig. 5.16	Safety index with time for different mean strength values.....	108
Fig. 5.17	Progressive probability of failure with time for different mean strength values.....	109
Fig. 5.18	Safety index with time for different coefficients of variation.....	110
Fig. 5.19	Progressive probability of failure with time for different coefficients of variation.....	111
Fig. 5.20	Force and energy as function of time in an impact test.....	112
Fig. 5.21	Displacement and velocity as function of time in an impact test.....	113
Fig. 5.22	Comparison between FEM solution and experimental results for an impact energy of 17.14 (ft-lb).....	114
Fig. 5.23	Tangential stress under the load at the bore for an impact energy of 17.14 (ft-lb).....	115
Fig. 5.24	Safety index with impact energy for different coefficients of variation.....	116
Fig. 5.25	Reliability with impact energy for different coefficients of variation.....	117
Fig. 5.26	Displacement and stress distribution (line/patch loads) along the interface under the load.....	118
Fig. 6.1	Geometry of the undeformed and deformed xz plane.....	136
Fig. 6.2	Center deflection for [90/0] S.S. plate under uniform load.....	137
Fig. 6.3	Center deflection for [45/-45] S.S. plate under time dependent load.....	138
Fig. 6.4	The vertical deflection of [+45/25]s simply supported plate under a uniform load of 1.3 psi or load factor of 50.....	139
Fig. 6.5	Mean and standard deviation of w for linear and nonlinear analyses.....	140

Fig. 6.6	Safety index with load for linear and nonlinear analyses.....	141
Fig. 6.7	Probability of failure with load for linear and nonlinear analyses.....	142
Fig. 6.8	Safety index with load for different values of R and nonlinear analysis.....	143
Fig. 6.9	Probability of failure with load for different values of R and nonlinear analysis...	144
Fig. 6.10	Probability of failure for different coefficients of variation and nonlinear analysis.	145
Fig. 6.11	Mean and standard deviation of w with time for linear and nonlinear analyses.....	146
Fig. 6.12	Safety index with time for linear and nonlinear analysis.....	147
Fig. 6.13	Progressive probability of failure with time for linear and nonlinear analyses.....	148
Fig. 6.14	Safety index with time for different values of R and nonlinear analysis.....	149
Fig. 6.15	Progressive probability of failure with time for different values of R and nonlinear analysis.....	150
Fig. 6.16	Progressive probability of failure with time for different values of d and nonlinear analysis.....	151
Fig. 6.17	Safety index with load for different strength distributions.....	152
Fig. 6.18	Reliability with load for different strength distributions.....	153
Fig. 6.19	Probability of failure with load for different strength distributions.....	154
Fig. 6.20	Compressive stress over the plate due to a 1.95 psi uniform load or 75 load factor and linear analysis.....	155
Fig. 6.21	Compressive stress contours over the plate due to a 1.95 psi uniform load or 75 load factor and linear analysis.....	156
Fig. 6.22	Safety index with strength for a 64 elements mesh and different failure modes....	157
Fig. 6.23	Safety index with strength for a 256 elements mesh and different failure modes...	158
Fig. 6.24	Safety index with strength based on the maximum compressive stress at the center of the plate for different meshes.....	159
Fig. 6.25	Reliability with strength based on the maximum compressive stress at the center of the plate for different meshes.....	160
Fig. 6.26	Probability of failure with strength based on the maximum compressive stress at the center of the plate for different meshes.....	161
Fig. 6.27	Safety index with strength based on the maximum compressive stress for different meshes (no size effect included).....	162
Fig. 6.28	Reliability with strength based on the maximum compressive stress for different meshes (no size effect included).....	163
Fig. 6.29	Probability of failure with strength based on the maximum compressive stress for different meshes (no size effect included).....	164

Fig. 6.30	Safety index with strength based on the maximum compressive stress for different meshes (size effect included).....	165
Fig. 6.31	Reliability with strength based on the maximum compressive stress for different meshes (size effect included).....	166
Fig. 6.32	Probability of failure with strength based on the maximum compressive stress for different meshes (size effect included).....	167
Fig. 6.33	Safety index with strength based on the maximum compressive stress for different meshes	168
Fig. 6.34	Reliability with strength based on the maximum compressive stress for different meshes.....	169
Fig. 6.35	Probability of failure with strength based on the maximum compressive stress for different meshes	170
Fig. 6.36	Safety index with strength for different meshes and modes of failure.....	171
Fig. 7.1	Safety index with load for a motor with orthotropic case.....	179
Fig. 7.2	Reliability with load for a motor with orthotropic case.....	180

List of Tables

Table 3.1	Values of a for an orthogonal central composite design.....	37
Table 4.1	Geometric, thermal and mechanical parameters.....	57
Table 4.2	Prony constants for tensile relaxation modulus.....	58
Table 5.1	Design variables for line and patch loaded motors.....	86
Table 5.2	Design variables for impact loads.....	87
Table 5.3	Radial stress at the interface for different angular locations compared with maximum tangential stress at the bore under the load.....	88
Table 5.4	Sensitivity analysis based on 11 variables.....	89
Table 5.5	Comparison between 6 and 11 random variables as a result of sensitivity analysis..	90
Table 5.6	Comparison between 4 and 8 random variables as a result of sensitivity analysis...	91
Table 5.7	Reliability analysis for different levels of correlation.....	92
Table 6.1	Design variables for laminated composite plate.....	135
Table 7.1	Comparison between different methods.....	178

Chapter I

INTRODUCTION

In classical mechanical and structural design, uncertainties in design parameters such, as material properties, loading and models used to describe stresses, are accounted for by factors of safety, chosen by experience and intuition. But reliability methods employing concepts of probability and statistics provide mathematical procedures for modeling uncertainty in a rational and consistent manner, thereby promising to produce a well engineered design.

Reliability analysis is defined as the application of probabilistic and statistical methods to the design process of a structure. Two important problems can be generated from this type of analysis. The first problem is reliability assessment in which the goal is to compute the reliability or the safety index for an existing or proposed structure. The second problem entails design where a target reliability is specified as a basic requirement for the structure.

Reliability analysis of structures has been carried out using various techniques, among them the First Order Second Moment (FOSM) method. In this technique a performance function is defined explicitly in terms of the design variables and separates

the failure region from the safe region. A minimum distance is computed from the origin of the design variables to a point on the performance function; this distance is called the safety index from which the reliability of the system can be computed, and the point on the performance function is called the failure point. The value of the safety index is obtained by taking the ratio of the first order approximation of the mean value of the performance function to its standard deviation evaluated at the failure point. Although there is some approximation associated with this method, it is efficient because it allows all the design variables to have any type of probability distribution as well as correlation between different variables.

Explicit or exact solutions are available when simple problems are considered. In most cases, however, explicit or exact solutions are not available. Such is the case for laminated composite structures subjected to various types of loads or rocket motors subjected to impact loadings. In fact, exact solutions become impossible when the analysis includes geometric or material nonlinearities. For such cases approximate methods are used.

Many statistical techniques have been developed to approximate the performance function in an explicit form in terms of the design variables. In fact, it has been a long-standing practice in engineering to approximate the mechanical behavior of structures to obtain simple solutions without significant loss of accuracy. A well known example is the discretization of continuous structures by the finite element method. From this point of view it seems to be obvious to follow this practice in order to reduce the computational efforts required for reliability analysis on an acceptable level. This approach led to the Response Surface Methodology (RSM), i.e., the approximation of the performance function by a simple function.

The use of Response Surface Methodology was first introduced in the late 1980's and early 1990's. Its main purpose is to approximate the performance function using a

polynomial function. The work that has been done in this area is not too deep. Some researchers dealt with approximation of the performance function by a polynomial which contains linear terms only, while others added quadratic terms without any interaction between different terms (mixed terms). The latest one applied RSM with mixed terms and made use of factorial design, which is an expensive design in terms of computation time, and when FOSM was applied, results were good if the variables were within one standard deviation of their mean values. Therefore, the need for an inexpensive and more general design is necessary.

A Response Surface Methodology (RSM) is presented in this work. In this technique the performance function is approximated by a second order polynomial expression, where all the design variables are included. In order to obtain the coefficients of the polynomial, central composite design is used in conjunction with fractional factorial analysis. Five levels for each variable are assumed and a design matrix is generated based on different combinations of these levels. Then the coefficients of the polynomial are obtained by solving a simple system of linear equations.

The main advantages for using this type of design are that it allows for interaction between different variables and uses fractional factorial design instead of a total factorial design. It uses five levels for each variable which increases the range in which the polynomial is valid. In other designs using two levels for each variable, the polynomial is valid within one standard deviation around the mean value, while here the polynomial will be valid up to three or more standard deviations around the mean value of each variable. This high range is important because it allows the performance function to handle small probability of failure values, especially for large safety indices. Another important advantage is that the central composite design is an orthogonal design, which means the system of linear equations to be solved for the coefficient of the polynomial is a set of decoupled equations (diagonal system). This technique has the capability of

converting all available deterministic finite element codes to probabilistic finite element codes.

In some engineering problems, where large numbers of design variables are included, the fractional factorial design becomes expensive too. Therefore, a sensitivity analysis will be used based on the t test to determine the relative importance of the design variables. This analysis will be performed on a first order polynomial which includes all design variables. Then a second order polynomial will be constructed and only important variables will be included.

Once the performance function is given in this explicit form in terms of the design variables, the FOSM can be applied to obtain the reliability of the structure. In fact, this gives the reliability at one point and is a good estimate for a structure with a single failure mode. In most structures, however, the failure domain is not just one point; they may have more than one critical point or mode of failure at different unknown locations. In this case the reliability must be computed at every critical point in the structure, and if the failure modes are independent, the reliability of the structure will be the product of these individual reliabilities.

The FOSM reliability method will be used to study the service life of Solid Rocket Motors subjected to environmental temperature variations. This problem is investigated for random temperature input and random strength with different probability distribution functions. In this study, all design parameters such as modulus, coefficient of thermal expansion, Poisson's ratio, etc. are assumed to be random. Correlation between design variables as well as different probability distributions such as normal, lognormal and Weibull will be considered. Three different locations will be examined. Point Barrow, AK. represents a cold site, Yuma, AZ. represents a warm site and Nashville, TN. represents a moderate site. Since the exact solution for stress analysis of this problem is available, the problem will be used to investigate the accuracy and efficiency

of the proposed technique. Comparisons will also be made with a FOSM method utilizing numerical differentiation.

The proposed technique will then be used to compute the reliability of rocket motors subjected to mechanical, static and time-dependent, loadings such as impact loads. An available deterministic finite element code will be converted to a probabilistic one to compute the reliability of the motor subjected to random design variables. Mean and standard deviation of any response quantity such as stresses and displacements will be computed too.

An important problem comes into the picture, especially when a finite element method is used for the analysis. Suppose, for example, a bar under uniform state of stress is analyzed using 10 elements in one case and then using 100 elements for another case. If it is assumed that failure of one element is independent from the others, the 10 element bar will give much higher reliability values than the 100 element bar, and since the bar is under uniform state of stress, the reliability values should be equal for both cases. In this research an important objective is to include the size of every element in the reliability analysis.

A more general example that includes nonlinear theory will be discussed, where the size effect plays an important rule. In this example a simply supported laminated composite plate subjected to static and time-dependent loads will be discussed; geometric nonlinearity will be included to account for large deformations. A deterministic finite element program is written to compute stresses and displacements; the program will be extended to include random design variables. Mean and standard deviation for any response quantity will be computed based on linear and nonlinear theories for both static and transient loadings. The reliability of the plate will be computed for every case, and a comparison will be made among the different cases based on central deflection. The reliability will also be computed for each element from which the total reliability of the

plate will be obtained for different numbers of elements. This will include the size of each element in the probabilistic model in order to obtain the same results for different numbers of elements.

Therefore, the objectives of this dissertation are summarized as follows:

1. Development of a reliability technique to be applied to problems where explicit or exact solutions are not available, large numbers of design variables are included, the failure region is unknown and correlated non-normal random variables are involved.
2. Calculation of any response statistics such as the mean and standard deviation of displacements and stresses when random design variables are included in such a case.
3. Investigation of the service life of rocket motors under thermal loads when all design variables are random. Here an exact analysis is available and will be compared to the developed technique.
4. Computation of the reliability of rocket motors under mechanical loads where stress analysis is performed using an available finite element code.
5. Analysis of laminated composite plates with geometric nonlinearities, random design parameters and multi-failure modes.

In this study the first problem of reliability assessment is discussed. An overview of the literature relevant to this study is presented in chapter II. Chapter III contains the theoretical development of the probabilistic model and the approach used to accomplish it. In chapter IV the reliability of a rocket motor under thermal loads is computed using exact analysis and is compared to the developed technique. The reliability of rocket motors subjected to mechanical loadings is discussed in chapter V and a probabilistic analysis of laminated composite plates with geometric nonlinearities is

presented in chapter VI. Chapter VII contains more examples to prove the efficiency of the developed technique, discussion of results, conclusions and recommendations for future work.

Chapter II

LITERATURE REVIEW

The analysis of structural reliability was first applied by Freudenthal [1]. The purpose of his paper was to analyze the safety factor in engineering structures in order to establish a rational method of evaluating its magnitude.

A second landmark work in structural reliability which began to formalize analyses was written by Freudenthal, Garrelts and Shinozuka [2]. This work dealt with the situation in which stress, S , and strength, R , are the basic random variables and these variables are both normally or lognormally distributed. The probability of failure was defined as the integral of the joint probability density function of these variables over the failure domain. The failure domain is the region where $R < S$ and the joint probability density function is obtained from the probability density function (PDF) and cumulative density function (CDF) for both variables. The integral was easy to obtain because of the simplicity of the assumption in the design variables.

In general, the joint probability density function is, however, a function of several variables and to obtain it for several variables is a very difficult, sometimes impossible task. Therefore the need for an alternative reliability technique exists.

The First Order Second Moment (FOSM) reliability method was introduced by Cornel [3] to circumvent this difficulty. In general the failure region can be separated from the safe region by what is called the limit state function or performance function, G , which is a function of n random variables. An approximation to the mean value of G , μ_g , and the standard deviation, σ_g , can be obtained using the first order terms of Taylor's series expansion.

Cornel defined the safety index, β , as μ_g divided by σ_g and probability of failure equal to $\Phi(-\beta)$, where Φ is the standard normal CDF. The technique was also called Mean Value First Order Second Moment method (MVFOSM).

The performance function depends on a physical model and not on a probabilistic model. However, MVFOSM fails to give the same result for β if the probabilistic model is changed; for example, changing G from $R - S$ to $R/S - 1$ produces different values of β . In 1974, Hasofer and Lind [4] proposed a new definition of the safety index which does not affect the way that the performance function is defined or its shape. The H-L scheme is based on normalizing every random variable with respect to its mean and standard deviation, substituting all random variables into the performance function to obtain the performance function in normalized coordinates, then computing the minimum distance from the origin of this coordinate system to a point on the performance function. This distance is called the safety index, β , and the point on the performance function which corresponds to the minimum distance is called the design point.

The major shortcoming of the H-L method is that it will not accept distributional information even if it is available. In 1978 Rackwitz and Fiessler [5] extended the H-L method in order to make it possible for the variables to have any distribution. The main idea in their method is to transform non-normal distribution functions into equivalent normal distributions. The equivalent normal distribution is obtained so that the PDF and CDF at the design point are the same as for a normal distribution. An equivalent

normal mean and standard deviation are then computed for every non-normal variable, and the safety index and the design point are calculated. The process is repeated until convergence occurs.

The probability of failure, p_f , as computed by the R-F method is close to exact in many cases, in contrast to others in which the error is significant [6]. Therefore, to improve p_f , Chen and Lind [7] in 1983 proposed a three-parameter normal tail approximation. The C-L algorithm is an extension of the R-F method as it added a third condition for the equivalent normal variable. In this method, not only are the PDF and CDF the same at the design point, but the slope of the PDF is also the same for the original distribution and the equivalent normal distribution.

Shinozuka [8] reviewed the FOSM method and showed that a Lagrange multiplier formulation can be used to evaluate the safety index and the location of the design point. The Monte Carlo technique was recommended for use in estimating limit state probabilities as a practical alternative to other methods. It was proposed that the point of maximum likelihood (failure point) should be used as the design point.

An efficient algorithm to compute the structural reliability has been available, where uncertainty can be included in any design variable [9]. But the problem is that, in computing the safety index, many derivatives of the performance function should be computed and the performance function should also be expressed in terms of β in order to solve for β . This was possible when the performance function was available in an explicit form in terms of the design variables. In most engineering problems, however, explicit or exact solutions are not available, especially with the use of numerical solutions such as the finite element method.

Thangjitham [10] has formulated the FOSM method in a numerical form. In this algorithm numerical differentiation of the performance function was used instead of exact differentiation. The algorithm is efficient for problems with a small number of design

variables. For problems with a large number of design variables, however, this algorithm becomes costly or may be impossible when analysis is performed using finite elements and when execution codes are provided instead of source codes. Moreover, when finite element analysis is performed based on nonlinear theory, the user should be extra careful when performing numerical differentiation, otherwise inaccurate solutions may be obtained.

Therefore, the use of statistical procedures such as Monte Carlo simulation became the only way for reliability calculations of structures with an implicit performance function. In this technique, sampling from known distribution functions is conducted where a large sample size must be used in order to converge to the correct reliability value [11]. The method becomes very expensive, as a finite element solution must be produced for each sample. This led to another statistical approach in which a planned set of experiments around the mean value of the different random variables is performed using a standard finite element code to determine response to different inputs. A regression analysis is then used to fit the response (performance function) to the different inputs.

In 1984 Wu [12-13], and Wu and Wirsching [14-15] developed an algorithm to compute structural reliability when the performance function is not available in explicit form in terms of the design variables. The algorithm, an extension of the R-F and C-L methods, employs an approximation of the performance function by a quadratic at the design point and transforms the quadratic form to a linear one, which gives a linear performance function in the normal design variables.

The quadratic form of the performance function defined by Wu did not include any mixed terms, such as x_1x_2 . This is because Wu had computed the coefficient of the quadratic by varying one variable at a time. Therefore, the need for more efficient methods to define G in an explicit form became one of the important goals for researchers in the area of probabilistic mechanics in the late 1980's and early 1990's.

Bucher et al. [16] and Schuëller et al. [17] introduced the RSM to approximate the performance function by a second order polynomial. They divided G into two parts, one part containing the linear and the quadratic terms and the other containing the mixed terms only. The former was computed by interpolation along each axis, while the latter was computed by interpolation between the axes. The reliability, in their work, was obtained using the Adaptive Sampling Method (ASM), also known as Iterative Fast Monte Carlo (IFM) procedure.

Nagpal, Rubinstein and Chamis [18] developed a methodology to quantify the influence of random variation on the performance of structural components and applied this methodology to quantify uncertainties in geometry, material properties and loadings. A factorial design was used and a t test was performed to determine whether a given variable was significant. A turbopump blade was chosen as an example where the mean and standard deviation of the natural frequency, stresses and displacements were obtained based on uncertainties in material properties and geometry.

Bucher and Bourgund [19] presented a new adaptive interpolation scheme which enables fast and accurate representation of the system behavior by a Response Surface (RS). The response surface approach utilizes elementary statistical information of the basic variables (mean values and standard deviations) to increase the efficiency and accuracy. Thus the RS obtained in their study is independent of the type of distribution or correlations among the basic variables. To obtain the reliability estimates, the RS is utilized in conjunction with the advanced Monte Carlo simulation technique. When compared with FOSM, this method was shown to be more efficient and accurate.

Tong and Wu [20] developed a method for reliability assessment that combines a fast convolution procedure with Response Surface. They established a quadratic performance function and transformed the quadratic function into a linear function, then applied a fast convolution procedure to obtain the PDF and CDF of the performance

function. In their work, mixed terms in the quadratic function were not used because the transformation can not be done if they were included. This reduced the accuracy of the method for cases when mixed terms are significant.

Ibrahim [21] presented a general strategy for structural-system reliability for use when deterministic structural analysis is expensive. The goal was to estimate the system-failure probability with a minimum number of structural analyses. The strategy relies upon the user to interpret and generate information about the system through the use of appropriate techniques such as RS and FOSM. But there are no concrete steps in the strategy, which make it inefficient for problems where the failure region is not easy to predict.

A different approach named Non-Statistical Approach was used to predict the reliability using the finite element method directly. This approach is also based on FOSM and Taylor's series expansion, where the mean and the standard deviation of the performance function are computed directly without using any statistical and design methods. Handa and Anderson [22] used this idea to study linear truss structures and the effect of correlation. Hisda and Nakagiri [23] used the same method to analyze structures with uncertain shapes, where geometrical coordinates were allowed to be random variables. Nakagiri et al. [24-27] applied this method to composite structures.

Liu et al. [28-31] introduced the term Probabilistic Finite Element Method. They applied the FOSM to nonlinear structural dynamics for correlated and uncorrelated random variables. Tokada and Shinozoka [32] developed a new method in which local integration of the continuous stochastic field was made in an element by element basis to form element stiffness matrices so that the random field is transformed into only a few random variables. This new method requires high computational time and was applied to linear problems only. Engelstad and Reddy [33] applied the FOSM to laminated composite shells, and material as well as geometric nonlinearities were included in the

analysis. The results obtained in this analysis were in a good agreement with Monte Carlo simulation, but only uncorrelated variables with normal distribution functions were considered in their study.

In the above approach, when FOSM is used, the safety index, β , is computed based on the mean and the standard deviation of the response function, which is the same as the original definition given by Cornel [3] and was shown to be invariant. Also, in computing the partial derivatives of the response function with respect to each random variable and as the number of random variables increases, it becomes apparent that a significant amount of storage becomes necessary to retain all the derivatives and high computational time is required to obtain these derivatives. This led to our focus in this research, which is the statistical method.

In Probabilistic Finite Element Method, the reliability is computed for each element and the total reliability is computed by multiplying the "element reliabilities". This means that the more elements in the domain, the less reliable the structure becomes. Therefore, the size of each element must be included in the reliability computations. In other words, the strength of each element must depend on the element size. Weibull [34,35] developed a statistical theory based on the "Weakest Link" hypothesis; a probability distribution function for the strength of the material was proposed. This Weibull distribution function has been widely used in various areas. Most of the applications are for brittle structures where failure of the structure occurs when one component of the structure has failed.

Some of the relevant studies in this area were performed by Margeson [36] and Stanley and Margeson [37]. They developed a statistical theory of brittle failure for an anisotropic structure and applied it to obtain the failure probability of a cylinder under thermal load. Heller [38,39], Heller, Schmidt and Deninghoff [40] and Heller, Thangjitham and Wall [41], applied the Weakest Link theory to a Proof-Loaded

isotropic material and to a composite plate with a hole. Thangjitham and Heller [42] computed the reliability of an infinite composite plate with a hole subjected to random load. Heller, Thangjitham and Yeo [43] investigated the size effect of a brittle composite beam and computed the reliability of the beam with random strength only. Yeo [44] extended the previous work for composite plates with stress concentration. However, none of these researches allow for all design variables to be probabilistic.

The use of reliability theories to predict the service life of Solid Rocket Motors was first started by Heller [45]. Input temperature as well as strength of the motor were assumed random variables, and the reliability of the motor was computed based on stress-strength interference. Cost [46] applied the Monte Carlo simulation technique to predict the service life of the motor. Heller et al. [47] and Heller and Singh [48] added the viscoelastic effect to the problem as well as cumulative damage and aging effect and obtained the service life of the motor based on the stress-strength interference. Zibdeh and Heller [49] used the First Passage method to predict the storage life of rocket motors, in which strength and stresses were assumed random variables. The uncertainty in the stress in their study was due to the uncertainty in the input temperature. In all of these studies, strength and input temperature are assumed independent random variables with different probability distribution functions, while in this proposed technique all design variables are allowed to have any probability function as well as correlation among them.

Chapter III

THEORY AND APPROACH

3.1 Introduction

In this chapter a formulation of a new technique (probabilistic model) will be developed based on Response Surface Methodology (RSM) to approximate the performance function (G) in an explicit form in terms of the design variables by a second order polynomial. Sensitivity analysis will be derived and used to test the relative importance of each random design variable based on which the number of variables in the probabilistic model will be reduced. The details of the First Order Second Moment (FOSM) reliability method will be presented for normal, non-normal and correlated random design variables.

The weakest link hypothesis and size effect will be discussed. A new formulation for probabilistic finite element analysis that includes the size of the element in the probabilistic model will be derived, too.

3.2 Response Surface Methodology

3.2.1 Generation of the Polynomial

The purpose of this technique is to obtain a good approximation to the performance function G . Consider a full second order polynomial

$$y = a_0 + \sum_{i=1}^n a_i x_i + \sum_{i=1}^n a_{ii} x_i^2 + \sum_{i=1}^{n-1} \sum_{j=i+1}^n a_{ij} x_i x_j + \varepsilon \quad (3.1)$$

where

y is the approximated response

$a_0, \dots, a_{(K-1)}$ are the regression coefficients; their total number is equal to $(n+1)(n+2)/2$ and denoted by K

x_1, \dots, x_n are the design variables

n is the number of design variables

ε is the error in the approximation.

In general, Eq. 3.1 can be written as

$$\{Y\} = [X]\{\hat{A}\} + \{\varepsilon\} \quad (3.2)$$

where

$$\{Y\} = \begin{bmatrix} y^1 \\ y^2 \\ \vdots \\ y^m \end{bmatrix}, \quad [X] = \begin{bmatrix} 1 & x_1^1 & \dots & x_n^1 & x_1^1 x_2^1 & \dots & x_n^1 x_n^1 \\ 1 & x_1^2 & \dots & x_n^2 & x_1^2 x_2^2 & \dots & x_n^2 x_n^2 \\ \vdots & \vdots & \dots & \vdots & \vdots & \dots & \vdots \\ 1 & x_1^m & \dots & x_n^m & x_1^m x_2^m & \dots & x_n^m x_n^m \end{bmatrix} \quad (3.3)$$

and

$$\{\hat{A}\} = \begin{bmatrix} a_0 \\ a_1 \\ \vdots \\ a_{(K-1)} \end{bmatrix}, \quad \{\varepsilon\} = \begin{bmatrix} \varepsilon_1 \\ \varepsilon_2 \\ \vdots \\ \varepsilon_m \end{bmatrix} \quad (3.4)$$

where m is the number of data sets.

The vector $\{\hat{A}\}$ should be calculated such that $\{\varepsilon\}$ is minimum [50]. This can be accomplished using least squares estimators, as

$$\begin{aligned} s(\{\hat{A}\}) &= \sum_{i=1}^m \varepsilon_i^2 = \{\varepsilon\}^T \{\varepsilon\} \\ &= (\{Y\} - [X]\{\hat{A}\})^T (\{Y\} - [X]\{\hat{A}\}) \\ &= \{Y\}^T \{Y\} - 2\{\hat{A}\}^T [X]^T \{Y\} + \{\hat{A}\}^T [X]^T [X] \{\hat{A}\} \end{aligned} \quad (3.5)$$

where $s(\hat{A})$ is the error produced by the difference between exact and approximated responses. To minimize this error, consider the following derivative:

$$\frac{\partial s}{\partial \{\hat{A}\}} = -2[X]^T \{Y\} + 2[X]^T [X] \{\hat{A}\} = 0 \quad (3.6)$$

or

$$[X]^T[X]\{\hat{A}\} = [X]^T\{Y\} \quad (3.7)$$

Therefore, the solution of the linear system in Eq. 3.7 gives the vector $\{\hat{A}\}$ which are the coefficients of the second order surface given by Eq. 3.1. But the question is how can the vector $\{Y\}$ and the data sets be generated! To answer this, the central composite design is discussed next.

3.2.2 Central Composite Design

Two levels for each variable are chosen as $-1, +1$; i.e, one standard deviation below and one above the mean value [51]. Using 2^n factorial experiments with each variable (factor) at two levels, a design matrix of order $2^n \times n$ can be obtained as

$$[D] = \begin{bmatrix} -1 & -1 & \dots & -1 \\ +1 & -1 & \dots & -1 \\ -1 & +1 & \dots & -1 \\ \vdots & \vdots & \ddots & \vdots \\ \vdots & \vdots & \ddots & \vdots \\ +1 & +1 & \dots & +1 \end{bmatrix} \quad (3.8)$$

If the design matrix, $[D]$, is augmented by

$$\begin{bmatrix} 0 & 0 & \dots & 0 \\ -\alpha & 0 & \dots & 0 \\ \alpha & 0 & \dots & 0 \\ \cdot & \cdot & \cdot & \cdot \\ \cdot & \cdot & \cdot & \cdot \\ \cdot & \cdot & \cdot & \cdot \\ 0 & 0 & \dots & -\alpha \\ 0 & 0 & \dots & \alpha \end{bmatrix} \quad (3.9)$$

where the value of α is chosen based on the number of random variables in the analysis (Table 3.1), the resultant matrix represents a new design matrix which is called the central composite design. In this design a total of five levels for each variable have been used, Fig. 3.1.

The response $\{Y\}$ is obtained by using each row in the resultant design matrix as an input. Then the design matrix is substituted in the $[X]$ matrix, and the resultant $[X]$ matrix and the vector $\{Y\}$ are substituted in Eq. 3.7 to produce an independent linear system. The solution will be the coefficients of the second order surface .

This design is an orthogonal central composite design, that is, $[X]^T[X]$ in Eq. 3.7 is a diagonal matrix, which provides ease in computation and an uncoupled linear system of equations.

The dimension of the design matrix, $[D]$, is usually large: $(2^n + 2n + 1) \times n$. For example, if 5 random variables are involved in the computation the dimension of $[D]$ is 45×5 . The dimension can be reduced without affecting the accuracy in the estimated second order surface by using fractional factorial analysis [52]. The above dimension is large because it allows for all possible interactions such up to $x_1x_2x_3\dots x_n$. However, the

second order surface defined in Eq. 3.1 needs only a second order interaction between variables. This means a large number of terms should drop out of the factorial design. This can be done by defining what is called a define contrast for certain levels of interaction for which this interaction is not included in the required surface. Each contrast will reduce the order of the design matrix by $\frac{1}{2}$; this can be done several times taking into consideration that each contrast will ignore some interaction terms that are not required and, more important, the combination of contrasts will also ignore more terms that are not required in the design surface [53].

The dimension of $[D]$ can be reduced more by using what is called sensitivity analysis. In this method the response (performance function) is tested with respect to the variation in each random variable in the design using the t test. As a result of this test, only significant variables will remain in the design matrix.

3.2.3 Polynomial Approximation vs. Taylor's Series Expansion

The rationale for the polynomial approximation of G is based on Taylor's series expansion of G around the mean values of the design variables. For example, the second order Taylor's series expansion of G around the mean values μ_{x_i} of the variables X_i , $i = 1, n$, can be written as

$$G(x_1, \dots, x_n) = G(\mu_{x_1}, \dots, \mu_{x_n}) + \sum_{i=1}^n \frac{\partial G}{\partial x_i} (x_i - \mu_{x_i}) + \sum_{i=1}^n \frac{\partial^2 G}{\partial x_i^2} (x_i - \mu_{x_i})^2 + \sum_{i=1}^{n-1} \sum_{j=i+1}^n (x_i - \mu_{x_i})(x_j - \mu_{x_j}) \frac{\partial^2 G}{\partial x_i \partial x_j} + \varepsilon \quad (3.10)$$

knowing that the mean value of the normalized variables x_i in Eq. 3.1 is equal to zero. A comparison between Eq. (3.10) and Eq. (3.1), makes it clear that a second order polynomial is the Taylor's series expansion of the performance function around the mean value of the design variables.

Similarly, a first order polynomial can be proven to be a first order Taylor's series expansion of the G function around the mean value of the design variables. In this case, the derivatives which correspond to the regression coefficients are indeed the gradient of the G function. In fact, they will be used to test the sensitivity of the G function with respect to each design variable and to determine the direction in which the second order polynomial has to be generated.

3.2.4 Sensitivity Analysis

It was noticed in the previous section that as the number of random variables in the probabilistic model increased, the number of runs or the number of times the physical model must be evaluated is increased as a multiple of two. However, when probabilistic analysis is performed and in the case of a large number of design variables, a major question arises: which of these variables should be included in the model, all of them or some of them, and how to distinguish between the importance of these variables.

The sensitivity analysis is used to answer all these questions. This can be done by constructing a probabilistic linear model, then testing the coefficient of each variable with respect to the standard error or the estimated standard deviation, t test [54] which can be written as

$$t = \frac{b_j}{s\sqrt{c_{jj}}} \quad (3.11)$$

where b_j is the regression coefficient, $s = \sqrt{\sum_{i=1}^m \frac{(y_i - \hat{y}_i)^2}{m - k}}$ is the standard error and c_{jj} is the j th diagonal of $([x]^T[x])^{-1}$

Myers and Walpole [55] show that t in Eq. 3.11 has a t or Student distribution with $(m - k)$ degrees of freedom. The probability density function for this distribution can be written as [56]

$$h(t) = \frac{\Gamma((v + 1)/2)}{\Gamma(v/2)\sqrt{\pi v}} \left(1 + \frac{t^2}{v}\right)^{-(v+1)/2} \quad -\infty < t < \infty \quad (3.12)$$

where $v = m - k$, m is the number of data sets, $k = n + 1$ is the number of regression coefficients and n is the number of random design variables.

Therefore, the probability that a random sample produces a value for t falling between any two specified values is equal to the area, A_0 , under the curve of the t distribution between the two ordinates corresponding to the specified values. Accordingly, the probability of not falling between these values is $1 - A_0$ and is designated as *prf*. This will be used to test the importance of each design variable; if *prf* is large, the variable will be removed from the probabilistic model. A value of 0.005 or more will be considered large here.

Thus, the use of sensitivity analysis can be summarized as follows:

1. All random variables are identified in the physical problem; if it is not clear whether some variables are random or not, they can be assumed random with 10% coefficient of variation.

2. A factorial design is constructed based on the number of random variables as $2^p > k$; for 10 variables a 2^4 design is needed for 30 variables a 2^5 design is needed, and so on.
3. The RSM is performed to obtain a first order polynomial based on the design variables in (1) and the factorial design in (2).
4. A sensitivity analysis is performed to obtain a *prf* value for the coefficient of each design variable in the first order polynomial. If *prf* > 0.005, the variable can be ignored from the probabilistic model.
5. The RSM is performed on the remaining variables to obtain a second order polynomial to which the FOSM is applied to obtain the reliability of the system.

Since y may represent any response quantity, such as stresses or displacements in a physical problem, the mean and standard deviation of y can be computed using Taylor's series expansion.

3.3 First Order Second Moment Reliability Analysis

Though the details for the FOSM have been available in many references [9], they are repeated here to show how complicated the method will be when the performance function is not available in an explicit form in terms of the design variables. In this method a performance function, G , is defined explicitly in terms of the design variables and separates the failure region from the safe region, Fig. 3.2. It can be written as

$$G = G(x_1, x_2, \dots, x_n) \quad (3.13)$$

when $G \leq 0$ failure takes place. The probability of failure, P_f , is then given as

$$P_f = P[G \leq 0] \quad (3.14)$$

where x_i are uncorrelated reduced variates

$$x_i = \frac{x_i^* - \mu_{x_i}}{\sigma_{x_i}} \quad (3.15)$$

with μ_{x_i} and σ_{x_i} the mean and standard deviation of the variable x_i^* .

The safety index, β , is defined as the minimum length vector from the origin of the coordinate system of x_i 's to the performance function G :

$$|\beta| = \sqrt{x_1^2 + x_2^2 + \dots + x_i^2} \quad (3.16)$$

The corresponding point, x_i^* , on G is called the design point. The direction cosines, γ_i , are calculated from the partial derivatives of G :

$$\gamma_i = \frac{\partial G}{\partial x_i^*} \sigma_{x_i} / \sqrt{\sum_{i=1}^n \left(\frac{\partial G}{\partial x_i^*} \sigma_{x_i} \right)^2} \quad (3.17)$$

A design value of the variables, x_i^* , is then obtained as

$$x_i^* = \mu_{x_i} - \gamma_i \sigma_{x_i} \beta \quad (3.18)$$

These variables are substituted into the performance function, Eq. 3.13, and the equation is solved for β .

The process is iterative, in that the new values of x_i^* (Eq. 3.18) are used in evaluating an improved set of γ_i and subsequently a new value of β .

For problems with large values of β , and in some other cases also, the polynomial shown in Eq. 3.1 has to be re-evaluated by using the design or the failure points obtained

in the first analysis as origin points (mean value) for the second design. A new polynomial can be obtained and will be much closer to the exact performance function. Then an increment for β can be computed and added to the previous value (as shown in Fig. 3.3) to obtain an accurate safety index for the problem under consideration. This process is repeated until the increment of β goes to zero. Usually it happens after one or two increments.

3.3.1 Uncorrelated Normally Distributed Variables

When all variables are normally distributed, the safety index β will also be normal and the probability of failure may be obtained from the normal integral as

$$P_f = \Phi(-\beta) \quad (3.19)$$

3.3.2 Correlated Normally Distributed Variables

It has been observed that strength and modulus for many materials are correlated variables. Such interdependence is characterized by the correlation coefficient ρ_{12} :

$$-1 < \rho_{12} < 1 \quad (3.20)$$

The procedure in such circumstances requires a transformation to uncorrelated variables [9].

In vector, form the means and standard deviations become

$$\vec{\mu}_x = \begin{pmatrix} \mu_{x_1} \\ \mu_{x_2} \end{pmatrix}, \quad \vec{\sigma}_x = \begin{pmatrix} \sigma_{x_1} \\ \sigma_{x_2} \end{pmatrix} \quad (3.21)$$

and the covariance matrix $[C]$ is

$$[C] = \begin{bmatrix} \sigma_{x_1}^2 & \rho_{12}\sigma_{x_1}\sigma_{x_2} \\ \rho_{12}\sigma_{x_1}\sigma_{x_2} & \sigma_{x_2}^2 \end{bmatrix} = \begin{bmatrix} \sigma_{x_1}^2 & C_{12} \\ C_{12} & \sigma_{x_2}^2 \end{bmatrix} \quad (3.22)$$

The two eigenvalues λ_1, λ_2 and eigenvectors are determined next by solving the matrix equation

$$\begin{bmatrix} (\sigma_{x_1}^2 - \lambda) & C_{12} \\ C_{12} & (\sigma_{x_2}^2 - \lambda) \end{bmatrix} = 0 \quad (3.23)$$

The eigenvectors are found from

$$\begin{bmatrix} (\sigma_{x_1}^2 - \lambda) & C_{12} \\ C_{12} & (\sigma_{x_2}^2 - \lambda) \end{bmatrix} \begin{pmatrix} \phi_1 \\ \phi_2 \end{pmatrix} = 0 \quad (3.24)$$

From these a modal matrix $[\Phi]$ and its transpose $[\Phi]^T$ are obtained as

$$[\Phi] = \begin{bmatrix} e_{11} & e_{12} \\ e_{21} & e_{22} \end{bmatrix} \quad (3.25)$$

$$[\Phi]^T = \begin{bmatrix} e_{11} & e_{21} \\ e_{12} & e_{22} \end{bmatrix} \quad (3.26)$$

The means of the uncorrelated normal variables $\{z\}$ are calculated as

$$\vec{\mu}_z = \begin{pmatrix} \mu_{z_1} \\ \mu_{z_2} \end{pmatrix} = [\Phi]^T \begin{pmatrix} \mu_{x_1} \\ \mu_{x_2} \end{pmatrix} \quad (3.27)$$

while the standard deviations of these uncorrelated normal variables are

$$\vec{\sigma}_z = \begin{pmatrix} \sigma_{z_1} \\ \sigma_{z_2} \end{pmatrix} = \begin{pmatrix} \sqrt{\lambda_1} \\ \sqrt{\lambda_2} \end{pmatrix} \quad (3.28)$$

For the calculation of the reliability index, β , the technique described earlier can be used with some modifications. First the variables $\{x^*\}$ are uncorrelated:

$$\{z\} = [\Phi]^T \{x^*\} \quad (3.29)$$

The derivatives of the performance function in terms of the uncorrelated variables are obtained as

$$\frac{\partial G}{\partial z} = [\Phi]^T \left\{ \frac{\partial G}{\partial x} \right\} \quad (3.30)$$

Next, the direction cosines $\{\gamma\}$ are found

$$\{\gamma\} = \left\{ \sigma_z \frac{\partial G}{\partial z} / \sqrt{\sum_{i=1}^n \left(\sigma_{z_i} \frac{\partial G}{\partial z_i} \right)^2} \right\} \quad (3.31)$$

New values of $\{z\}$ are calculated:

$$z_i = \mu_{z_i} + \gamma_i \beta \sigma_{z_i} \quad (3.32)$$

The original variables are obtained by the transformation

$$\{x^*\} = [\Phi]\{z\} \quad (3.33)$$

These are substituted into the performance function

$$G(x_1^*, x_2^*, \dots, x_i^*) = 0 \quad (3.34)$$

which is then solved for β . The process is repeated until convergence occurs.

3.4 Non-Normal Variables

When variables are not normally distributed, transformations to equivalent normal distributions are first performed. If the density function and probability distribution are $f_x(x^*)$ and $F_X(x^*)$, respectively, while the corresponding normal density and distribution at the design point are $\phi(x_i^*)$ and $\Phi(x_i^*)$, for equivalence

$$f_x(x^*) = \phi(x^*) \quad (3.35)$$

$$F_X(x^*) = \Phi(x^*) \quad (3.36)$$

The equivalent normal standard deviation is obtained from the relation

$$\sigma_x^N = \phi[\Phi^{-1}(F_X^*)]/f_x(x^*) \quad (3.37)$$

and the normal mean from

$$\mu_x^N = X^* - \sigma_x^N \Phi^{-1}[F_X(x^*)] \quad (3.38)$$

These values are then used to replace the standard deviation and the mean in Eqs. 3.17 and 3.18.

The probability of failure is calculated from Eq. 3.19.

3.4.1 Log Normal Variables

When variables are log-normally distributed,

$$f_x(x) = \frac{1}{\sqrt{2\pi} \zeta_x x} e^{-\frac{1}{2} \left(\frac{\ln x - \lambda_x}{\zeta_x} \right)^2} \quad (3.39)$$

the parameters of the distribution, λ_x , the mean value of $\log x$ and ζ_x , the standard deviation of $\log x$, must be computed

$$\lambda_x = \ln \mu_x - \frac{1}{2} \zeta_x^2 = \ln \hat{x} \quad (3.40)$$

$$\zeta_x = \sqrt{\ln(1 + \delta_x^2)} \quad (3.41)$$

where $\delta_x = \sigma_x/\mu_x$ is the coefficient of variation and \hat{x} is the median value.

With these parameters, Eqs. 3.37 and 3.38 are simplified

$$\sigma_x^N = \zeta_x x^* \quad (3.42)$$

and

$$\mu_x^N = x^* \left(1 - \ln \frac{x^*}{\hat{x}} \right) \quad (3.43)$$

3.4.2 Weibull Distributed Variables

The density and probability functions of the Weibull distribution are given in terms of three parameters, x_c , the characteristic value, x_0 , the minimum value and m , the shape parameter, as

$$f_x(x) = \frac{m}{x_c - x_o} \left(\frac{x - x_o}{x_c - x_o} \right)^{m-1} \exp \left[- \left(\frac{x - x_o}{x_c - x_o} \right)^m \right] \quad (3.44)$$

and

$$F_X(x) = 1 - \exp \left[- \left(\frac{x - x_o}{x_c - x_o} \right)^m \right] \quad (3.45)$$

x_c and m are related to the mean and standard deviation of the variable:

$$\mu_x = x_o + (x_o + x_c) \Gamma \left(1 + \frac{1}{m} \right) \quad (3.46)$$

$$\sigma_x = (x_c - x_o) \left[\Gamma \left(1 + \frac{2}{m} \right) - \Gamma^2 \left(1 + \frac{1}{m} \right) \right]^{\frac{1}{2}} \quad (3.47)$$

with $\Gamma(\cdot)$ the gamma function. The shape parameter may be approximated for the two parameter case ($x_o = 0$) as

$$m = \frac{1.2}{\delta_x} \quad (3.48)$$

3.4.3 General Strategy for Non-Normal Variables

The following steps will be used to perform probabilistic analysis for problems with design variables that have non-normal probability functions.

1. All five steps that are described in section 3.2.4 are used under one condition which is that the mean and standard deviation for each variable that enter the design must come from a normally distributed function, i.e., Eqs. 3.36 and 3.37 are used to obtain an equivalent normal mean and standard deviation for every non-normal variable.

2. New values for the equivalent mean and standard deviation are computed based on the design points obtained in step 5 of 3.2.4.
3. Step 5 of 3.2.4 is repeated using the new values of the mean and the standard deviation for each variable, and a new design point as well as an increment for the safety index are obtained.
4. Steps 2 and 3 are repeated till the increment of the safety index becomes less than 0.001. This normally happens after 2 to 3 trials.

3.5 Progressive Probability of Failure

The probabilities of failure calculated in the previous section lead to the concept of failure rate or hazard rate [57], $h(t)$, which is the probability that a structure that survived to time t will fail during the next time unit. It is based on the application of a single stress and is defined as the ratio

$$h(t) = \frac{p_f(t)}{L(t)} \quad (3.49)$$

When a sequence of stresses is applied to the motor, its reliability $L(t)$ is calculated as

$$L(t) = \exp\left[-\int_0^t h(t) dt\right] \quad (3.50)$$

In summation form

$$L(t_n) = \exp\left[-\sum_{j=1}^n \frac{p_f(t_j)}{L(t_{j-1})}\right] \quad (3.51)$$

with $L(0) = 1.0$.

The progressive probability of failure is

$$p_f(t_j) = 1 - L(t_j) \quad (3.52)$$

3.6 Weakest Link and Size Effect

3.6.1 Independent Failure Modes

In the probabilistic finite element method, the reliability for each element is computed based on FOSM in conjunction with the RSM described above. In some problems, failure of one element represents total failure of the system. Normally, this is the case for problems where brittle materials are involved in their design or the case of independent failure modes in the system. The total reliability will be computed based on Weakest Link theory which requires multiplying element reliabilities by each other. This technique depends on the number of elements in the finite element domain, i.e., for less elements a better reliability value will be obtained. In fact, this should be true when the domain in reality consists of several elements, but the discretization of the domain is done by the user and is different from one user to another. Therefore, the following is proposed to overcome this difficulty and obtain the same reliability value regardless of the number of elements in the domain.

The proposed technique is based on including the size of the element in the strength distribution of the material. The technique described above will be used to compute the

reliability for each element. The Weibull probability density function has been a good choice for the strength of the material [34,35] and can be written as

$$f_R(r) = \frac{m}{R_c} \left(\frac{r}{R_c} \right)^{m-1} \exp\left[- \left(\frac{r}{R_c} \right)^m \right] \quad (3.53)$$

with the cumulative distribution function

$$F_R(r) = 1 - \exp\left[- \left(\frac{r}{R_c} \right)^m \right] \quad (3.54)$$

R_c and m are related to the mean and standard deviation of the variable:

$$\mu_R = R_c \Gamma\left(1 + \frac{1}{m}\right) \quad (3.55)$$

$$\sigma_R = R_c \left[\Gamma\left(1 + \frac{2}{m}\right) - \Gamma^2\left(1 + \frac{1}{m}\right) \right]^{\frac{1}{2}} \quad (3.56)$$

with $\Gamma(\cdot)$ the gamma function.

The FOSM is performed at the element level; therefore the above equations should include the element size. Probability functions are always nondimensional, thus the size of the element should be normalized with respect to the total size of the domain. Eqs. 3.53-3.56 can be written as

$$f_R(r) = c \frac{m}{R_c} \left(\frac{r}{R_c} \right)^{m-1} \exp\left[- c \left(\frac{r}{R_c} \right)^m \right] \quad (3.57)$$

$$F_R(r) = 1 - \exp\left[- c \left(\frac{r}{R_c} \right)^m \right] \quad (3.58)$$

and the mean and standard deviation of the strength become

$$\mu_R = R_c \left(\frac{1}{c} \right)^{\frac{1}{m}} \Gamma\left(1 + \frac{1}{m}\right) \quad (3.59)$$

$$\sigma_R = R_c \left(\frac{1}{c} \right)^{\frac{1}{m}} \left[\Gamma\left(1 + \frac{2}{m}\right) - \Gamma^2\left(1 + \frac{1}{m}\right) \right]^{\frac{1}{2}} \quad (3.60)$$

where c is the ratio between the element size and the total size of the domain. In 1-D problems, c is the ratio of the length of the element to the total length; in 2-D problems it is the area of the element to the total area, and in 3-D problems it is the ratio of the volume of the element to the total volume. The FOSM described above will be used based on non-normal variables, with strength probabilistic information given in Eqs. 3.57-3.60.

3.6.2 General Strategy for Multi-Independent Failure Modes

When more than one failure mode is included in the analysis, more than one performance function must be considered. Moreover, since the Weibull distribution function described in the previous section is adapted for the strength of the material, at least one of the variables is a non-normal random variable. To achieve this, the following steps are used:

1. Step one in section 3.4.3 is applied for each failure mode, i.e., for each failure region. In this case, however, the results of sensitivity analysis for each failure mode must be combined together in order to decide on the retained variables that will be used in the second order approximation, i.e., only common variables must be dropped out of the design.
2. The reliability of the system is computed by multiplying the reliabilities at each failure mode by each other.
3. The safety index of the system is computed by taking the inverse of the normal density function at the resultant reliability value.

4. The procedure is terminated after this step because more than one set of design points is obtained (one set for each failure mode) and it is impossible to decide which one to choose in order to reevaluate the performance function.

Table 3.1 Values of α for an Orthogonal Central Composite Design

n	α
2	1.000
3	1.216
4	1.414
5	1.596
6	1.761
7	1.910
8	2.045

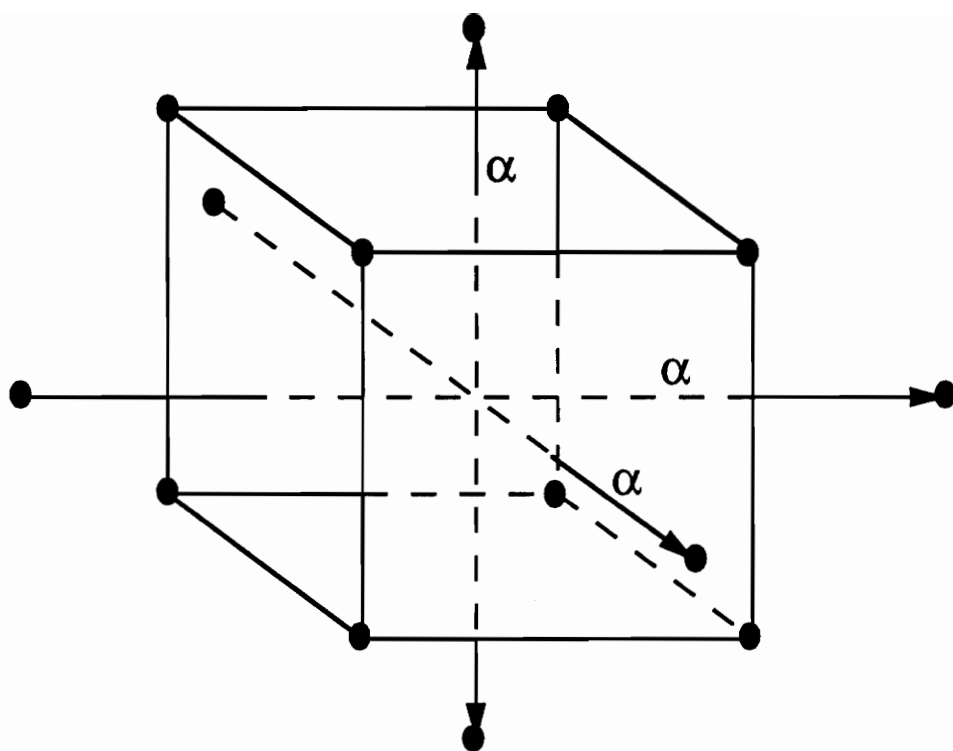


Fig. 3.1 Central composite design for $n = 3$

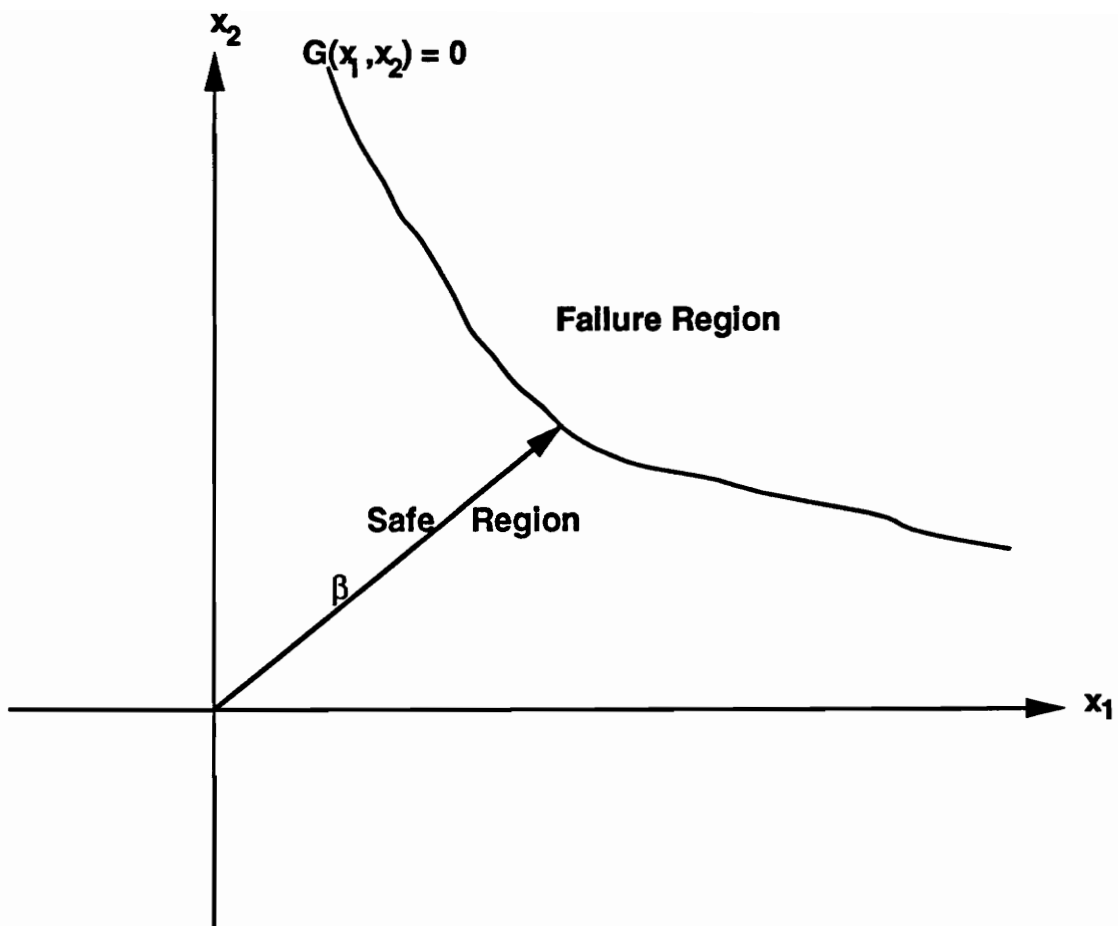


Fig. 3.2 A typical performance function

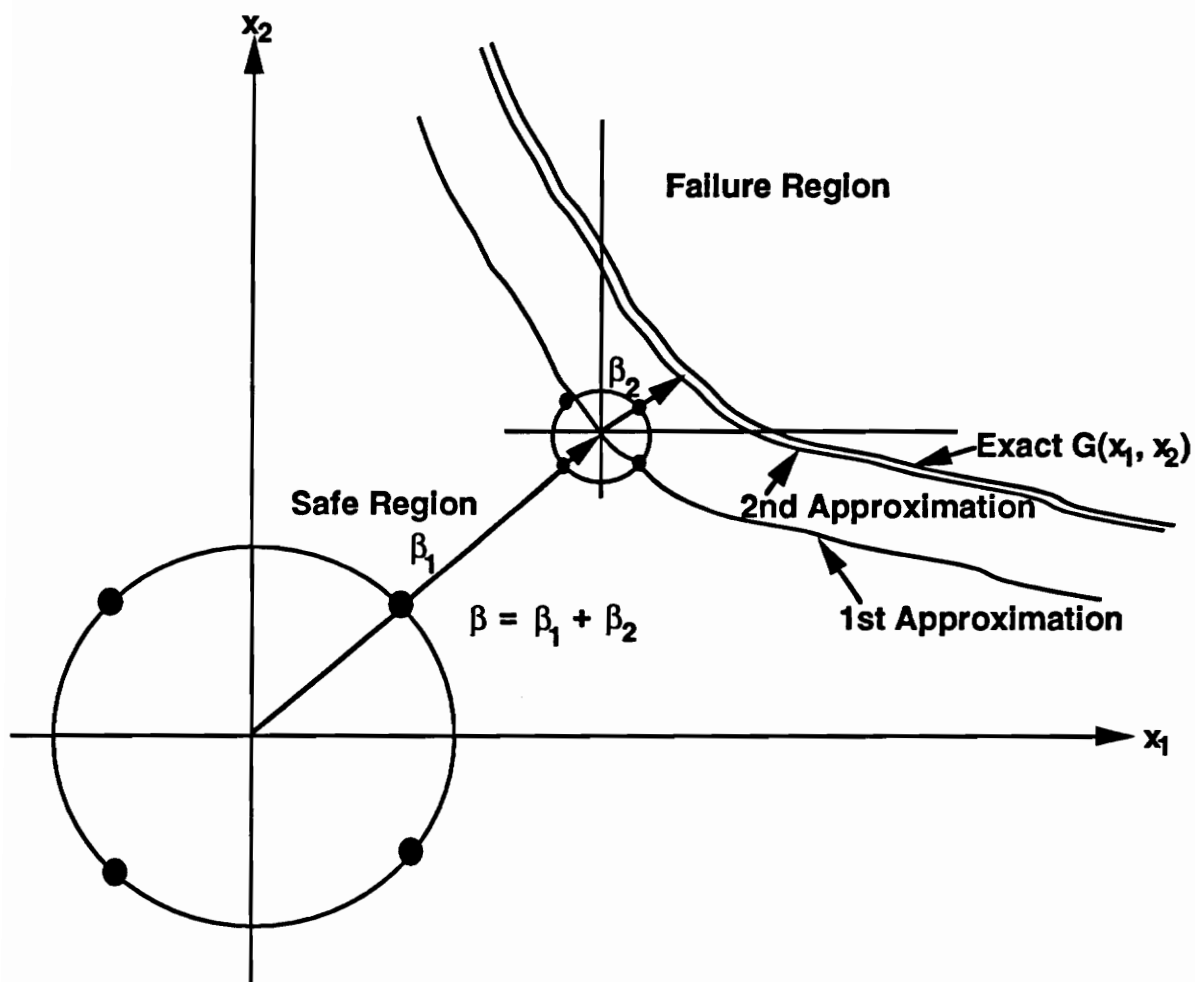


Fig. 3.3 A performance function obtained by RSM

Chapter IV

RELIABILITY OF ROCKET MOTORS UNDER THERMAL LOAD

4.1 Introduction

Solid propellant rocket motors when stored under field conditions are subjected to environmental temperature changes which will eventually produce thermal stresses, cumulative damage as well as aging in the propellant. These stresses will cause structural damage and consequently structural failure. Since all design variables as well as temperature parameters are random variables, a probabilistic analysis based on the First Order Second Moment (FOSM) reliability method will be used to determine the service life of these motors.

Motors are considered to be long, hollow, elastic, cylindrical shells, surrounded by a layer of insulation and filled with a viscoelastic propellant whose strength is degraded by cumulative damage and aging. Temperature is symmetric with respect to the axis of

the motor, and the outside surface temperature is the same as the air temperature. Failure of the motor is based on the maximum tangential stress at the bore, for which an exact solution can be derived.

The new technique that has been developed in chapter 3 will be applied here too and a comparison between the two solutions will be made to demonstrate the accuracy of the developed technique. The new developed technique will be referred to as the approximate solution.

4.2 Exact Analysis

The First Order Second Moment (FOSM) reliability method is used to predict the service life of rocket motors. The technique allows different probability distributions for each variable and allows for dependence between variables in terms of correlation such as propellant strength and modulus. Before the induced thermal stresses are calculated at a certain point in the motor, the temperature at that point must be known. Hence the first task is to determine the temperature at the instant at which the stresses are desired, and the second one is to compute the stresses themselves.

In previous studies, [47,48,58], a recorded time series of actual hourly temperatures has been used as an input. Such a detailed series has been found to be unnecessarily costly in terms of computer time. In the present analysis, only seasonal and diurnal temperature variations are considered without significant loss of accuracy and with considerable savings in computational costs.

4.2.1 Thermal Stress Analysis

Though the thermal stress analysis of a layered cylinder has been presented in many papers [44,45], it is repeated here in a shortened form for the sake of completeness.

Assuming an axisymmetric temperature distribution around the cylinder, the heat conduction equation in cylindrical coordinates is used for each layer Fig. 4.1,

$$\frac{\partial^2 T_j}{\partial^2 r} + \frac{1}{r} \frac{\partial T_j}{\partial r} = \frac{1}{\bar{\alpha}_j} \frac{\partial T_j}{\partial t} \quad (4.1)$$

The temperature of the j^{th} layer, $T_j(r,t)$ is a function of both radial coordinate, r , and time, t , with $\bar{\alpha}_j$ the thermal diffusivity of the j^{th} layer. Using the frequency response function approach, the temperature can be written as

$$T_j(r,t) = \bar{T}_j(r, \omega) e^{i\omega t} \quad (4.2)$$

Substituting Eq.4.2 into Eq. 4.1, the solution of Eq. 4.1 becomes

$$\bar{T}_j(r, \omega) = C_j^1 Br(x_j) + C_j^2 Kr(x_j) \quad (4.3)$$

where $\bar{T}_j(r, \omega)$ is the frequency response function of the j^{th} layer, $x_j = \sqrt{\omega/\bar{\alpha}_j} r_j$, Br , Kr are Kelvin functions [56] and C_j^1 , C_j^2 are coefficients to be determined from the following boundary conditions:

B.C. 1: $T_1(0,t)$ temperature at the center is finite

B.C. 2, 3, 4, 5: $T_j(r,t) = T_{j+1}(r,t)$, temperatures are the same on both sides of an interface

B.C. 6, 7, 8, 9: $K_j \frac{\partial T_j(r,t)}{\partial r} = K_{j+1} \frac{\partial T_{j+1}(r,t)}{\partial r}$, the heat flux across an interface is continuous

B.C. 10: $T_3(r_3,t) = e^{i\omega t}$, the temperature on the surface of the fifth layer varies sinusoidally with a unit amplitude and a frequency, ω

While temperature is evaluated in all five layers, stresses are of interest only in layers 2 and 3. The frequency response function of the temperature is used to evaluate the frequency response functions for the stress components $S_r(r, \omega)$ and $S_\theta(r, \omega)$ for the following boundary conditions: continuity of radial displacements and radial stresses on interfaces and zero radial stresses on the bore and the external surface of layer 3.

Because storage life is limited by the deterioration of the propellant rather than the case, only stresses in the second layer (propellant) are evaluated. These are given as

$$S_r(r, \omega) = \frac{r_2^2}{r_2^2 - r_1^2} \left(1 - \frac{r_1^2}{r^2}\right) E_2 \frac{q_1}{q_2} + \frac{\alpha_2 E_2}{(1 - \nu_2)(r_2^2 - r_1^2)} \left(1 - \frac{r_1^2}{r^2}\right) \int_{r_1}^{r_2} \bar{T}_2(r, \omega) r dr - \frac{\alpha_2 E_2}{(1 - \nu_2)r^2} \int_{r_1}^r \bar{T}_2(r, \omega) r dr \quad (4.4)$$

$$S_\theta(r, \omega) = -\frac{r_2^2}{r_2^2 - r_1^2} \left(1 + \frac{r_1^2}{r^2}\right) E_2 \frac{q_1}{q_2} + \frac{\alpha_2 E_2}{(1 - \nu_2)(r_2^2 - r_1^2)} \left(1 + \frac{r_1^2}{r^2}\right) \int_{r_1}^{r_2} \bar{T}_2(r, \omega) r dr + \frac{\alpha_2 E_2}{(1 - \nu_2)r^2} \int_{r_1}^r \bar{T}_2(r, \omega) r dr - \frac{\alpha_2 E_2 \bar{T}_2(r, \omega)}{1 - \nu_2} \quad (4.5)$$

where

$$q_1 = 2\alpha_2(1 + \nu_2) \int_{r_1}^{r_2} \bar{T}_2(r, \omega) r dr - \alpha_3(1 + \nu_3)(r_2^2 - r_1^2) \bar{T}_2(r_2, \omega) \quad (4.6)$$

$$q_2 = (1 + \nu_2)(1 - 2\nu_2)r_2^2 + (E_2/E_3)(1 - \nu_3^2)r_2(r_2^2 - r_1^2)/(r_3 - r_2) \quad (4.7)$$

The stress frequency response functions, Eqs. (4.4) and (4.5), are complex quantities. Their magnitudes are obtained as

$$|S(r, \omega)| = [S^2(r, \omega)_{RE} + S^2(r, \omega)_{IM}]^{1/2} \quad (4.8)$$

They are the response to a sinusoidal temperature input of unit amplitude and frequency ω . A temperature input consists of several constant and sinusoidal components:

$$T = T_f - [T_m + A_y \sin(\omega_y t + \phi_y) + A_d \sin(\omega_d t + \phi_d)] \quad (4.9)$$

All constants in Eq. 4.9 are defined in Table 4.1.

Calculations indicate that the tangential stress at the bore is significantly greater than the radial stress at the bond line. Therefore only the time dependent tangential stress will be considered. This can be written as

$$S_\theta(r, t) = T_f S_\theta(r, 0) - T_m S_\theta(r, 0) - A_d \sin(\omega_d t + \phi_d) S_\theta(r, \omega_d) - A_y \sin(\omega_y t + \phi_y) S_\theta(r, \omega_y) \quad (4.10)$$

4.2.2 Viscoelastic Properties of the Propellant

Both modulus and strength of the material are time and temperature dependent properties.

Since in storage, thermal loads are essentially cyclic in nature, it is expedient to convert the time-dependent relaxation modulus into the frequency-dependent complex modulus representation. This is accomplished by performing sine and cosine Fourier-transformations which yield a real and an imaginary term

$$E'(T, \omega)_{RE} = E_{\infty} + \sum_{i=1}^8 \frac{E_i \omega^2 a_i^2 \tau_i^2}{1 + \omega^2 \tau_i^2 a_i^2} \quad (4.11)$$

and

$$E''(T, \omega)_{IM} = 2\pi \sum_{i=1}^8 \frac{E_i \omega a_i \tau_i}{1 + \omega^2 \tau_i^2 a_i^2} \quad (4.12)$$

Hence

$$E(T, \omega) = E'(T, \omega) + iE''(T, \omega) \quad (4.13)$$

For the seasonal and diurnal frequencies, the imaginary part can be neglected [48].

In Eqs. (4.11) and (4.12), E_i , τ_i are moduli and relaxation times for parallel Maxwell elements [58], shown in table 4.2, and a_i is the viscoelastic shift function [59] which for the material under investigation can be written as

$$\log a_i = 1.42 \left\{ -\frac{8.86(T + 34.0)}{181.9 + (T + 34.0)} + 3.32 \right\} \quad (4.14)$$

with T in $^{\circ}F$. The shift function for the propellant under consideration is plotted in Fig. 4.2. Substituting Eq. (4.14) into Eq. (4.11), the daily modulus can be computed as a function of temperature, and the result is shown in Fig. 4.3.

The mean strength, $R(T, t)$ (psi) of a viscoelastic material is given in [60] as

$$R(T, t) = R_0 \left(\frac{t}{4a_i} \right)^{-n} \quad (4.15)$$

For the propellant under consideration $n = 0.0857$, $R_0 = 139$ when t is measured in minutes, and $R_0 = 98$ when t is in hours. Experiments conducted by the U.S. Army Missile Command [61] indicate that the bond line for room temperature and above is approxi-

mately twice as strong as the tensile strength of the propellant. Only at low temperatures is the bond line weaker than the propellant. At $0^{\circ}F$ their ratio is 0.8.

4.2.3 Cumulative Damage and Aging

The linear cumulative damage rule proposed in [62] states that damage produced in time spent at a particular stress level, S_i , is inversely proportional to the time, t_{fi} , required to produce failure in the material at that stress level:

$$d_i = \frac{1}{t_{fi}} \quad (4.16)$$

The total damage produced by N stress levels is

$$D = \sum_{i=1}^N \frac{t_i}{t_{fi}} \quad (4.17)$$

where t_i is the duration for each stress level. A relationship between constant stress and reduced time to failure is given as

$$\frac{t_{fi}}{a_t} = CS_i^{-B} \quad (4.18)$$

where C and B are material parameters ($C = 1.6 \times 10^{16}$, $B = 8.76$ are being used here). The cumulative damage, D , becomes

$$D = \frac{1}{C} \sum_{i=1}^N \frac{S_i^B t_i}{a_t} \quad (4.19)$$

Therefore, the degraded mean strength can be written as

$$R'(T,t) = R(T,t)(1 - D) \quad (4.20)$$

Aging is defined as the change in physical and thermal parameters in an unloaded condition. It is accelerated in warm climates and during summer periods. It has been shown that the ratio, $\eta(T,t)$, of the current value of a property to its initial value is proportional to the logarithm of time [63].

In the case of strength,

$$\eta_R(T,t) = \frac{R(T,t)}{R(T,0)} = 1 - \beta_R(T) \log t \quad (4.21)$$

where the coefficient, $\beta_R(T)$, is an exponentially decreasing function of absolute temperature, T . Hence,

$$\beta_R(T) = A_R e^{-B_R/T} \quad (4.22)$$

$$R(T,t) = \eta_R R_0 \left(\frac{t}{4a_t} \right)^{-n} \quad (4.23)$$

Here $A_R = 1.15 \times 10^{10}$, $B_R = 1.53 \times 10^4$ with t in days and T in $^{\circ}\text{Rankin}$.

In the case of the modulus, E_2 , the coefficients of Eqs. (4.22) and (4.23) are replaced by $A_E = 4.1 \times 10^5$, $B_E = 8.75 \times 10^3$.

Variable temperature aging will be calculated based on the concept of reduced time. If the propellant is aged at temperature T_1 for the period of t_1 days, the aging factor becomes equal to

$$\eta_1 = 1 - \beta_1 \log t_1 \quad (4.24)$$

where $\beta_1 = Ae^{-B/T_1}$. The same aging factor may be obtained at a different temperature, T_2 , in time, t'_1 , called equivalent time Hence the equivalent time during which the same aging parameter is reached at T_2 becomes equal to

$$t'_1 = t_1^{\beta_1/\beta_2} \quad (4.25)$$

If aging is now continued at T_2 for an additional time, Δt , the total aging time, t_2 , will be the sum

$$t_2 = t'_1 + \Delta t \quad (4.26)$$

The process is then repeated for other temperatures.

Because the aging at practical service temperatures is relatively slow , it has been found that diurnal temperature variations have an insignificant effect on aging factors. As a consequence, only seasonal thermal changes have been included in aging calculations. Aging factors are evaluated for the average daily temperature.

4.2.4 Results for Exact Analysis

4.2.4.1 Evaluation of Stresses

The motor configuration shown in Fig. 4.1 with geometric, thermal and mechanical parameters presented in Table 4.1 has been analyzed. Coefficients of variation are given in the same table. Three different locations are considered. Point Barrow, AK. represents a cold site, Yuma, AZ. represents a warm site and Nashville, TN. represents a moderate site.

First, the frequency response function for temperature at the bore is evaluated for seasonal and diurnal frequencies. Then the tangential bore stress is calculated and the results are plotted in Fig. 4.4 for the three locations.

Cumulative damage is presented in Fig. 4.5. The damage at Point Barrow becomes 1 after 2200 days, which corresponds to 0 strength, and further calculations are terminated. Aging factors are plotted in Fig. 4.6 for both strength and modulus. It is seen that the modulus and consequently the stresses are affected more by this phenomenon than is the strength of the material. Both indicate accelerated deterioration during the hot summer months. This explains why there is no aging effect on the strength at Point Barrow.

The seasonal variations of the modulus including aging are depicted in Fig. 4.7. The change in the slope is due to high variation of the modulus at low temperature levels. The plot presented in Fig. 4.4 indicates the seasonal changes in thermal stresses. The gradual deterioration of the core strength is seen in Fig. 4.8. The strength at Point Barrow becomes 0 after 2200 days, the same period in which the damage effect is 1.

4.2.4.2 Evaluation of the Safety Index and the Progressive Probability of Failure

4.2.4.2.1 Uncorrelated Non-Normal Variables (aging and cumulative damage included)

The safety index, β , is a measure of the reliability of a structure. A high value of β corresponds to high reliability. Utilizing Eqs. (3.13) to (3.18) with the performance function, $G = R - S$, where, R is given in Eq. 4.15 and S is given in Eq. 4.10, the safety index may be determined for each day. The daily variations in the safety index are

plotted in Fig. 4.9 for the three different locations, where strength and modulus have Weibull probability distributions and other variables have normal distributions. The influence of the temperature variation is clearly visible here.

Because low temperature produces high modulus and consequently high stresses, where the latter produces a high damage factor which gives rise to a significant reduction in the strength, therefore the lowest value of β occurred at Point Barrow, AK. The daily probability of failure may be calculated from Eq. (3.19) while the progressive probability of failure is obtained from Eqs. (3.51) and (3.52).

The progressive probability is presented in Fig. 4.10 again for the above three cases. Because a low value of the safety index corresponds to high probability, the Point Barrow curve rises fastest, followed by the Nashville curve and the Yuma curve. To illustrate the effect of probability distributions on the analysis, different probability distributions are assumed for the strength and the modulus at Nashville, TN. Results are shown in Fig. 4.11 for the safety index and Fig. 4.12 for the progressive probability of failure.

The probability of failure is less for the Weibull distributed modulus than for the lognormally distributed modulus, Therefore, if the actual probability distribution of the modulus is lognormal and the prediction was made based on Weibull, then the service life will be over estimated.

4.2.4.2.2 Correlated Non-Normal Variables (aging and cumulative damage included)

To illustrate the effects of correlation, three different levels of correlation are considered at the moderate site. Correlation is assumed between strength and modulus of

the propellant. Weibull probability distribution is assumed for both the strength and the modulus of the propellant, and normal probability distribution is assumed for the other variables. These cases are shown in Fig. 4.13 for the safety index and Fig. 4.14 for the progressive probability of failure.

As correlation increases, the probability of failure decreases because higher stresses (higher modulus) are applied to a stronger material while a weaker material is subjected to lower stresses. In the absence of correlation such matching does not take place. The assumption of independence of variables results, therefore, in conservative estimates for reliable storage lives of motors.

4.3 Approximate Analysis

4.3.1 Solution by Approximate Analysis

The importance of this approximation is to get the function G in a simplified explicit form in terms of the design variables.

The reliability of the motor described above will be computed based on RSM and a comparison will be made with the exact solution. Let

- $x_1 =$ propellant modulus E_2
- $x_2 =$ case modulus E_3
- $x_3 =$ Poisson's ratio of case ν_3
- $x_4 =$ coefficient of thermal expansion of propellant α_2
- $x_5 =$ coefficient of thermal expansion of steel case α_3
- $x_6 =$ daily temperature amplitude A_d
- $x_7 =$ yearly temperature amplitude A_y
- $x_8 =$ propellant strength R

By assuming two levels for each variable, and making use of central composite design, with $\alpha = 2.045$ from table 3.1, the design matrix, D , Eq. 3.8 and Eq. 3.9 can be obtained. The fractional factorial analysis is used to reduce the order of the design matrix from $256 + 17$ to $64 + 17$. This fraction is called $\frac{1}{4}$ of 2^8 fractional factorial analysis. Each row of the design matrix is substituted into Eq. 3.11 to obtain the corresponding response y . The design matrix is also substituted into the X matrix, Eq. 3.3, and the elements of the X matrix are obtained. Then the linear system given by Eq. 3.7 is solved and the solution is the set of coefficients of the approximated surface of the second order.

This second order surface can be written as

$$y = a_0 + \sum_{i=1}^8 a_i x_i + \sum_{i=1}^8 a_{ii} x_i^2 + \sum_{i=1}^7 \sum_{j=i+1}^8 a_{ij} x_i x_j + \varepsilon \quad (4.27)$$

The FOSM reliability method is ready to be applied by using y as the performance function G , where the probability of failure is

$$P_f = P(y \leq 0) \quad (4.28)$$

Then the same procedures as in Eqs. 3.13-3.18 can be followed. In order to obtain the derivatives of y with respect to each variable x , y should be rewritten as

$$y = a_0 + \hat{x}^T b + \hat{x}^T B \hat{x} \quad (4.29)$$

where

$$\hat{x} = \begin{bmatrix} x_1 \\ x_2 \\ \cdot \\ \cdot \\ \cdot \\ \cdot \\ \cdot \\ x_8 \end{bmatrix}, \quad b = \begin{bmatrix} a_1 \\ a_2 \\ \cdot \\ \cdot \\ \cdot \\ \cdot \\ \cdot \\ a_8 \end{bmatrix}, \quad B = \begin{bmatrix} a_{11} & a_{12} & a_{13} & a_{14} & a_{15} & a_{16} & a_{17} & a_{18} \\ & a_{22} & a_{23} & a_{24} & a_{25} & a_{26} & a_{27} & a_{28} \\ & & a_{33} & a_{34} & a_{35} & a_{36} & a_{37} & a_{38} \\ & & & a_{44} & a_{45} & a_{46} & a_{47} & a_{48} \\ & & & & a_{55} & a_{56} & a_{57} & a_{58} \\ & & & & & a_{66} & a_{67} & a_{68} \\ & & & & & & a_{77} & a_{78} \\ \cdot & \cdot & \cdot & \cdot & \cdot & \cdot & \cdot & a_{88} \end{bmatrix} \quad (4.30)$$

Off diagonal elements are divided by 2. Therefore

$$\frac{\partial y}{\partial x} = b + 2B\hat{x} \quad (4.31)$$

The transformed variables can be written as

$$x_i = -\gamma_i \beta \quad (4.32)$$

Substituting Eq. 4.31 into Eq. 3.17, γ_i are evaluated. Then substituting Eq. 4.32 into Eq. 4.29, the safety index, β , is obtained. Then the derivatives in Eq. 4.31 can be updated and new values of γ can be obtained. The process is iterative until convergence occurs.

4.3.2 Results for Approximate Analysis

Fig. 4.15 represents a comparison between exact analysis and the new approximate analysis. The stress, S , the strength, R , and the performance function, $R - S$, are calculated based on the exact analysis. The function $R - S$ is also calculated using approximate analysis and the results are plotted in Fig. 4.15. An excellent agreement is obtained between the two techniques.

Fig. 4.16 represents a comparison between the two analyses in terms of the safety index. The safety index is obtained by substituting Eq. 3.18 into Eq. 3.13 and solving

for β for the exact analysis and by substituting Eq. 4.32 into Eq. 4.29 for the approximated analysis. The two curves overlap.

Fig. 4.17 represents the progressive probability of failure for the two solutions. The solution is obtained based on Eq. 3.51 and Eq. 3.52. The two curves are in good agreement, indicated by the overlap in the safety index curves.

4.4 Conclusions

The FOSM method of structural reliability has been applied to estimate the storage life of motors subjected to environmental temperatures. Variables with various statistical distributions and degrees of correlation have been assumed.

Under or over estimates of the service life of rocket motors might result if the design variables are given unreasonable probability distributions. The assumption of independence between variables produces more conservative estimates than correlated variables.

Results have shown that storing rocket motors at a warm site make them more reliable than storing them at a cold site.

The accuracy of the approximate solution has been demonstrated by the excellent agreement that has been obtained between the two analyses. This allows for more complicated examples to be investigated where solutions are obtained using finite element analysis. An example is the case of rocket motors subjected to static and dynamic patch and line loadings where reliability analysis is required. This example will be covered in the next chapter.

A computer program entitled ROCKT2 has been developed [64] for the calculation of reliabilities and storage lives of solid propellant motors.

Table 4.1 Geometric, Thermal and Mechanical Parameters

Material	Air (core)	Propellant	δ	Case	δ	Air(gap)	Insulation
r (in)	1.875	4.302	---	4.400	---	5.400	6.400
Conductivity K							
Btu/hrft F°	0.0145	0.7641	---	14.600	---	0.0145	0.0160
Diffusivity $\bar{\alpha}$							
in^2 /hr	109.872	4.378	---	48.960	---	109.872	1.235
Elastic modulus E		E_∞					
(psi)	---	281.84	0.10	30.0×10^6	0.05	---	---
Poisson's ratio ν	---	0.492	0.0	0.253	0.05	---	---
Coefficient of thermal expansion $\alpha(\text{in/in}F^\circ)$	---	5.7×10^{-5}	0.05	6.5×10^{-6}	0.05	---	---
Strength	---	Eq. (13)	0.10	---	---	---	---
Stress Free Temperature $T_f(F^\circ)$	---	165	---	---	---	---	---
Characteristics	Point Barrow, AK	δ	Nashville, TN	δ	Yuma, AZ	δ	
Mean Temperature (T_m) F°	9.356	---	58.536	---	73.49	---	
Daily Amplitude (A_d) F°	1.602	0.10	7.495	0.10	11.530	0.10	
Yearly Amplitude (A_y) F°	30.690	0.10	20.678	0.10	19.224	0.10	
ω_d	$2\pi/24$	--	$2\pi/24$	---	$2\pi/24$	---	
ω_y	$2\pi/8760$	---	$2\pi/8760$	---	$2\pi/8760$	---	
Daily Phase (ϕ_d)	$15\omega_d$	---	$16\omega_d$	---	$16\omega_d$	---	
Yearly Phase (ϕ_y)	$5088\omega_y$	---	$4871\omega_y$	---	$4920\omega_y$	---	

Table 4.2 Prony Constants for Tensile Relaxation Modulus

$$E_{\infty} = 281.84\text{psi} (1.943E + 06N/m^2)$$

i	$E_i, \text{psi}(N/m^2)$	$\tau_i, \text{hrs.}$
1	1.979E + 04 (1.364E + 08)	3.333E-12
2	7.990E + 03 (5.509E + 07)	3.333E-10
3	2.522E + 03 (1.739E + 07)	3.333E-08
4	1.153E + 03 (7.947E + 06)	3.333E-06
5	7.346E + 02 (5.065E + 06)	3.333E-04
6	2.041E + 02 (1.497E + 06)	3.333E-02
7	2.718E + 02 (1.873E + 06)	3.333E±00
8	8.643E-15 (5.959E-16)	3.333E + 02

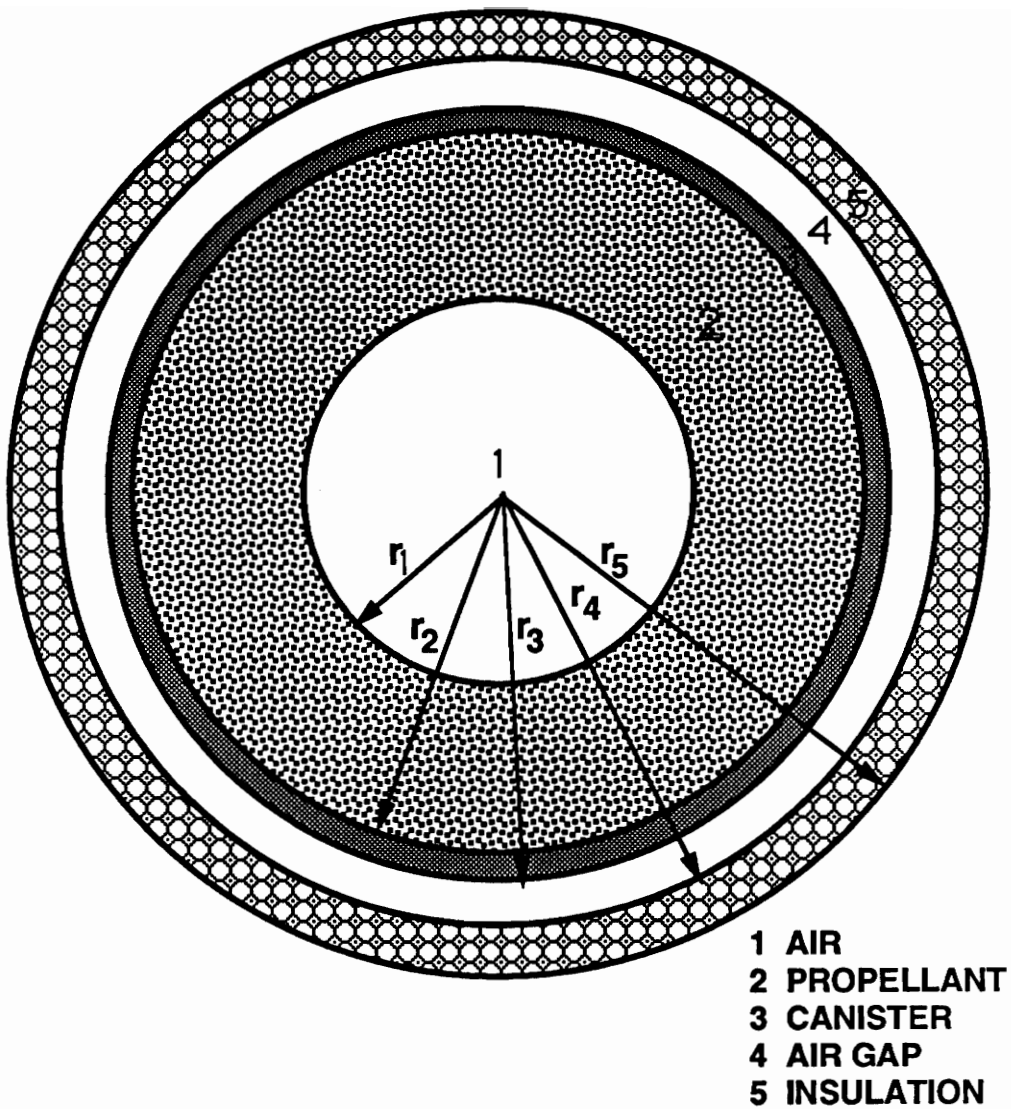


Fig. 4.1 Configuration of the solid propellant rocket motor

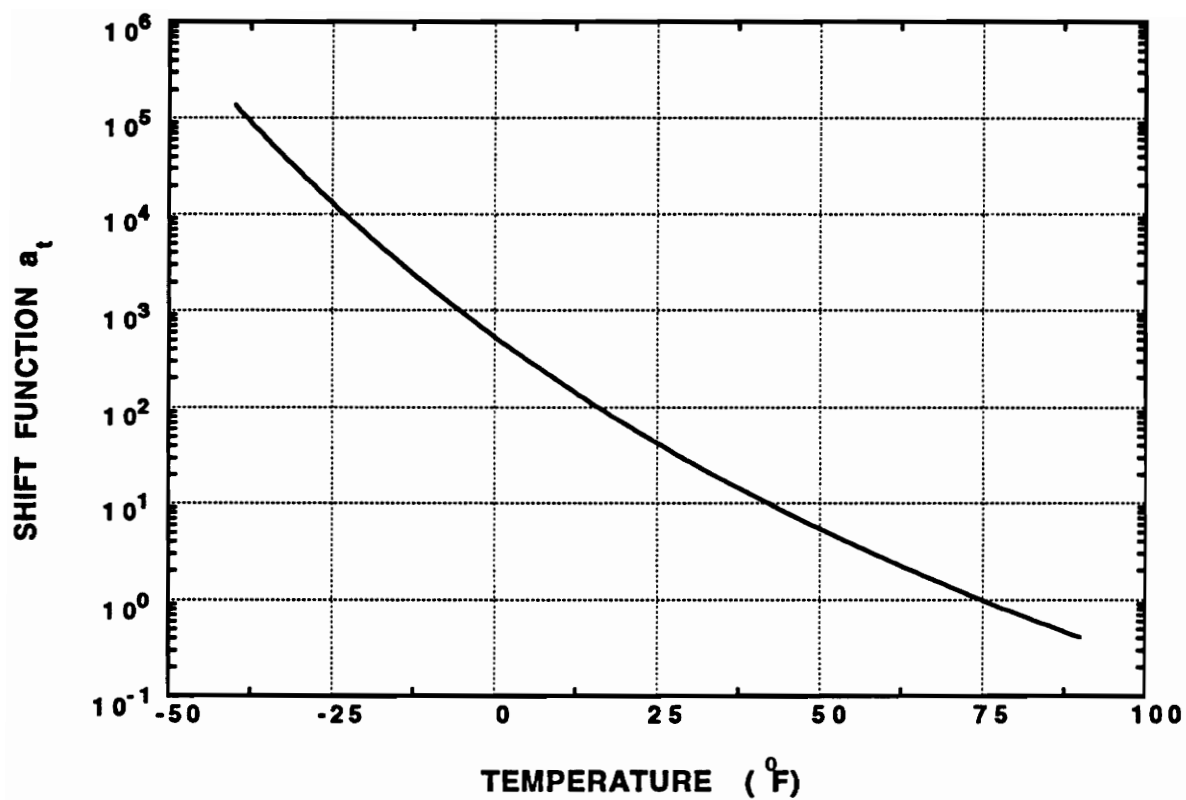
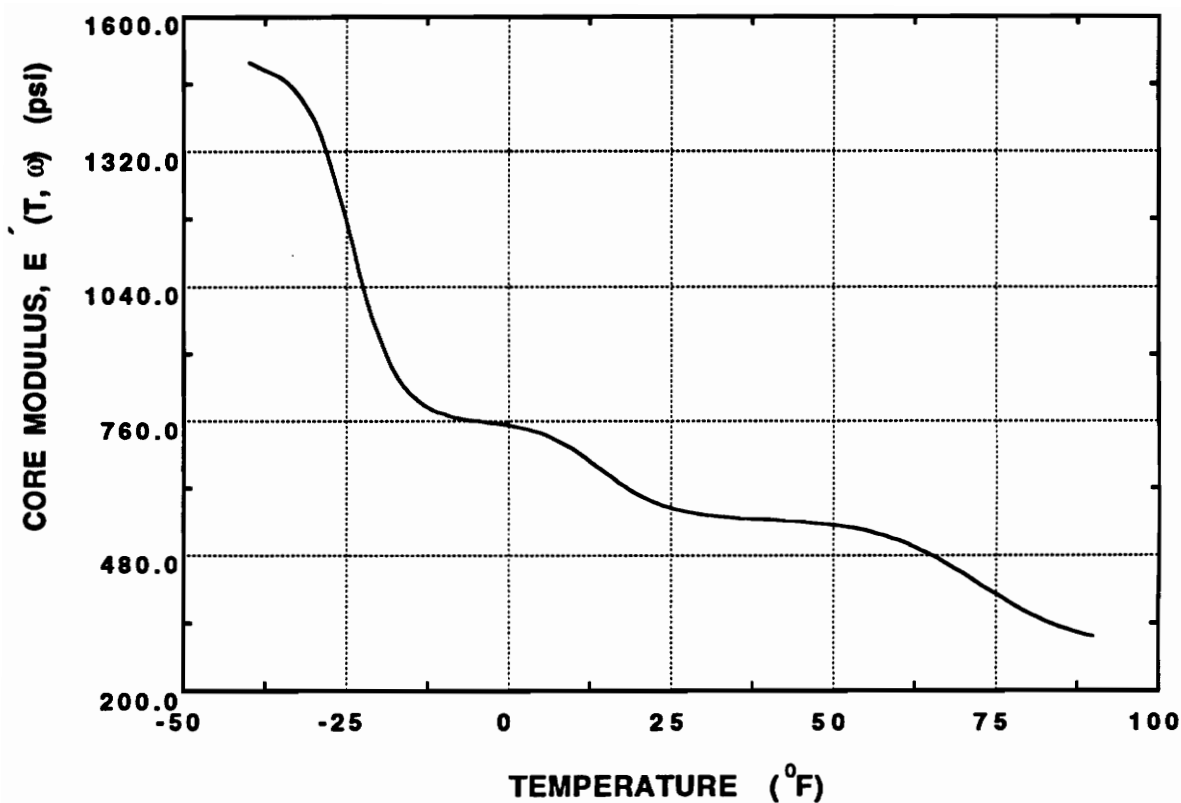


Fig. 4.2: The shift function of the core under consideration at different temperatures



**Fig. 4.3: Core modulus, $E(T, \omega)$, at different temperatures for daily frequency,
Note that the variation in the modulus is very high in the low temperature range which corresponds to Point Barrow, AK and low in the high temperature range which corresponds to Yuma, AZ.**

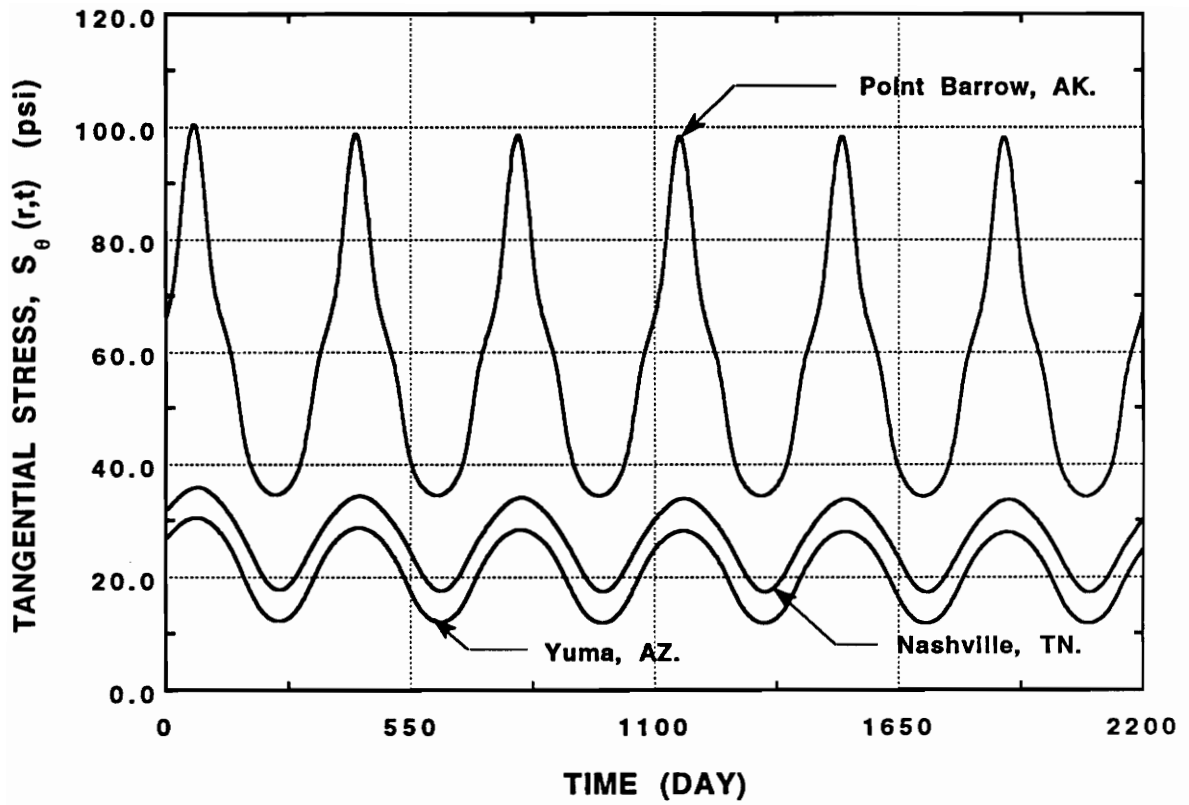


Fig. 4.4: Tangential stress, $S_{\theta}(r,t)$, at the bore due to cyclic temperature with time at different locations.

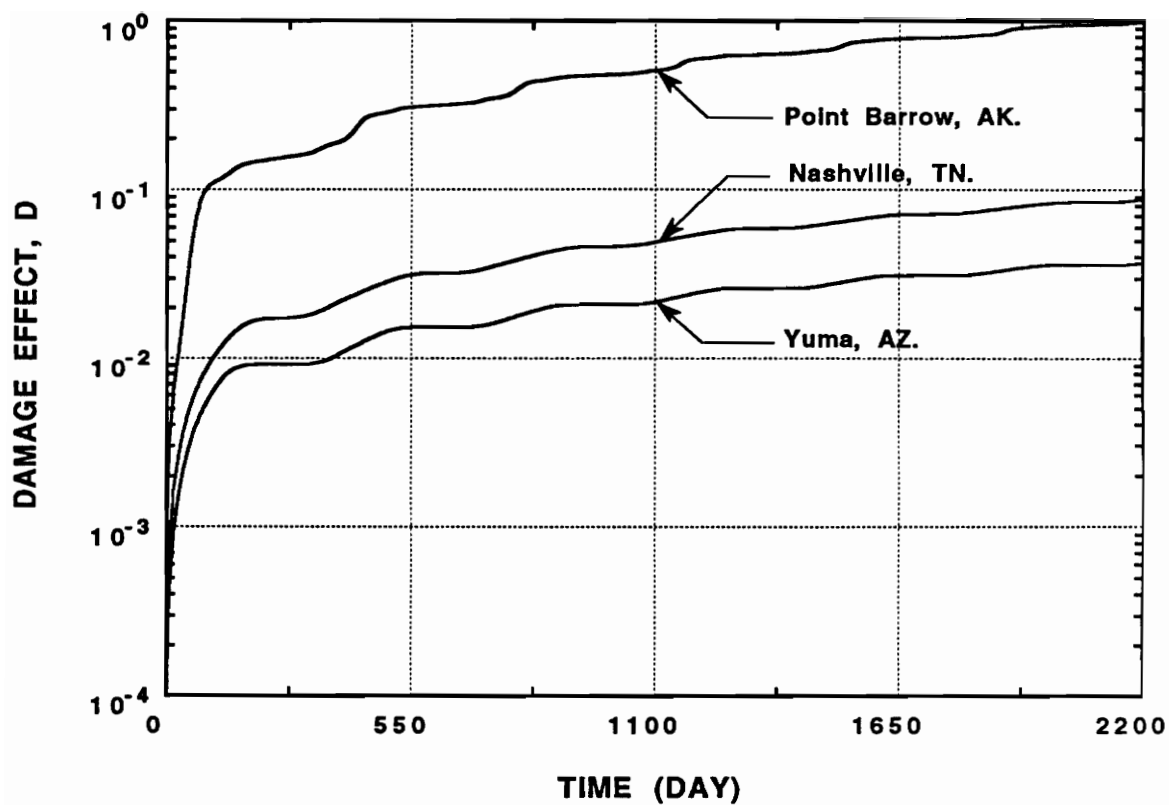


Fig. 4.5: The damage effect, D , on the strength of the core at different locations

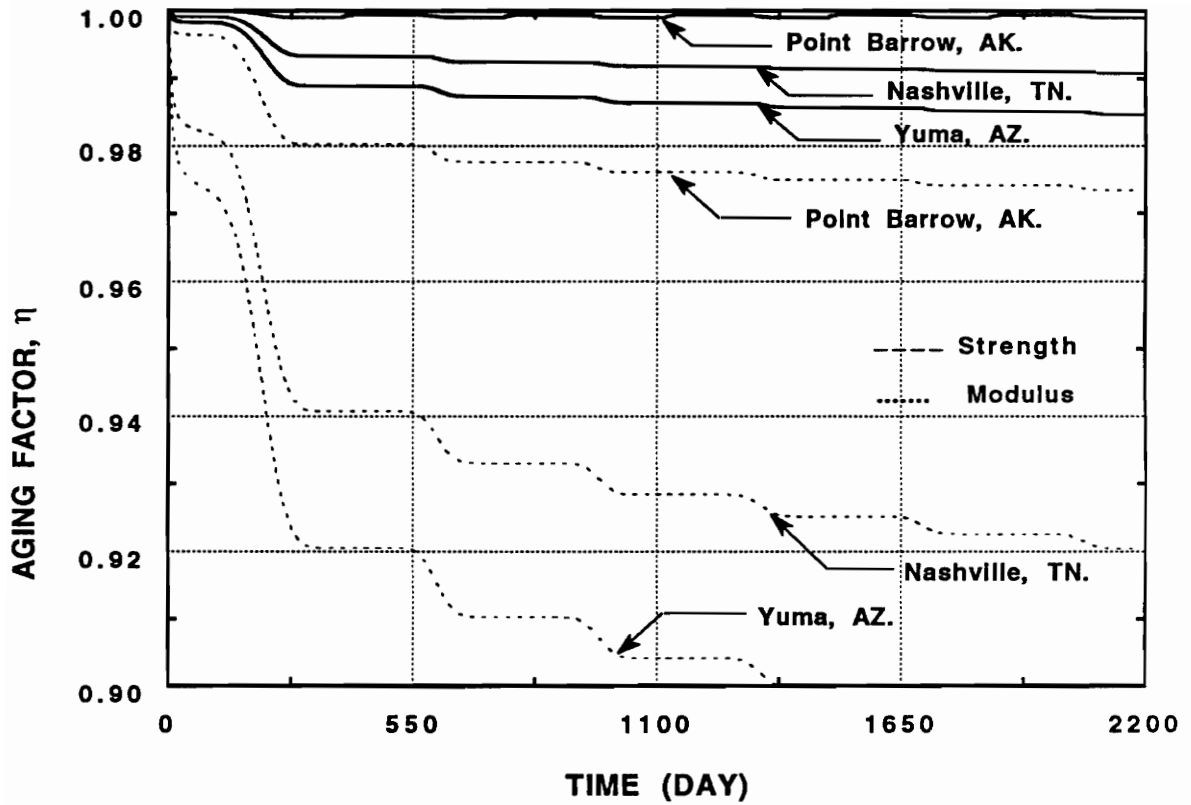


Fig. 4.6: Aging factor, η , with time at different locations

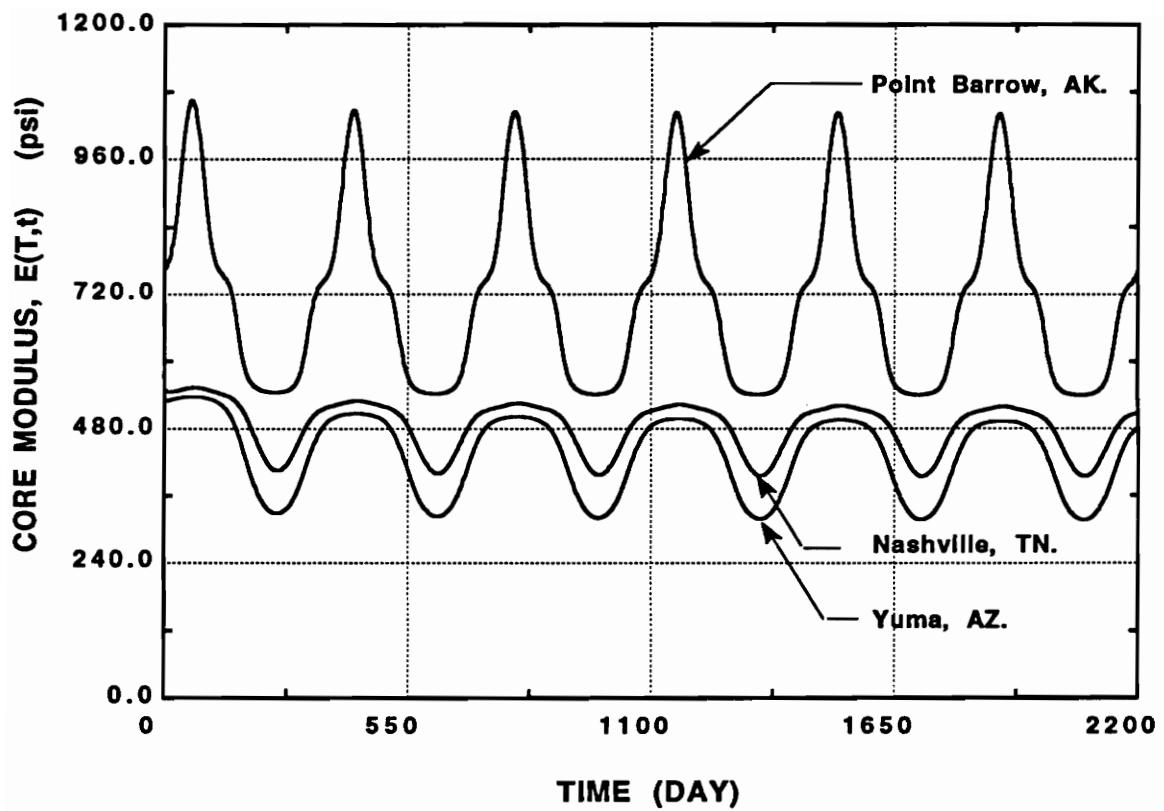


Fig. 4.7: Core modulus, $E(T,t)$ with time at different locations (aging effects are included); note that the change in the slope is due to high variation of the modulus at low temperature levels (see Fig. 4.3)

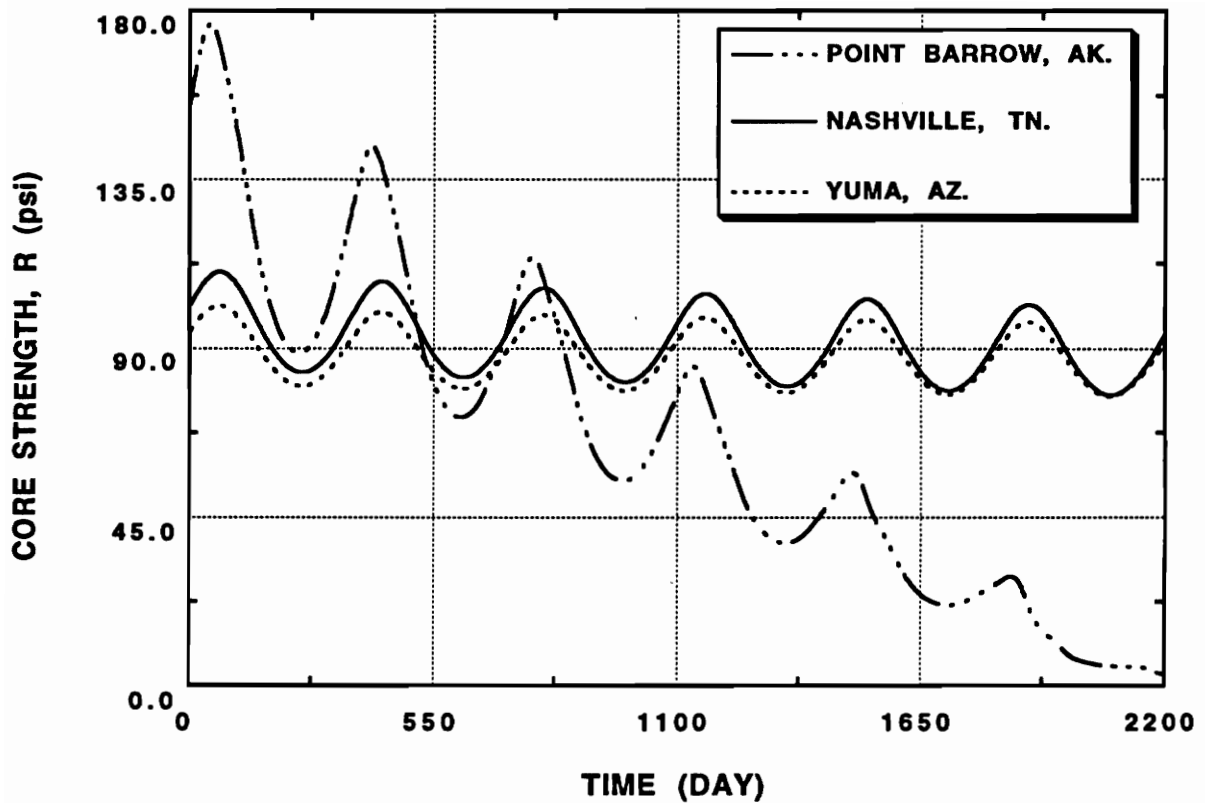


Fig. 4.8: Core strength, R, with time at different locations (aging and damage effects are included); note that the strength at Point Barrow, AK. becomes 0 after 2200 days, the same period in which damage effect is 1.

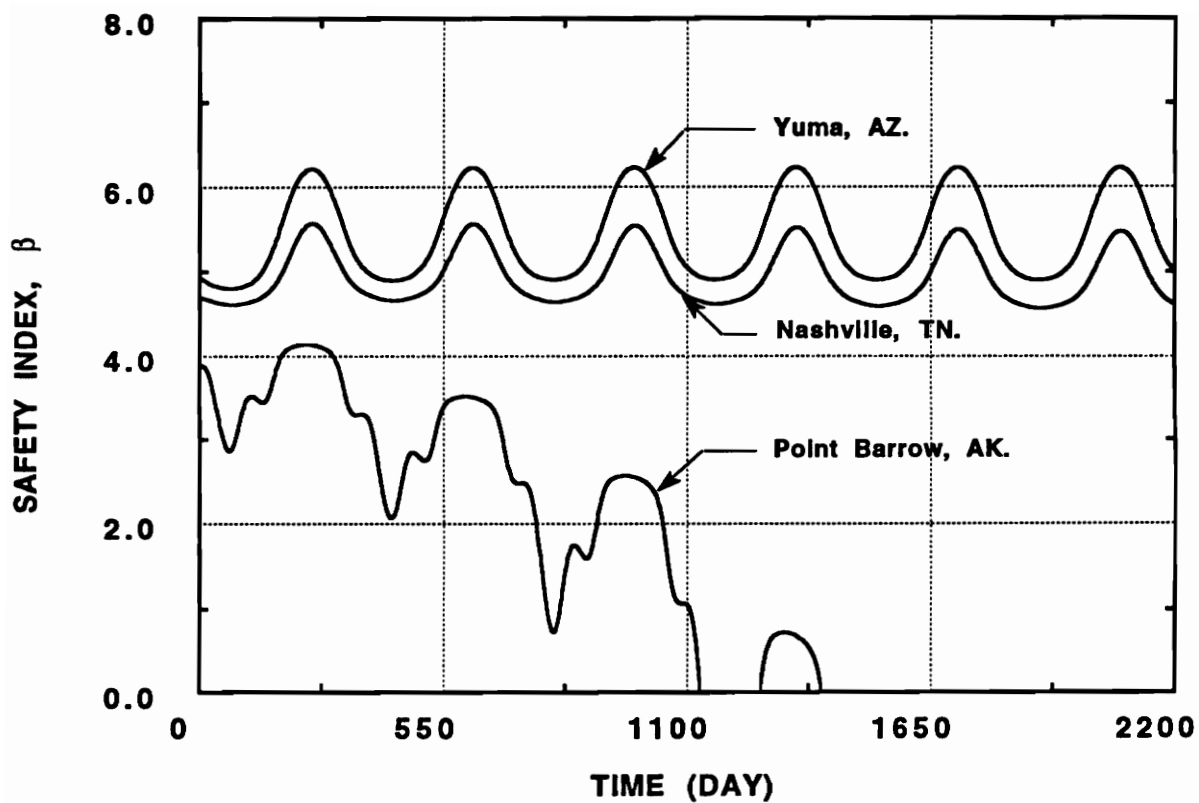


Fig. 4.9: Safety Index, β , with time at different locations, strength and modulus are Weibull, other variables are normal.

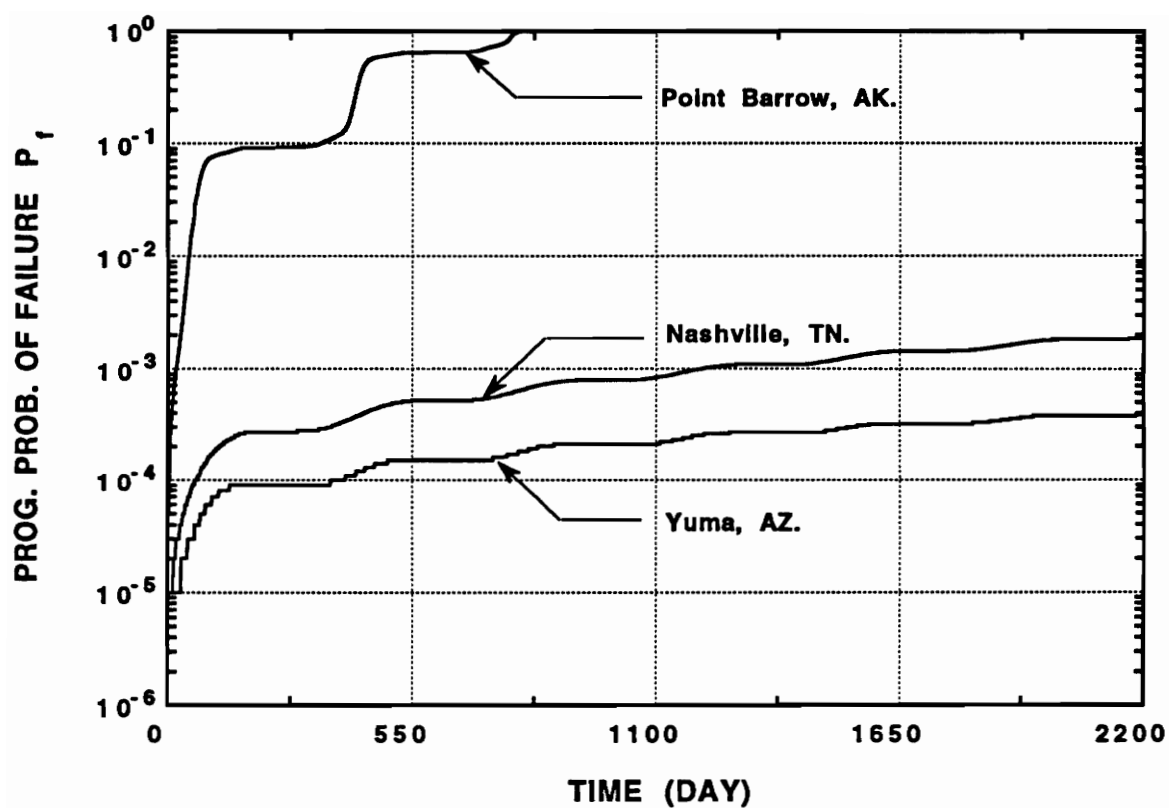


Fig. 4.10: Progressive probability of failure with time at different locations; strength and modulus are Weibull, other variables are normal

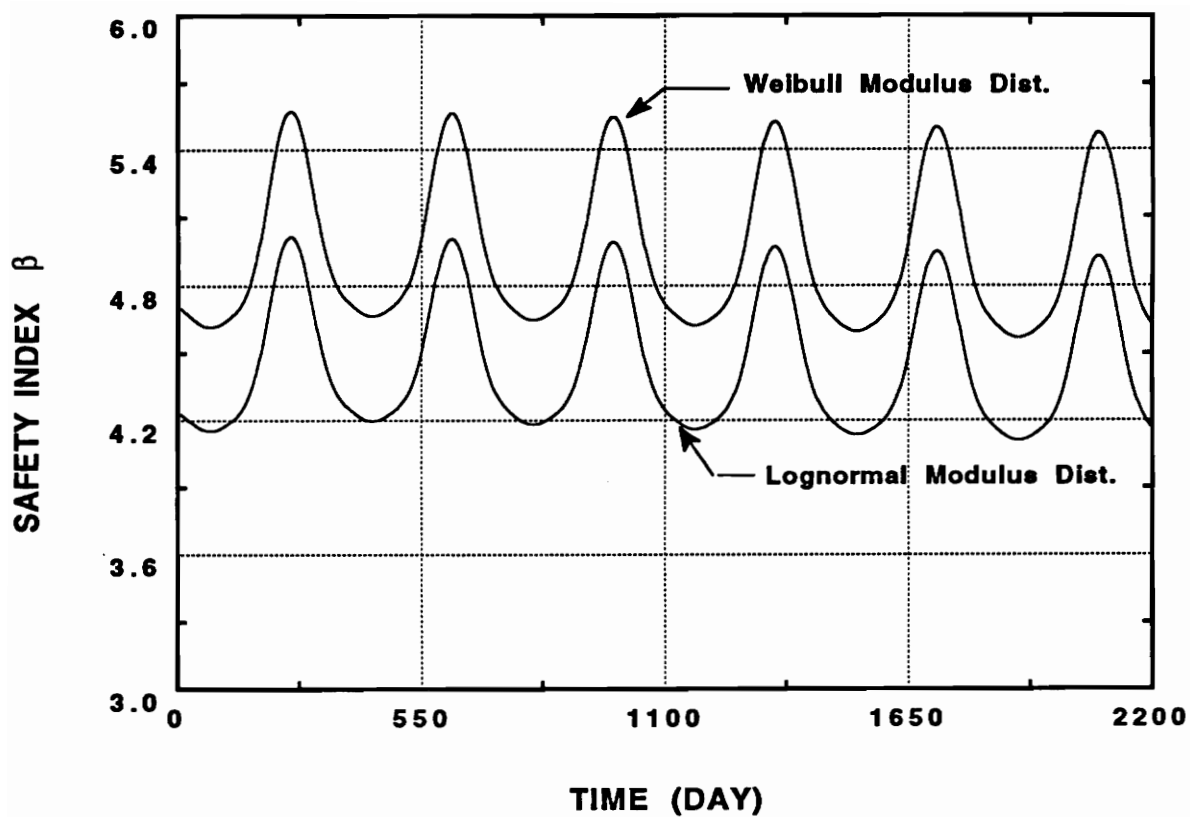


Fig. 4.11 Safety index, β , with time for Weibull and lognormal modulus distributions; strength is Weibull and other variables are normal.

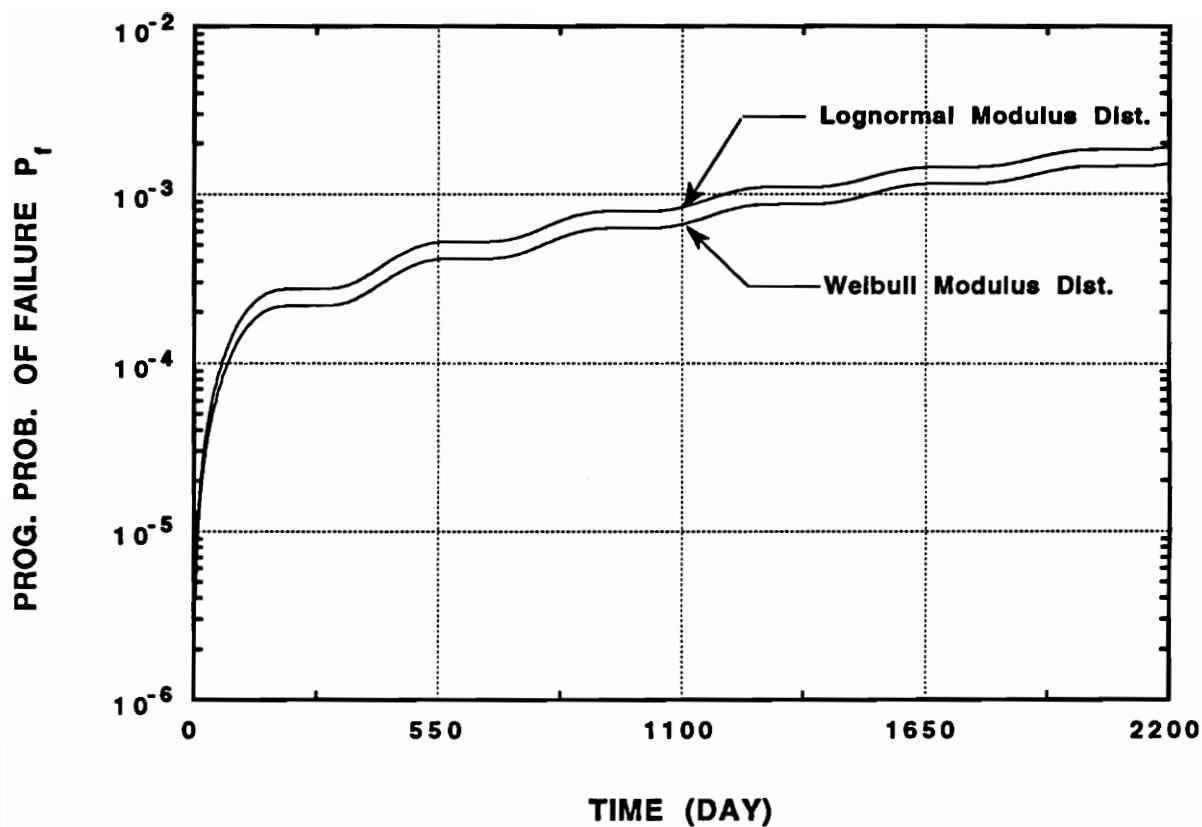


Fig. 4.12: Progressive probability of failure for Weibull and lognormal modulus distributions; strength is Weibull and other variables are normal

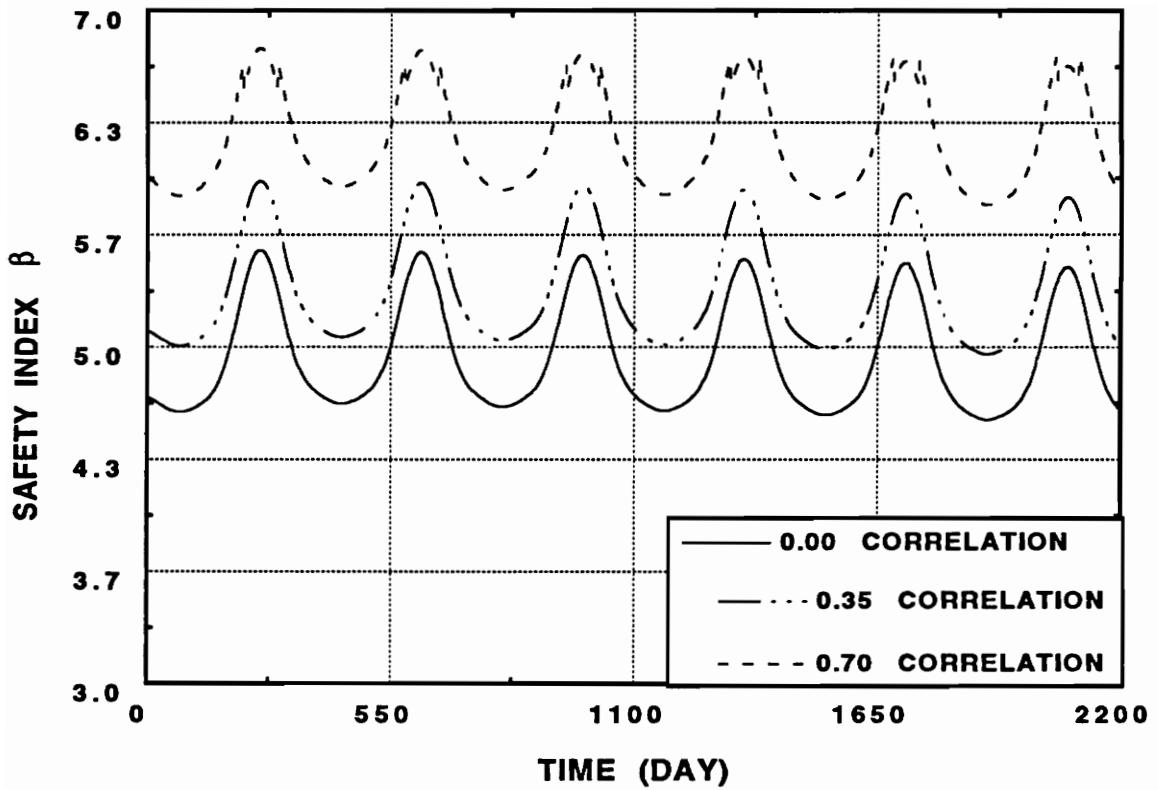


Fig. 4.13 Safety Index, β , with time at different levels of correlation at Nashville, TN.; strength and modulus are Weibull, other variables are normal

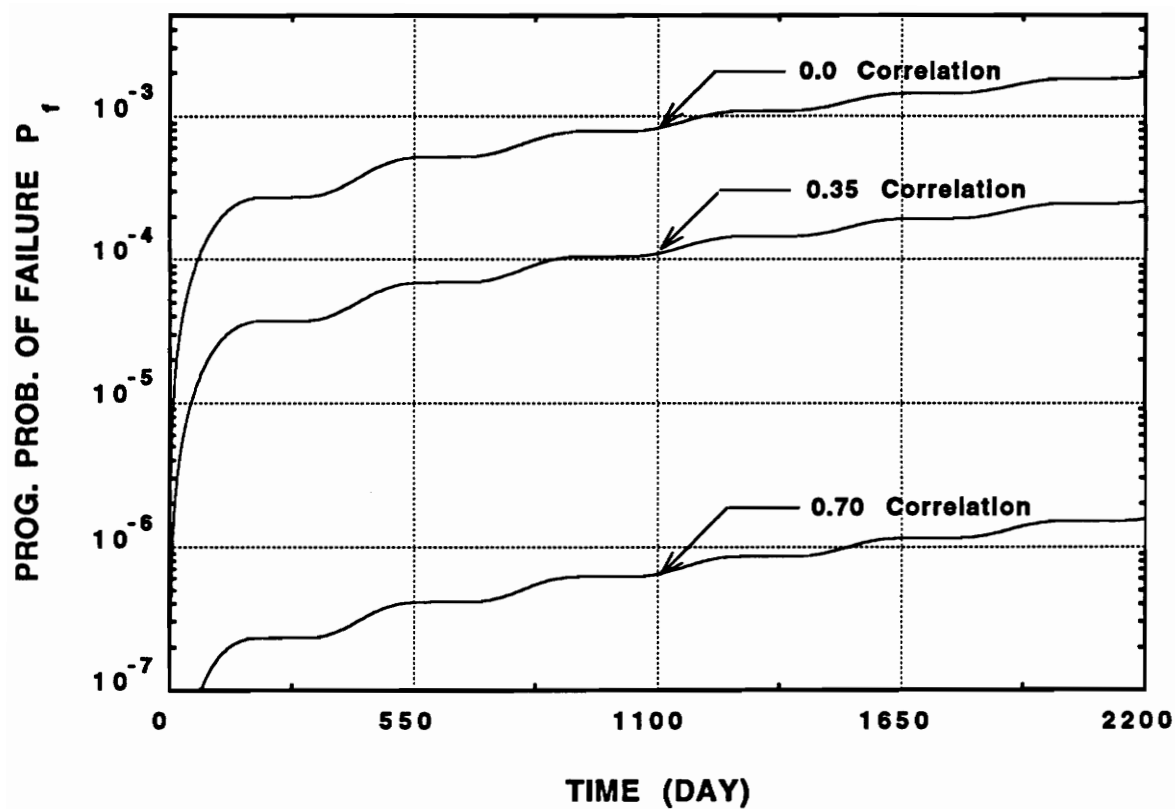


Fig. 4.14 Progressive probability of failure with time for different levels of correlation at Nashville, TN.; strength and modulus are Weibull, other variables are normal.

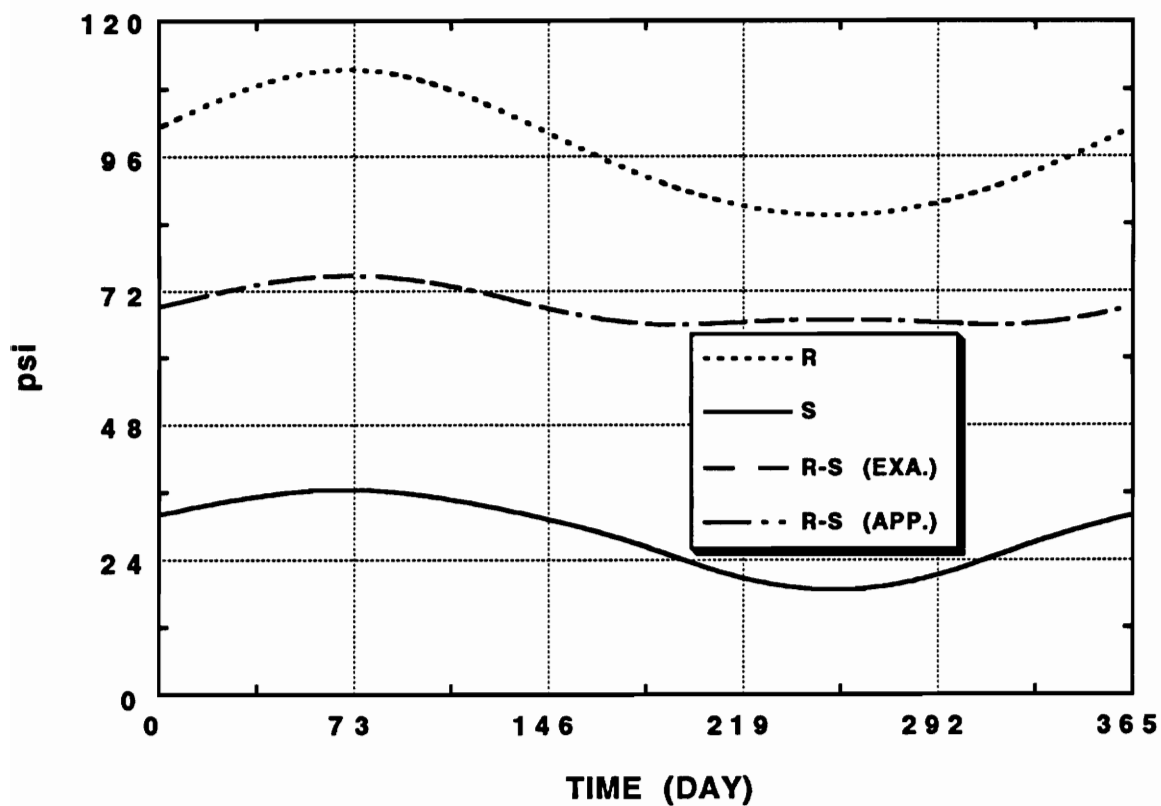


Fig. 4.15 Comparison between exact and approximate analyses in terms of (R-S); the two curves overlap

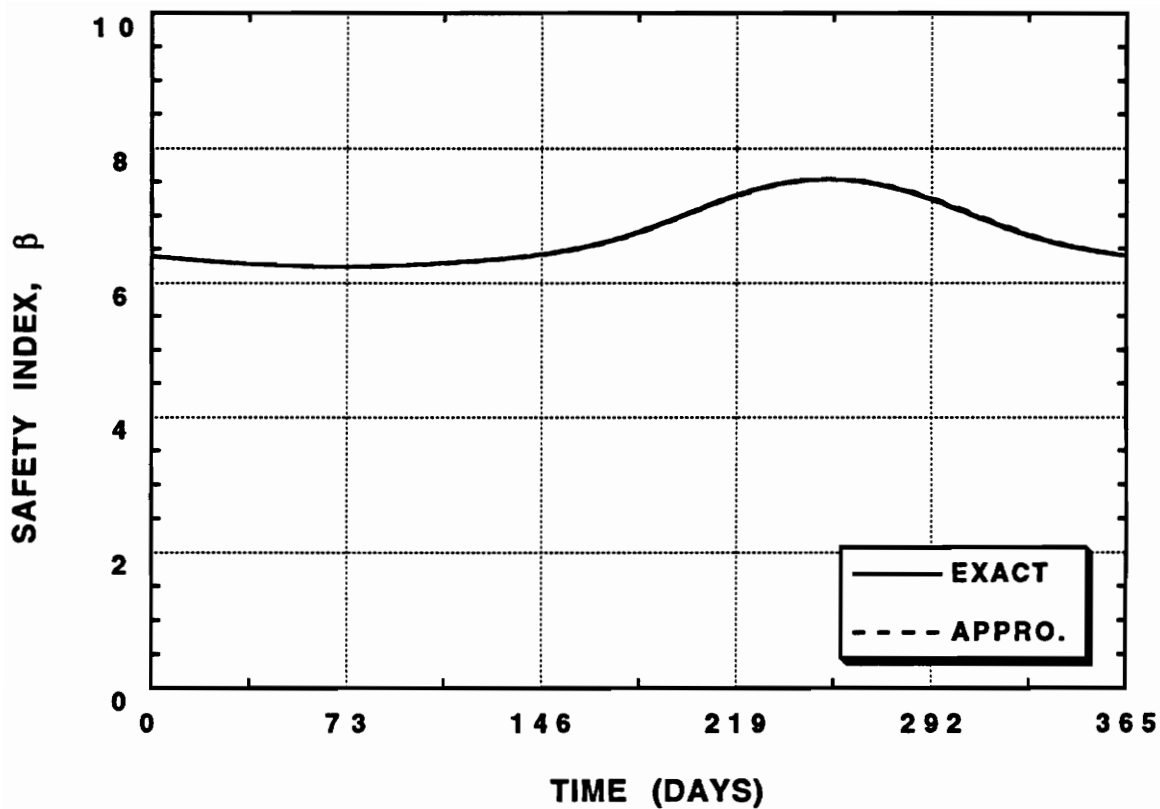


Fig. 4.16 The safety index based on exact analysis and polynomial approximation; the two solutions overlap

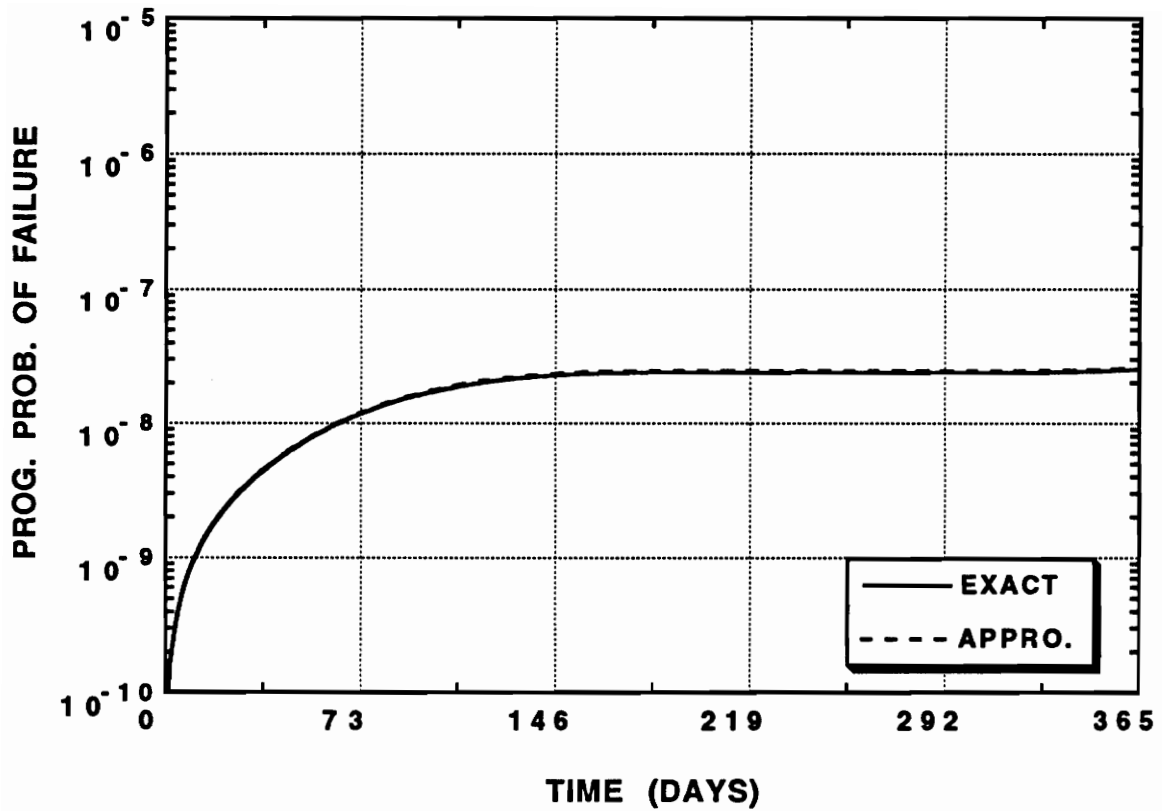


Fig. 4.17 Progressive probability of failure based on exact analysis and polynomial approximation; the two solutions overlap

Chapter V

RELIABILITY OF ROCKET MOTORS UNDER MECHANICAL LOAD

5.1 Introduction

Storing rocket motors under field conditions produces thermal stresses which have been investigated in the previous chapter. During storing or loading, however, rocket motors may be accidentally dropped or hit by an object. The stress distribution due to such cases can result in extensive damage and consequently in termination of the service life of the motor.

In this chapter, the reliability of rocket motors subjected to mechanical loadings will be investigated. All design parameters will be assumed random variables with correlation among some of them. Static and time-dependent loading with real time history will be considered. These loads will be treated as two opposite line loads, one patch load and one line load, especially in the case of impact loads. Response statistics such as

mean and standard deviation of stress and displacements will be computed and the efficiency of the sensitivity analysis will be demonstrated too.

Experiments have shown that failure of the motor occurs at the bore under this loading condition, i.e., the tangential stress at the bore exceeds the propellant strength. Therefore, the performance function is defined as $(R - S)$ where R is the propellant strength and S is the maximum tangential stress at the bore. Once the stress analysis is performed, the RSM method is applied to produce an analytical expression for the performance function followed by the FOSM analysis.

Stresses are analyzed with the aid of a finite element program [65] (MCYL1). Because no explicit performance function can be written in this case, the RSM method is used.

5.2 Probabilistic Finite Element Program

The finite element method is used in computing stresses and displacements. A deterministic finite element program (MCYL1) was developed by Heller and Lin [65] to perform the analysis and it will be extended to allow for probabilistic analysis. The deterministic finite element model was developed based on a mixed finite element formulation where stresses and displacements were treated as the unknown nodal values.

The deterministic finite element program will be converted to a probabilistic one based on the following steps:

1. Random design variables such as modulus, strength, Poisson's ratio, load parameters, inner radius, etc. are identified in terms of mean and standard deviation

2. A design matrix is obtained based on factorial design, where $2^p > n + 1$, $p = 4$ for $n = 8$ and $p = 5$ for $n = 11$
3. The performance function, G , is defined as $R - S$ with R the propellant strength and S the maximum tangential stress at the bore
4. The finite element program MCYL1 is called to perform the analysis at each data set to obtain the corresponding G value
5. The RSM is used to build a first order probabilistic model as a function of the random design variables defined in step 1
6. The sensitivity analysis is used to scan the variables and determine which variables should be retained in the probabilistic model
7. A fractional factorial design is built based on the retained variables
8. A central composite design is constructed as shown in 3.2.2
9. The finite element program MCYL1 is called again to perform the analysis at each data set
10. The RSM is used to build a second order performance function in terms of the retained variables
11. If response statistics are required, such as mean and standard deviation of stresses and displacements, G is replaced by that response quantity, Taylor's series expansion is used to compute the response statistics and further calculations are terminated; if reliability analysis is required, this step may be ignored
12. The FOSM is used to obtain the safety index β and, consequently, probability of failure and reliability; design points are obtained too
13. If the value of β obtained is large and for some special cases, step 9 is repeated with the design points obtained in step 12 used as new mean values of the variables; in this manner, an increment for β is obtained

14. The process may be repeated until the increment of β goes to zero (normally after two trials)

A flow chart has been developed based on the above steps and is shown in Fig. 5.1 for this case. Any available deterministic finite element program is used as a subroutine in the main algorithm and each data set can be run separately. This makes the developed technique efficient because it can handle problems where only execution codes are available and there is no way to access the structure of these codes, such as is the case for ABAQUS. In fact, all the probabilistic finite element programs that have been used in this work (chapters V and VI) are and will be developed based on this flow chart.

5.3 Rocket Motor Loaded by Static Line Loads

A rocket motor subjected to two line loads (Fig. 5.2) is examined. Geometrical and mechanical properties are given in Table 5.1. In this case the reliability curve is required as a function of the applied load for different mean strength values.

Fig. 5.3 represents the tangential stress at the bore as a function of the applied load. Fig. 5.4 shows the performance function ($R - S$) as a function of the applied load for different strength values. Fig. 5.5 presents the safety index, β , with load for different strength values; the high safety index curve corresponds to high values of strength. Fig. 5.6 represents the reliability of the motor with load for different strength values, where high reliability corresponds to high safety index and high strength value. For a constant strength, the reliability of the motor decreases as load increases.

As a good check of the results, consider the fact that when strength and stress are equal, the reliability is equal to 0.5. This can be proven by the results in Fig. 5.6 and

Fig. 5.3. In Fig. 5.6 the applied load corresponding to 0.5 reliability can be obtained for each curve. Then these load values can be entered into Fig. 5.3 to obtain the corresponding stress value. These stresses will be equal to the strength from which the load is obtained, i.e., stress and strength are equal.

5.4 Rocket Motors Loaded by Patch Loads.

The motor of section 5.3 is analyzed under the action of a line load and a patch load combination as shown in Fig. 5.7. Static as well as dynamic loads are considered, the dynamic load is applied over a short period of time to represent impact. The FEM code (MCYL1) used above is used for the static and dynamic responses such as stresses and displacements. The RSM is applied to predict the mean and standard deviation for any response quantity. Then the RSM with FOSM is used to obtain the reliability and the progressive probability of failure of the motor.

5.4.1 Static Loads

Fig. 5.8 presents the mean and standard deviation of the radial displacement with load at the interface under the load. In Fig. 5.9 the mean and the standard deviation of the tangential stress is plotted at the same location. Utilizing the RSM and FOSM, the safety index with load is presented in Fig. 5.10 for different propellant strengths. In Fig. 5.11 the safety index is plotted for different coefficients of variation, while in Fig. 5.12 the probability of failure is plotted based on these safety indices.

5.4.2 Impact Patch Loads

Patch loads are applied to the motor of section 5.3 as functions of time, shown in Fig. 5.13. Because the total duration of the load is 5 msec it is considered to be an impact. The mean and the standard deviation of the radial displacement at the interface and the tangential stress at the bore are computed under the action of random impact load as functions of time (Figs. 5.14 and 5.15). The safety index with time for different strength values is presented in Fig. 5.16, and the progressive probability of failure is computed for this case and plotted in Fig. 5.17. The safety index and the progressive probability of failure are computed also for different coefficients of variation as functions of time (Figs. 5.18 and 5.19). In this analysis the load-time function used is a half sine wave.

5.4.3 Experimental Impact Loads

In a parallel experimental investigation of the effect of impact loads on motor segments, a drop tester is used for tests on 4 in. long, inert propellant filled cylinders. The equipment consists of a 10.5 lbs drop-weight with an instrumented, $\frac{3}{4}$ in. diameter spherical impactor. The cylinders have the dimensions shown in Fig. 5.2. Their dynamic mechanical properties have been computed from Eqs. 4.11-4.15 and are given in Table 5.2.

The drop tester measures the impact force and the velocity of the impactor as functions of time and automatically plots these variables in addition to the displacement of the tup and the impact energy also as functions of time.

A typical set of such curves is presented in Figs. 5.20 and 5.21 for a drop height of 20 in. and a maximum energy of 17.14 ft-lbs. As seen in Fig. 5.20, the load-time trace is not sinusoidal and reaches a maximum value of 992 lbs.

This load-time history is used in a digitized form as an input first to the finite element analysis (MCYL1) and then in the RSM reliability analysis.

The experimental results and finite element results are compared in terms of the radial displacements under the load and are shown in Fig. 5.22 for a load duration of 10 msec. Fig. 5.23 represents the tangential stress with time at the bore for the same energy level.

A reliability analysis is performed based on the developed technique for different energy levels. The safety index β is computed as a function of energy levels for different coefficients of variation. The results shown in Fig. 5.24 and Fig. 5.25 represent β and the reliability of the motor as functions of energy levels.

Specimens subjected to drop tests were dissected. A close examination indicated that in the majority of cases cracks originated at the bore and propagated radially under the influence of circumferential stresses. In some specimens, however, cracks developed near the interface (bond line) and traveled in the circumferential direction under the influence of radial tension stresses.

A stress analysis indicated that radial stresses in this region vary from compression directly under the load (0°) to tension around 30° from the loading direction and back to compression again at right angles to the load. Fig. 5.26 taken from reference [66] shows the variation of radial stress around the circumference of the cylinder.

Tangential stresses at the bore and radial stresses near the bond line at various angles from the loading direction are presented in Table 5.3. It is seen that tangential bore stresses are considerably higher than radial bond-line stresses and consequently cracks

at the bond-line are expected to initiate only when some imperfections are present in the material. This fact has been observed in the experiments.

5.5 Application of Sensitivity Analysis and Correlated Variables

5.5.1 Application of Sensitivity Analysis

To demonstrate the efficiency of the sensitivity analysis, three more variables with 10% coefficients of variation are assumed to be random, bringing the total number of random design variables to 11 which, are

- x_1 = applied patch load
- x_2 = propellant modulus
- x_3 = case modulus
- x_4 = Poisson's ratio of propellant
- x_5 = Poisson's ratio of case
- x_6 = density of propellant
- x_7 = density of case
- x_8 = propellant strength
- x_9 = inner radius
- x_{10} = half angle range of the patch load
- x_{11} = half angle range of the line load

A first order G function is constructed based on RSM in terms of all the above variables. The sensitivity analysis described in section 3.2.4 is performed to determine which variable must be retained in the probabilistic model, and the results are shown in Table 5.4. It is clear that x_4 , x_5 , x_6 , x_7 and x_{11} are insignificant with respect to the other variables; therefore, these 5 variables are removed from the probabilistic model.

In order to prove the accuracy of the sensitivity analysis, the FOSM is applied to the first order G function obtained above and a similar polynomial is constructed based

on the 6 retained variables to which the FOSM is again applied. A comparison between the two solutions is made in terms of the safety index, β , the probability of failure, P_f , the reliability, R_i , and the design points. The comparison is shown in Table 5.5 where a good agreement is obtained. A second order G function is constructed also in terms of the 6 retained variables. A ($\frac{1}{2}$ of $2^6 + 12 + 1$) number of points instead of ($\frac{1}{8}$ of $2^{11} + 22 + 1$) are used, resulting in the same accuracy; the finite element code is evaluated 45 times instead of 278 times.

According to the results in Table 5.4, 4 out of the 8 original random variables are significant and must be retained in the probabilistic model. The RSM is applied to construct a second order G function, then the FOSM is used to obtain β , P_f , R_i and the design points. This is performed based on 4 and 8 random variables and the comparison is shown in Table 5.6.

5.5.2 Application of Correlated Variables

Four random variables are found to be significant, the patch load (x_1), the propellant modulus (x_2), the case modulus (x_3) and the propellant strength (x_4). It has been found that propellant modulus, x_2 , and strength, x_4 , are correlated random variables, since both are time and temperature dependent. The RSM in conjunction with FOSM for correlated variables is applied to obtain β , P_f , R_i and the design points for correlation coefficients, ρ_{24} , of 0.0, 0.4 and 0.8 (Table 5.7).

To increase the accuracy of the solution, the G function for 0.0 and 0.4 correlation coefficient is re-evaluated using the design points as the new mean values. An incremental value for β is computed and added to the previous one. New values for

β , P_f , R_i and design points are obtained and are shown in the same table. Because β is small, the re-evaluation of G does not change these values significantly.

5.6 Conclusions

Reliability of motors subjected to static and impact loads was calculated, using the developed technique, for two different loading conditions: two opposite line loads and patch-line load combinations. Response statistics such as the mean and the standard deviation of stresses and displacements were calculated too.

The efficiency of the sensitivity analysis was demonstrated by considering all random variables and obtaining the same safety index when insignificant ones are considered as deterministic. This will reduce the computations by a significant amount. Correlated variables were tested and it was found that the assumption of correlation between propellant strength and modulus will increase the safety index and consequently the reliability of the motors.

The technique uses an available deterministic computer code as a subroutine. This allows the extension of all available finite element codes or any other numerical codes to be adapted to a probabilistic analysis.

A computer program entitled ROCKT3 has been developed [67] for the calculation of reliabilities of rocket motors under mechanical loadings.

Table 5.1. Design variables for line and patch loaded motors

Variable	Mean	Coefficient of variation δ
Propellant		
Strength R (psi)	25.0 to 100.0	0.10
Modulus E_p (psi)	281.0	0.10
Poisson's ratio ν_p	0.49	0.005
Density ρ_p (lb/in ³)	0.0623	0.10
Case		
Modulus E_c (psi)	2.0 E + 06	0.10
Poisson's ratio ν_c	0.30	0.10
Density ρ_c (lb/in ³)	0.0600	0.10
Applied load		
P(lb)	1 to 200	0.10

Table 5.2 Design variables for impact loads

Variable	Mean	standard deviation	Coefficient of variation δ
E (propellant) (psi)	1076	107.6	0.10
R (propellant) (psi)	319	31.9	0.10
	319	63.8	0.20
E (case) (psi)	3.0E + 06	3.0E + 05	0.10

Table 5.3 Radial stress at the interface for different angular locations compared with maximum tangential stress at the bore under the load

location θ°	radial stress at interface psi	Max. tangential stress at bore psi
0	-160	280
30	75	
45	46	
90	-40	

Table 5.4 Sensitivity analysis based on 11 variables

Coefficient	Value	t Value	PRF
intercept	0.66824937E + 02	0.49196245E + 02	0.00000102
x_1	-0.25307438E + 02	-0.18631232E + 02	0.00004885
x_2	-0.13999063E + 02	-0.10306053E + 02	0.00050004
x_3	0.13222188E + 02	0.97341203E + 01	0.00062375
x_4	-0.30398125E + 01	-0.22378975E + 01	0.08882885
x_5	-0.79043750E + 00	-0.58191685E + 00	0.59184263
x_6	0.13005625E + 01	0.95746879E + 00	0.39255109
x_7	-0.24643750E + 00	-0.18142628E + 00	0.86485538
x_8	0.31354938E + 02	0.23083377E + 02	0.00002087
x_9	-0.88980625E + 01	-0.65507172E + 01	0.00280780
x_{10}	-0.23738563E + 02	-0.17476233E + 02	0.00006294
x_{11}	-0.13256875E + 01	-0.97596571E + 00	0.38434388

Table 5.5 Comparison between 6 and 11 random variables as a result of sensitivity analysis

No. of random variables	safety index β	Reliability R_i	Prob. of failure P_f	
11 (1st order G)	1.29801	0.9028576500E+00	0.9714235000E-01	
6 (1st order G)	1.30271	0.9036628641E+00	0.9633713590E-01	
6 (2nd order G)	1.24774	0.8939373171E+00	0.1060626829E+00	

Variable	Mean value	Design value 11 r. v. 1st order	Design value 6 r.v. 1st order	Design value 6 r.v. 2nd order
x_1	-0.28590E+06	-0.30414E+06	-0.30418E+06	-0.30379E+06
x_2	0.10767E+04	0.11147E+04	0.11137E+04	0.11136E+04
x_3	0.30000E+07	0.29000E+07	0.28970E+07	0.28905E+07
x_4	0.49000E+00	0.49019E+00	0.49000E+00	0.49000E+00
x_5	0.30000E+00	0.30060E+00	0.30000E+00	0.30000E+00
x_6	0.62300E-01	0.62096E-01	0.62300E-01	0.62300E-01
x_7	0.60000E-01	0.60037E-01	0.60000E-01	0.60000E-01
x_8	0.31946E+03	0.29421E+03	0.29399E+03	0.29655E+03
x_9	0.75000E+00	0.76683E+00	0.76647E+00	0.76660E+00
x_{10}	0.10000E+01	0.10599E+01	0.10605E+01	0.10593E+01
x_{11}	0.10000E+01	0.10033E+01	0.10000E+01	0.10000E+01

Table 5.6 Comparison between 4 and 8 random variables as a result of sensitivity analysis

No. of random variables	safety index β	Reliability R_i	Prob. of failure P_f
8 (2nd order G)	1.45135	0.9266592171E+00	0.7334078289E-01
4 (2nd order G)	1.45864	0.9276683596E+00	0.7233164038E-01

Variable	Mean value	Design value 8 r. v.	Design value 4 r. v.
x_1	-0.28590E+06	-0.30939E+06	-0.30959E+06
x_2	0.10767E+04	0.11250E+04	0.11254E+04
x_3	0.30000E+07	0.28533E+07	0.28520E+07
x_4	0.49000E+00	0.49034E+00	0.49000E+00
x_5	0.30000E+00	0.29943E+00	0.30000E+00
x_6	0.62300E-01	0.62300E-01	0.62300E-01
x_7	0.60000E-01	0.60000E-01	0.60000E-01
x_8	0.31946E+03	0.28797E+03	0.28763E+03

Table 5.7 Reliability analysis for different levels of correlation

Corr. coeff. ρ_{24}	safety index β	Reliability R_i	Prob. of failure P_f	
0.0(1st time)	1.45864	0.9276683596E+00	0.7233164038E-01	
0.0(2nd time)	1.48401	0.9310967550E+00	0.6890324400E-01	
0.4(1st time)	1.60376	0.9456162171E+00	0.5438378289E-01	
0.4(2nd time)	1.69604	0.9550608270E+00	0.4493917000E-01	
0.8	1.81678	0.9653743731E+00	0.3462562693E-01	

Variable	x_1	x_2	x_3	x_4
Mean value	-0.28590E+06	0.10767E+04	0.30000E+07	0.31946E+03
Design value				
0.0 1st time	-0.30959E+06	0.11254E+04	0.28520E+07	0.28763E+03
0.0 2nd time	-0.31008E+06	0.11263E+04	0.28496E+07	0.28717E+03
0.4 1st time	-0.31417E+06	0.10863E+04	0.28180E+07	0.28827E+03
0.4 2nd time	-0.31614E+06	0.10692E+04	0.28085E+07	0.28683E+03
0.8	-0.32170E+06	0.10272E+04	0.27578E+07	0.28984E+03

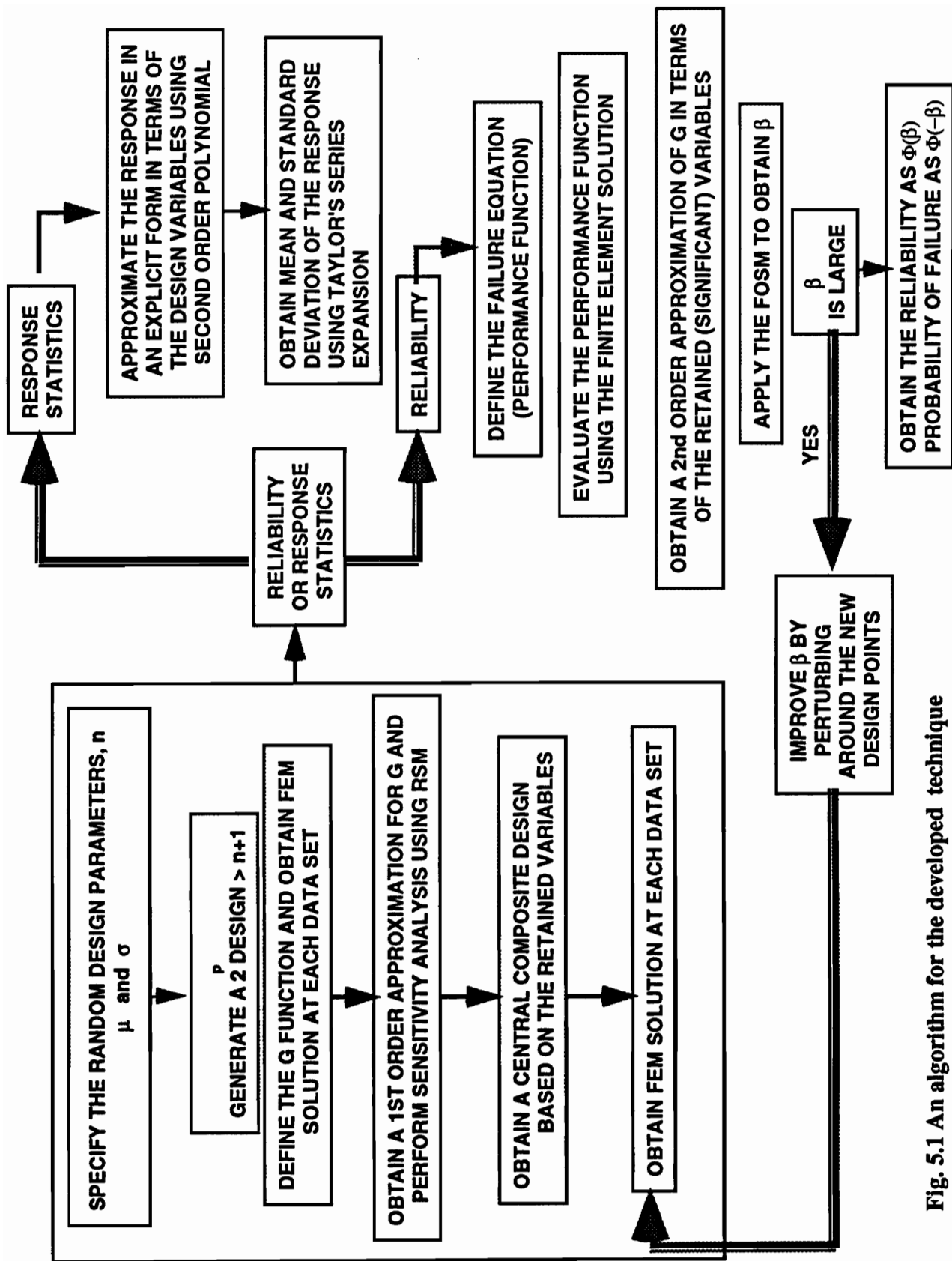


Fig. 5.1 An algorithm for the developed technique

MOTOR UNDER LOADING

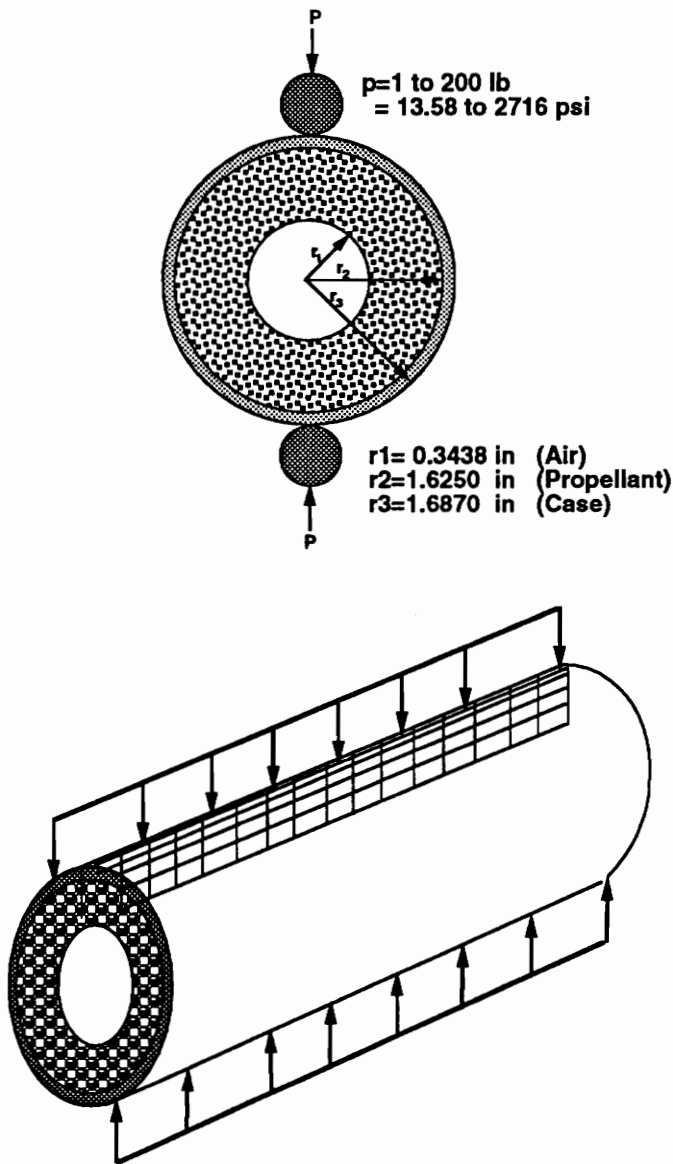


Fig. 5.2 Motor under two opposite line loads

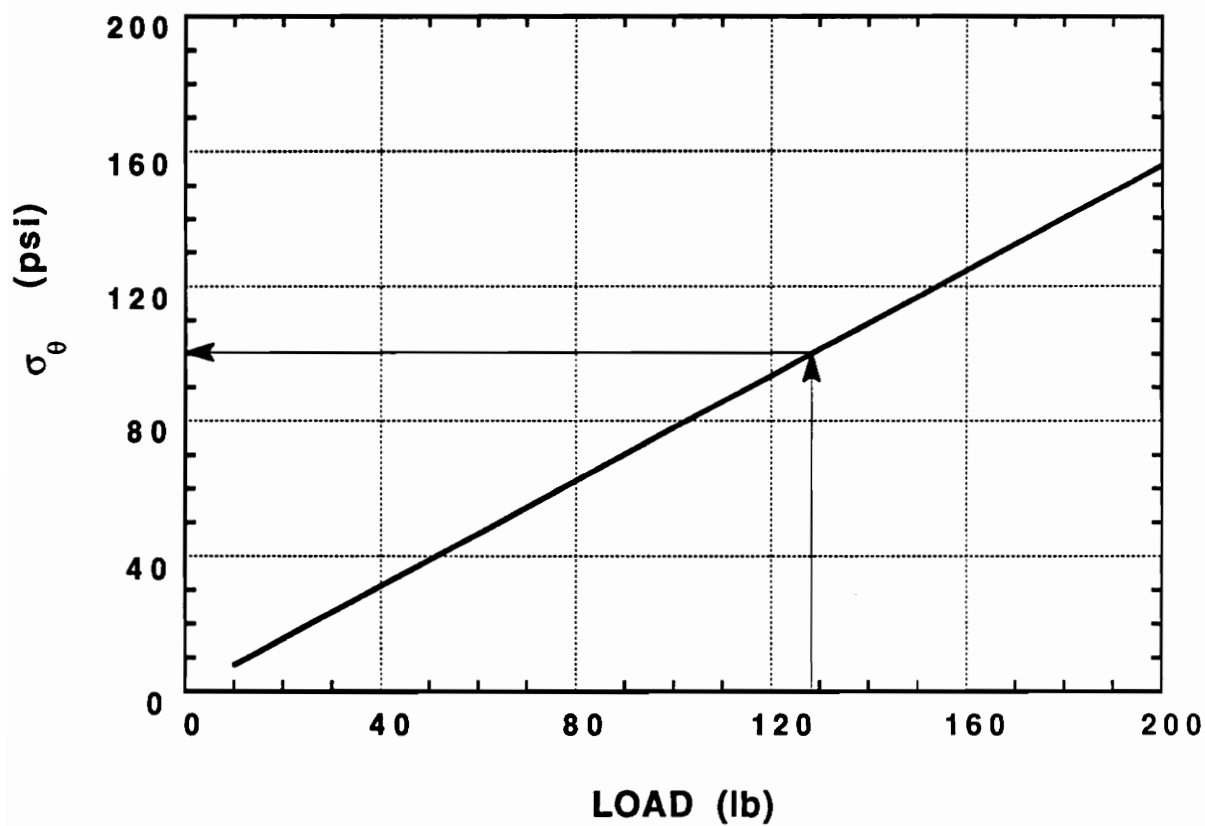


Fig. 5.3 Tangential stress at the bore with load

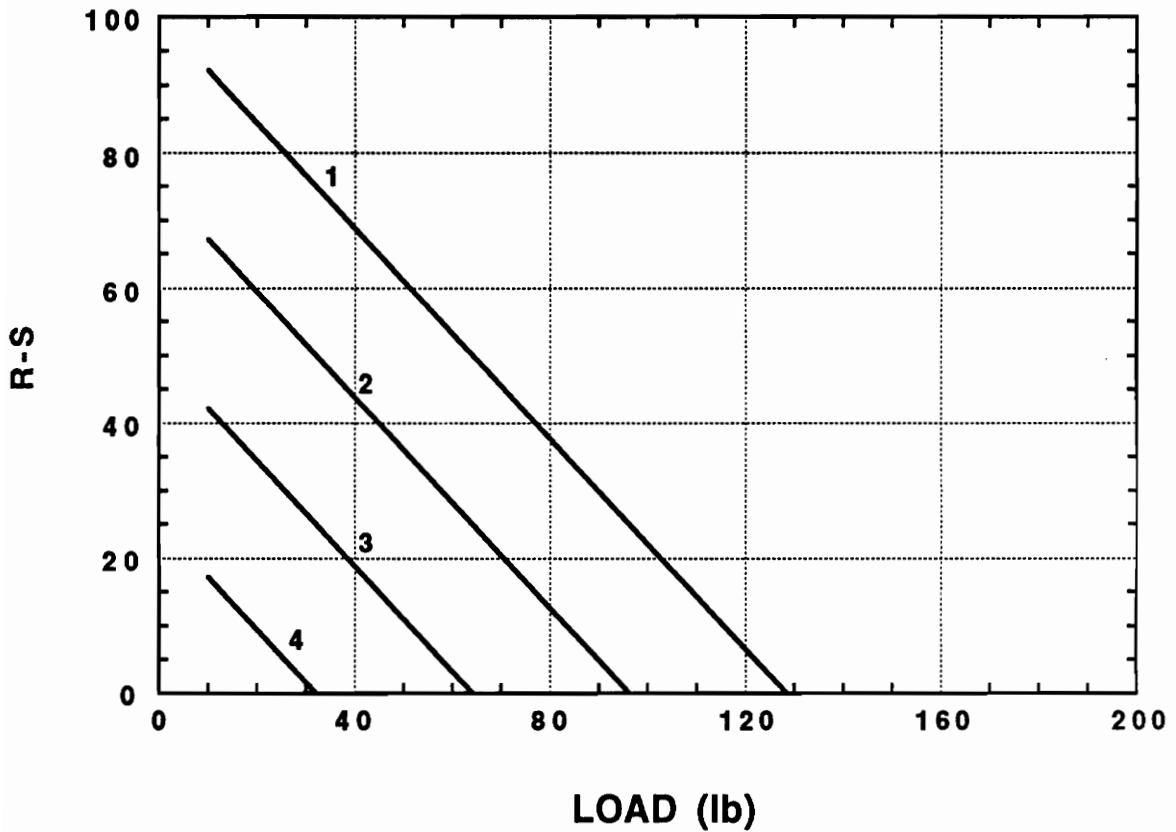


Fig. 5.4 Response (R-S) with load for different mean strength values:

- (1) Propellant strength = 100.0 psi , (2) 75.0 psi
 (3) 50.0 psi , (4) 25.0 psi

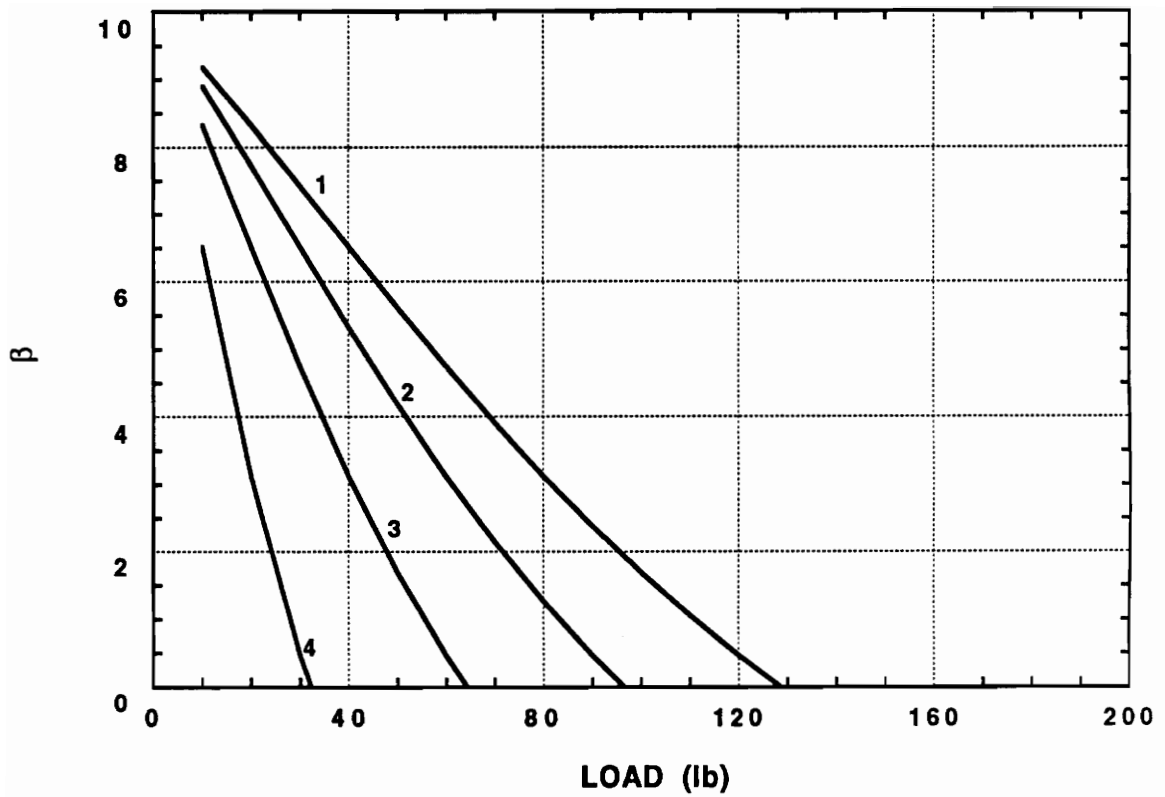


Fig. 5.5 Safety index with load for different mean strength values:

- (1) Propellant strength = 100.0 psi , (2) 75.0 psi
 (3) 50.0 psi , (4) 25.0 psi

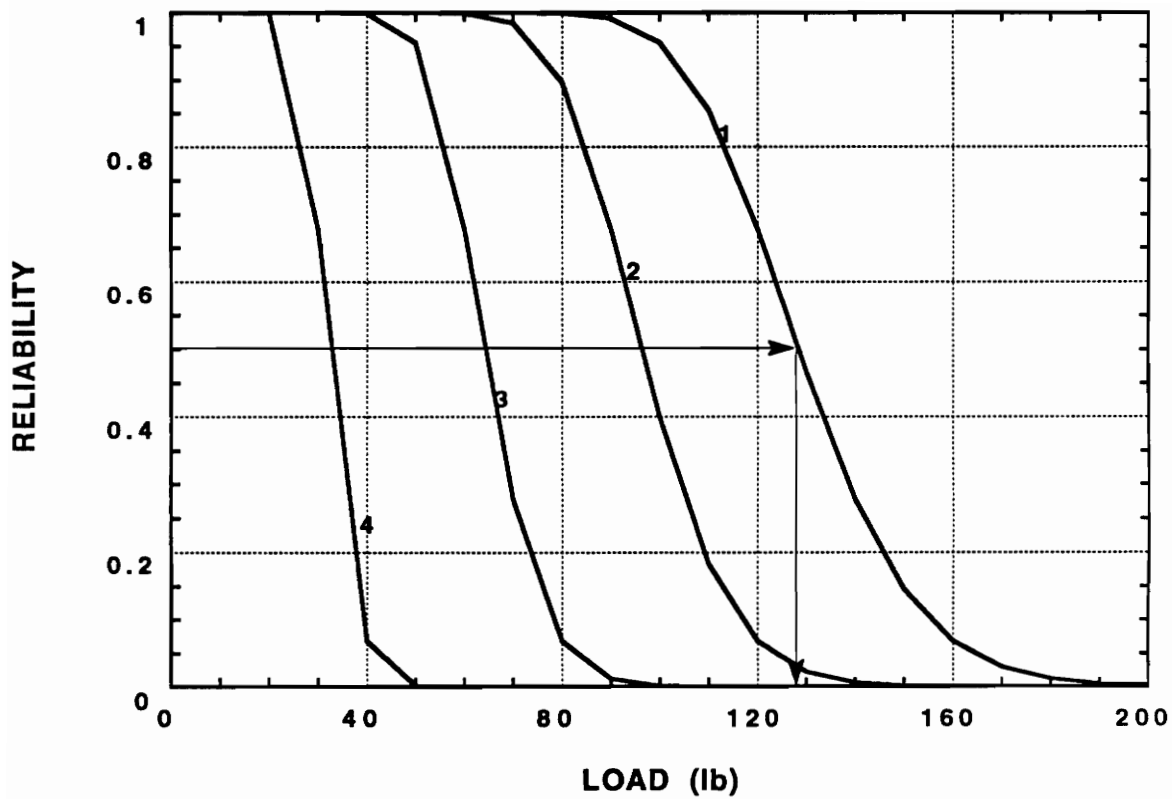


Fig. 5.6 Reliability with load for different mean strength values:

- (1) Propellant strength = 100.0 psi , (2) 75.0 psi
 (3) 50.0 psi , (4) 25.0 psi

MOTOR UNDER LOADING

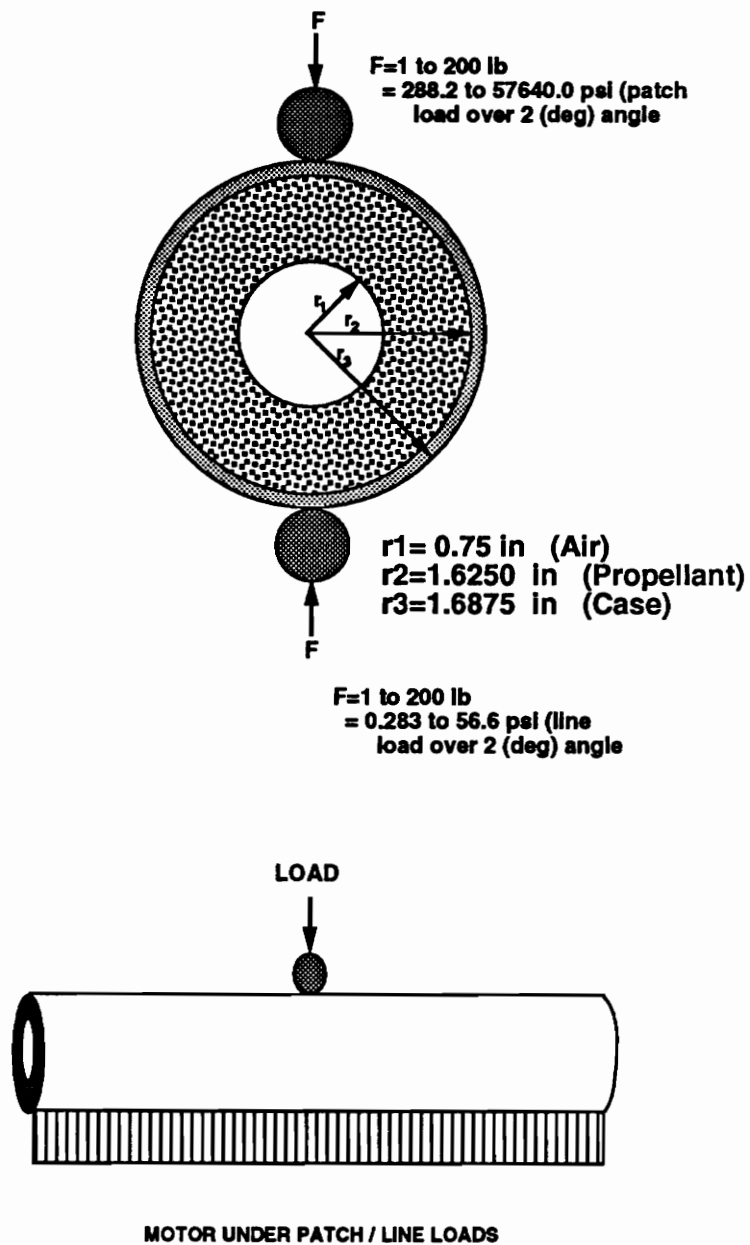


Fig. 5.7 Motor under patch/line loads compination

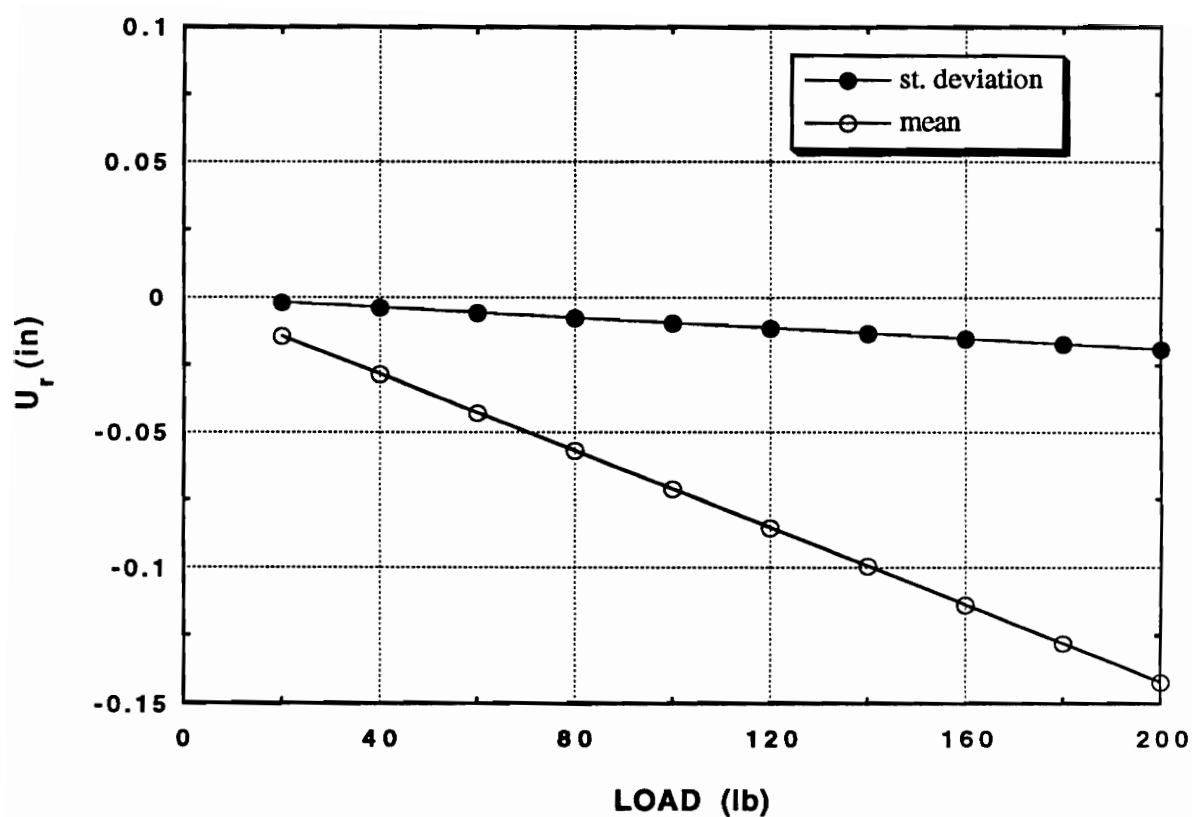


Fig 5.8 Mean and standard deviation of the radial displacement with load at the interface under the load

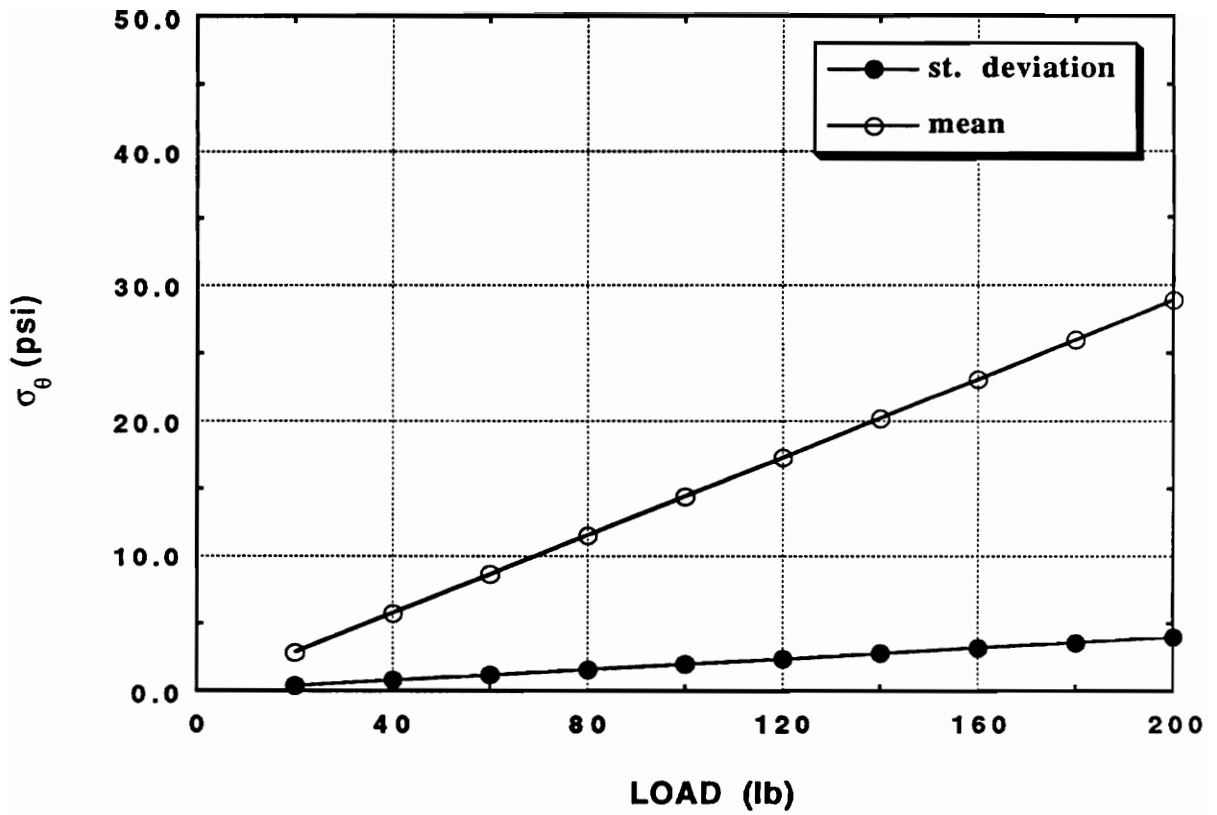


Fig. 5.9 Mean and standard deviation of the tangential stress with load at the bore under the load

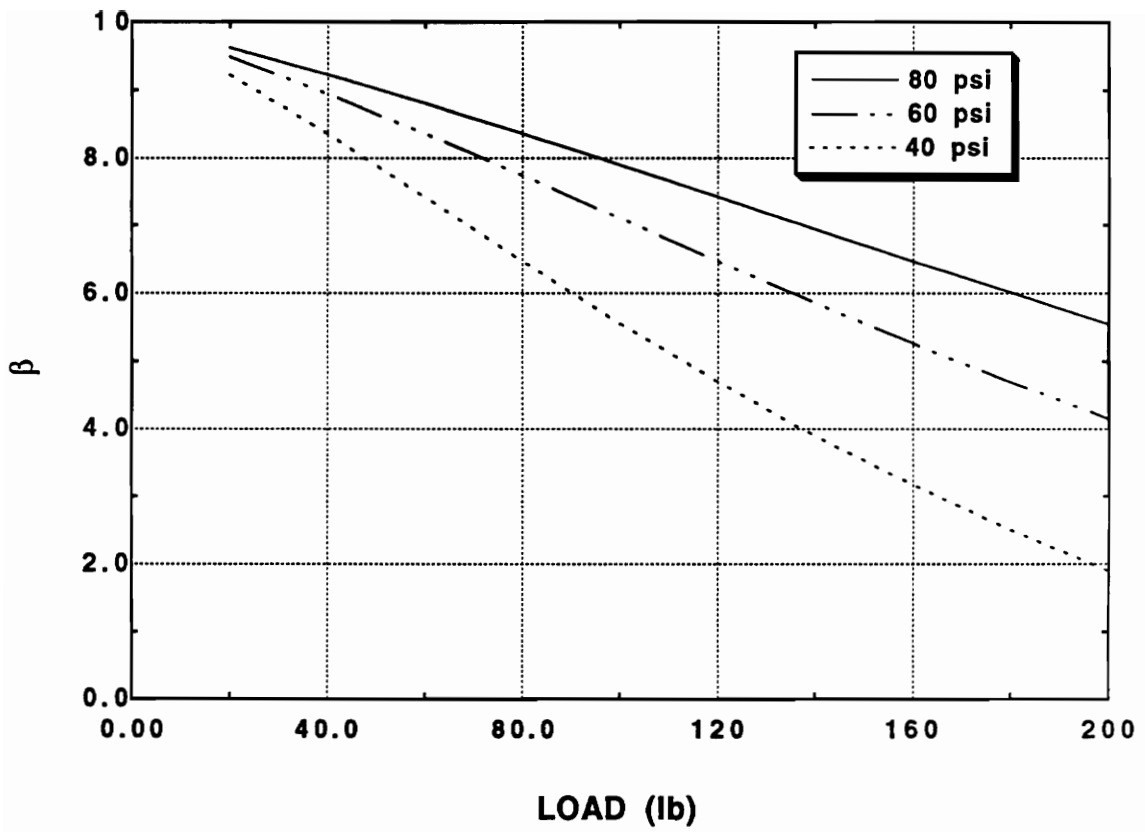
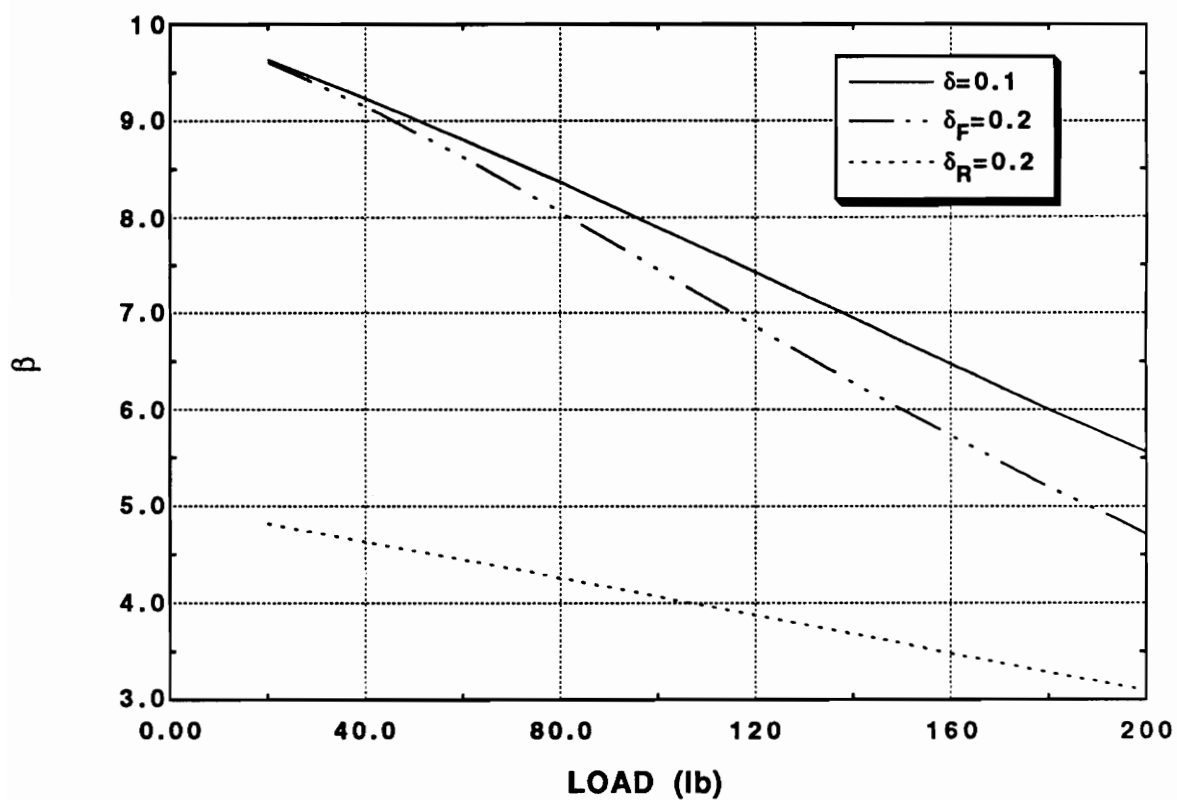


Fig. 5.10 Safety index with load for different mean strength values



**Fig. 5.11 Safety index with load for different coefficients of variations:
(R= Strength, F= Load, Mean (R)= 80 psi)**

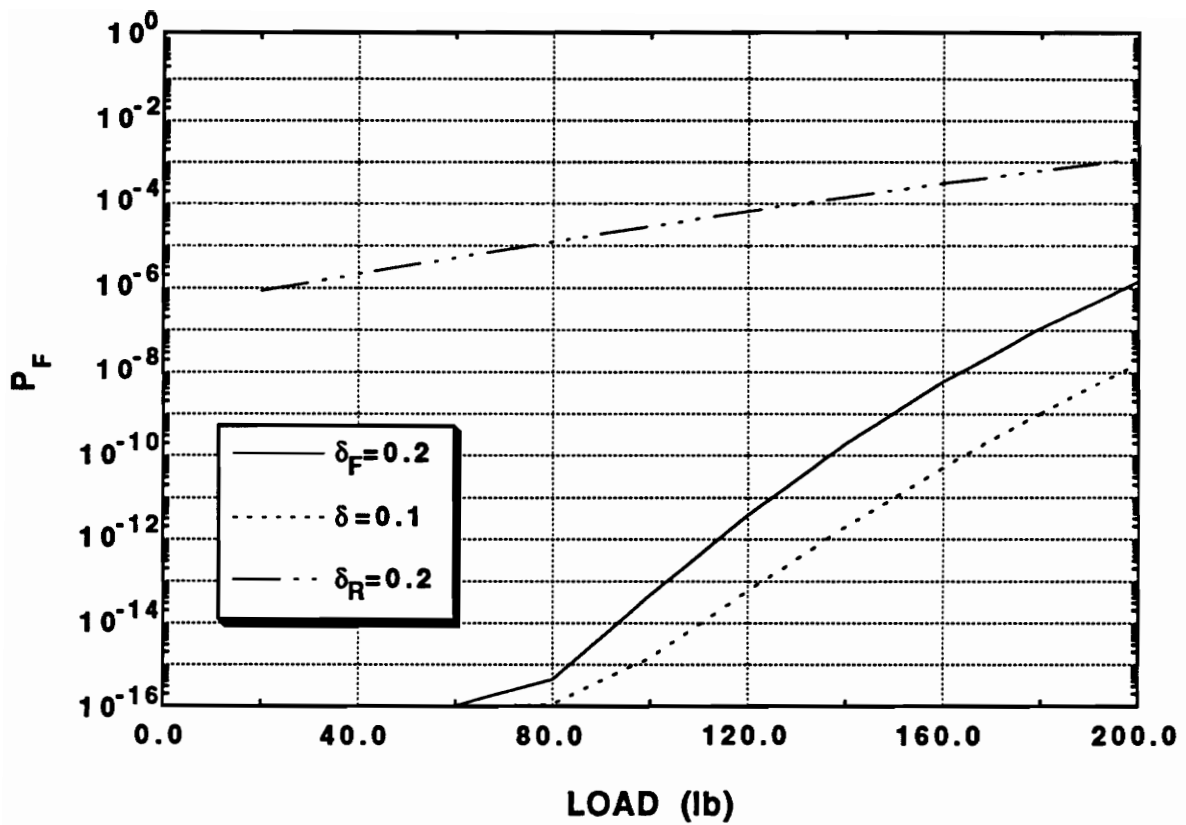


Fig. 5.12 Probability of failure with load for different coefficients of variations: (R= strength, F= Load, Mean (R)= 80 psi)

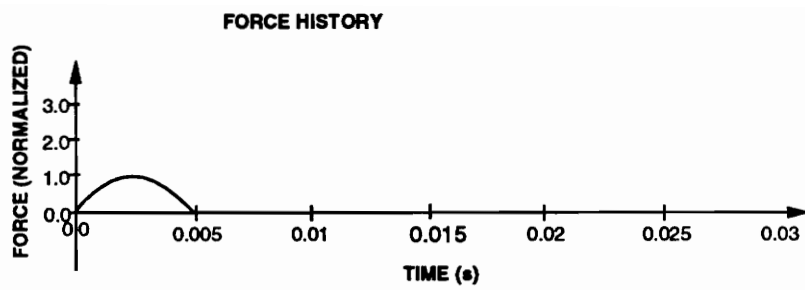


Fig 5.13 Sine wave impact load

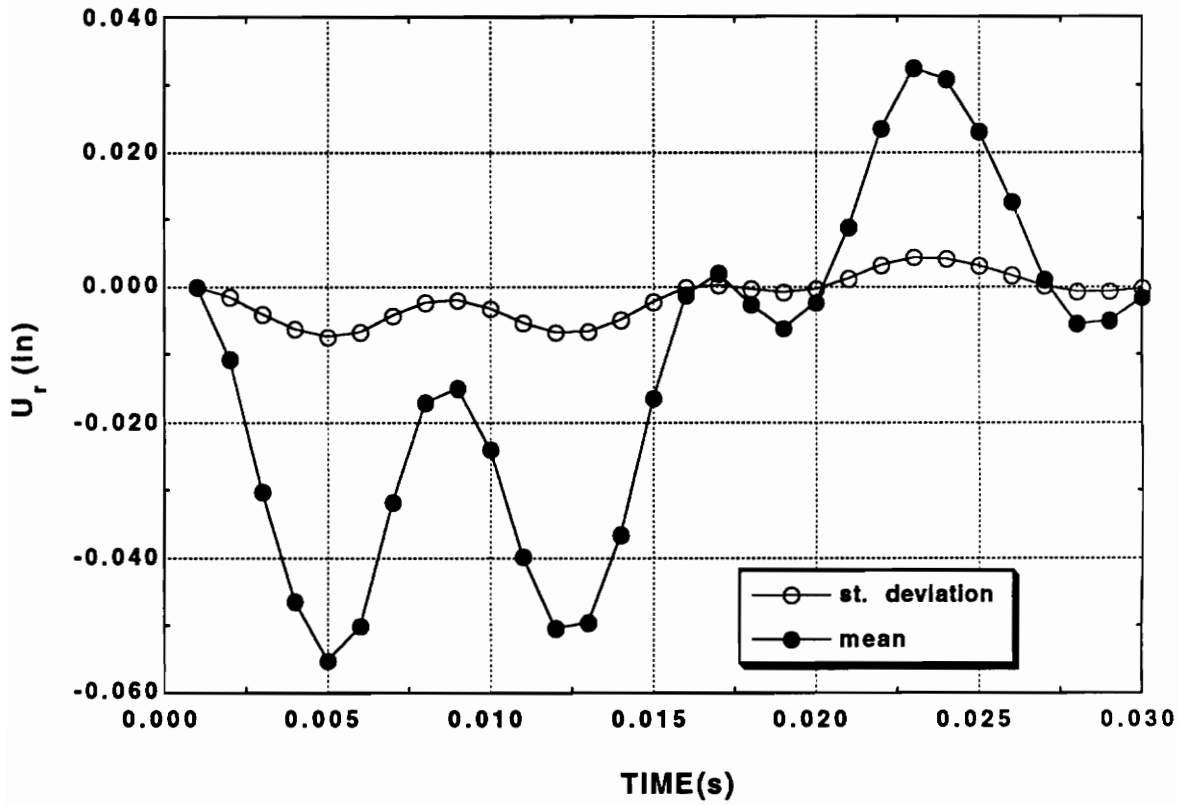


Fig. 5.14 Mean and standard deviation of radial displacement with time at the interface under the load due to sine wave load

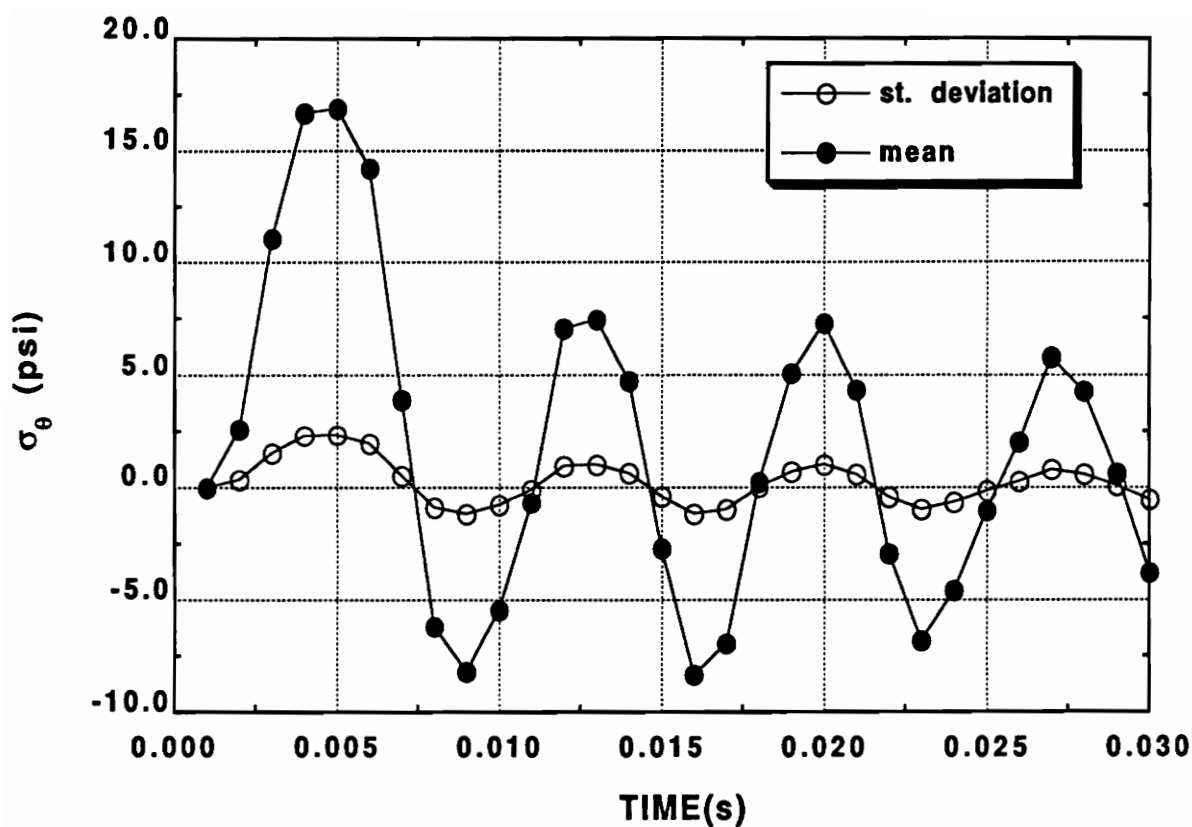


Fig. 5.15 Mean and standard deviation of the tangential stress with time at the bore under the load due to sine wave load

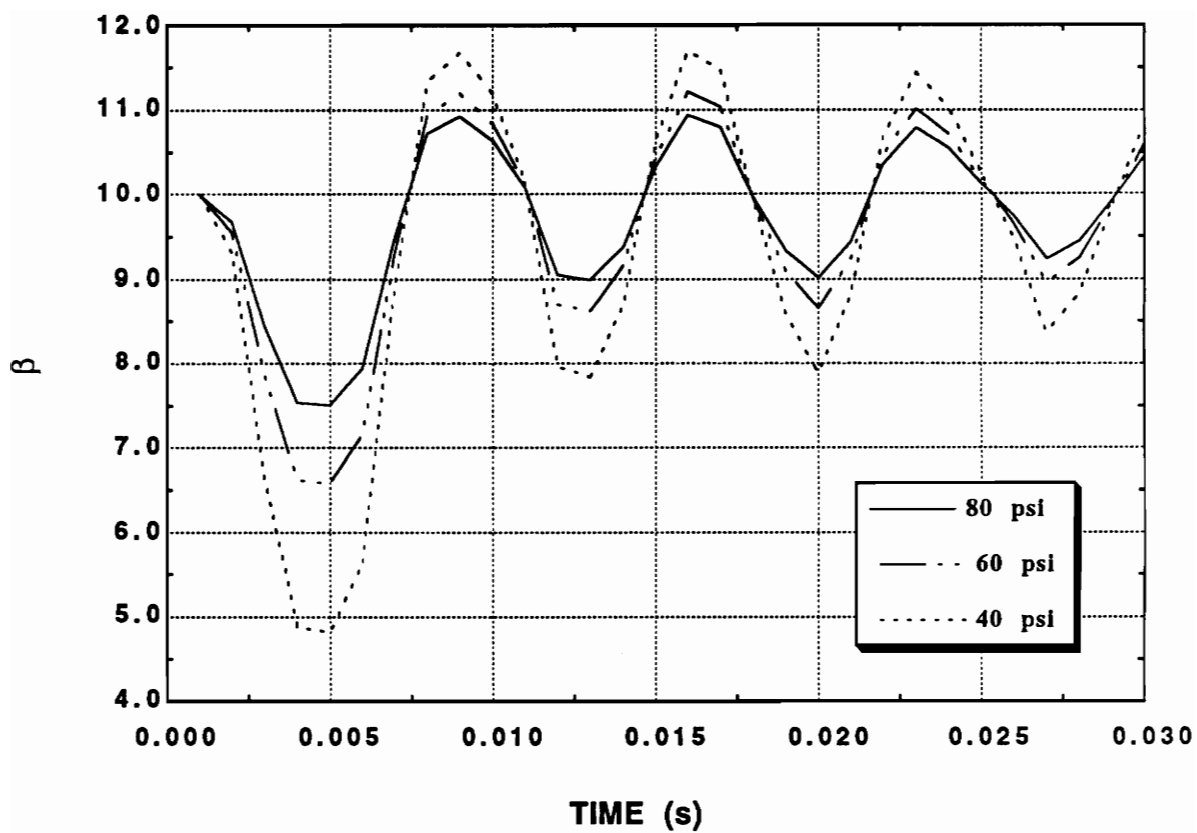


Fig. 5.16 Safety index with time for different mean strength values

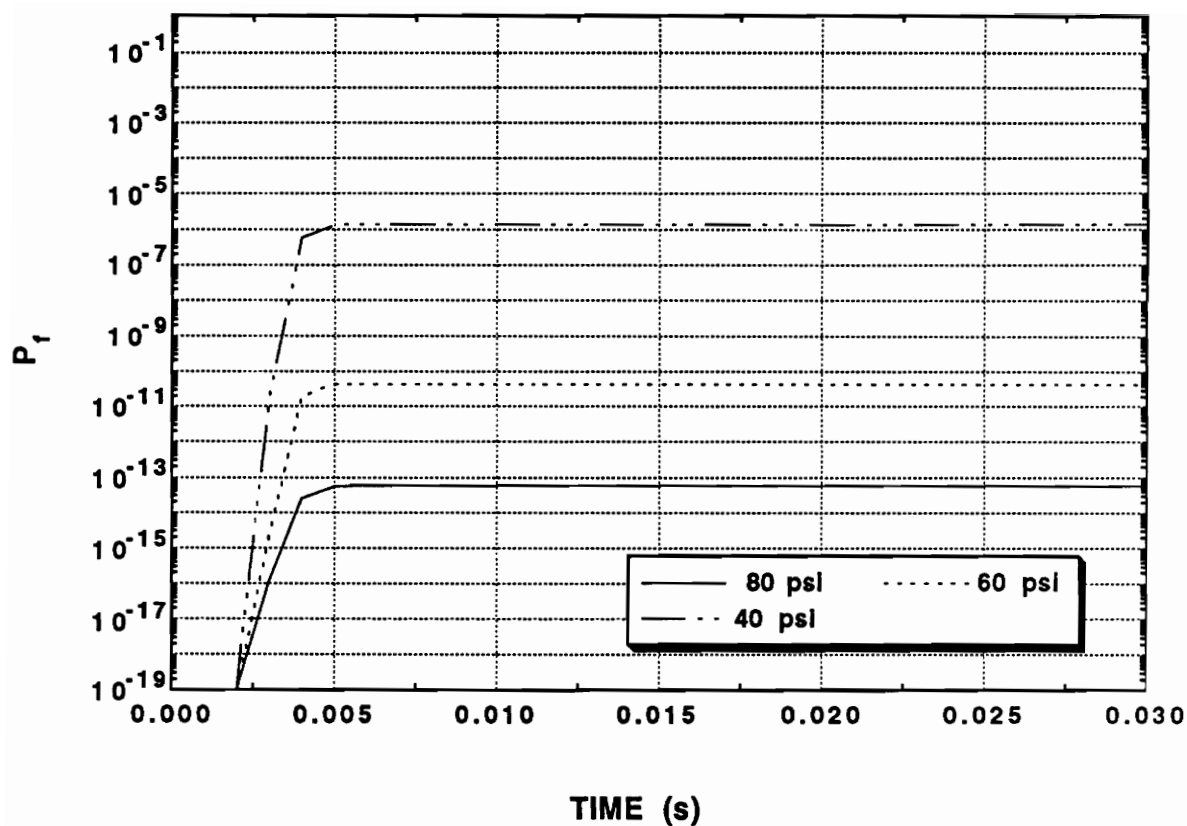
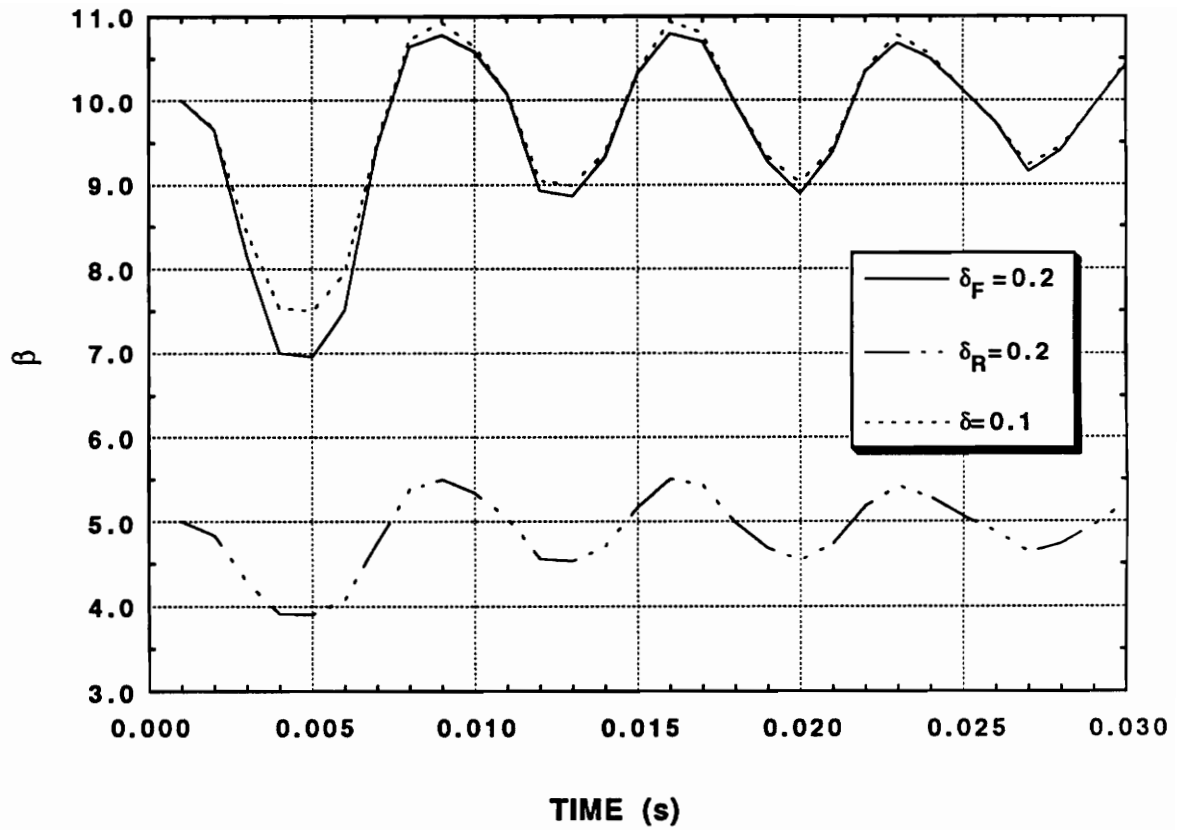


Fig. 5.17 Progressive probability of failure with time for different mean strength values



**Fig. 5.18 Safety index with time for different coefficients of variations:
(R= Strength, F= Load)**

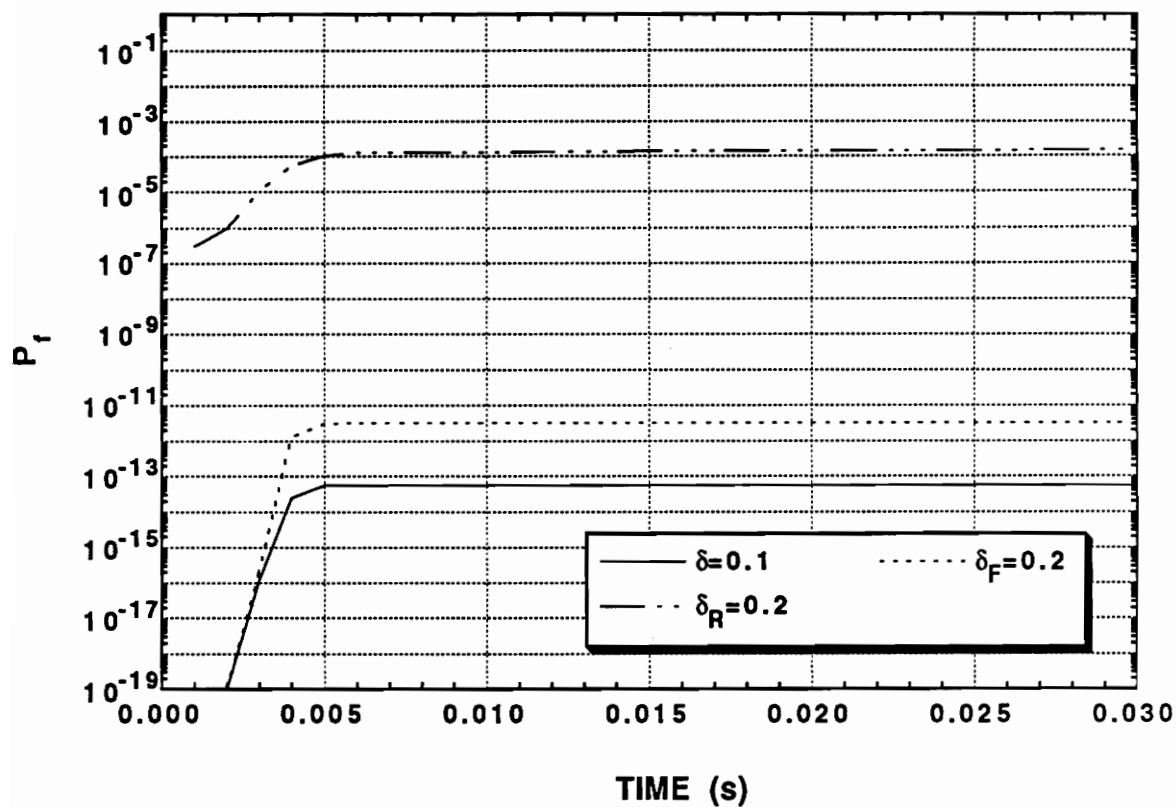
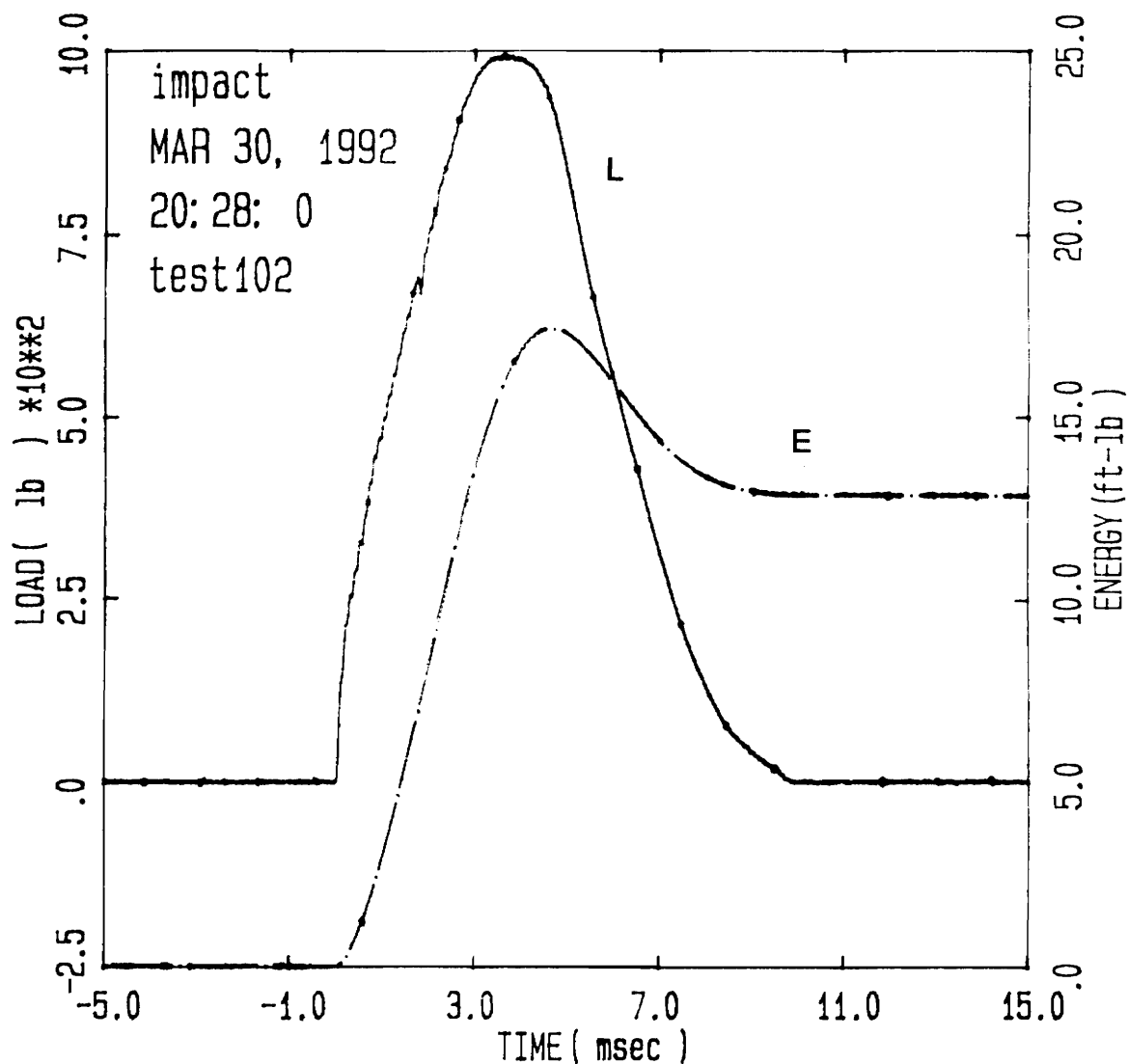


Fig. 5.19 Progressive probability of failure with time for different coefficients of variations: (R= Strength, F= Load)

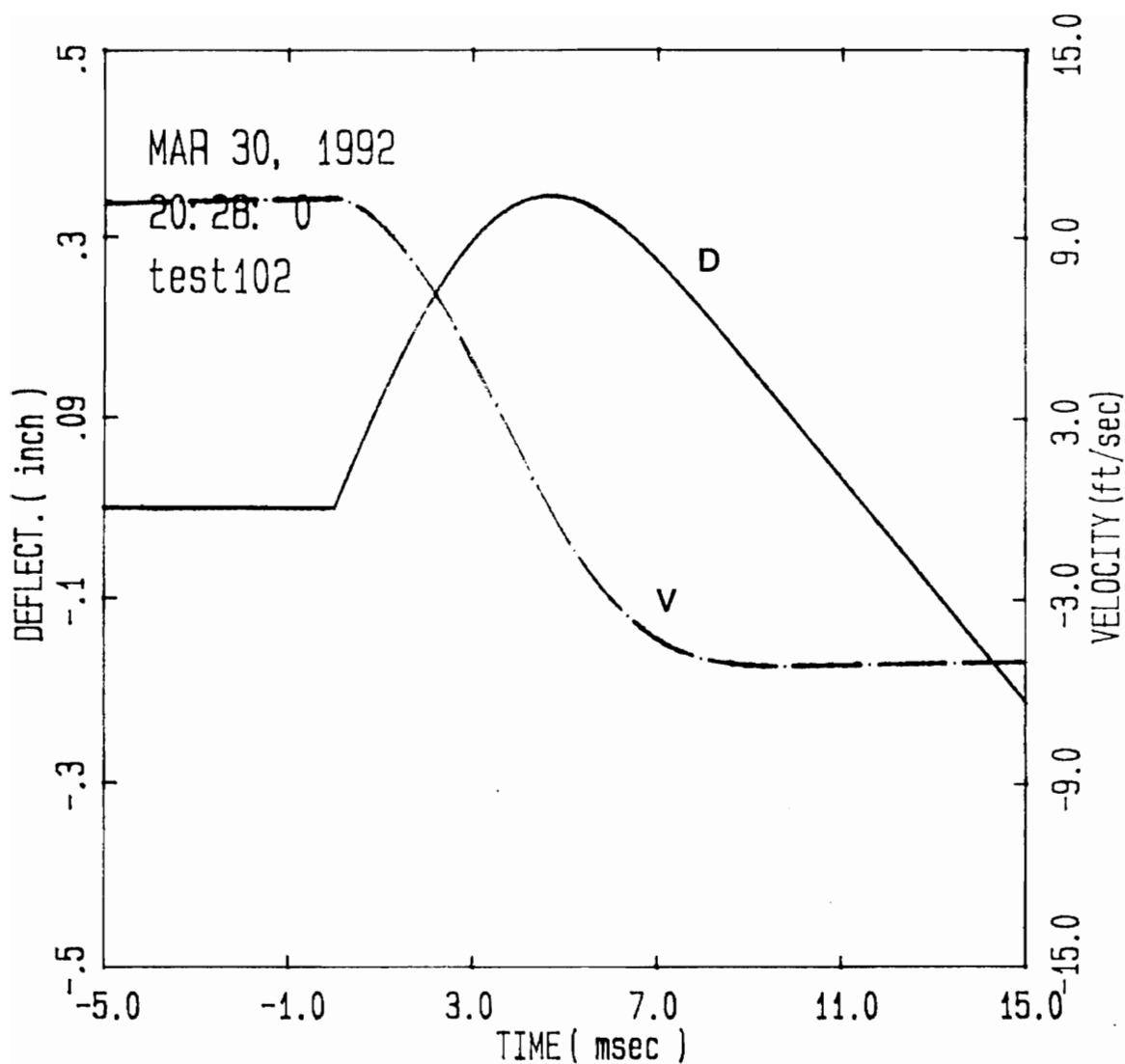


Specimen Id	Impact			Time		Load		Energy	
	Temp (f)	Veloc. (ft/sec)	Energy (ft-lb)	(msec)		(lb)		(ft-lb)	
				Max	Ld	Total	Max	Maxld	Total
test102	70.	10.25	17.14	3.60		9.95	992.0	15.835	12.854

Filter No.- 1. No Smoothing.

Comments:

Fig. 5.20 Force and energy as function of time in an impact test



Specimen Id	Temp (f)	Impact		Time (msec)		Load (lb)		Energy (ft-lb)	
		Veloc. (ft/sec)	Energy (ft-lb)	Max Ld	Total	Max	Maxld	Total	
test102	70.	10.25	17.14	3.60	9.95	992.0	15.835	12.854	

Filter No.= 1, No Smoothing.

Comments:

Fig. 5.21 Displacement and velocity as function of time in an impact test

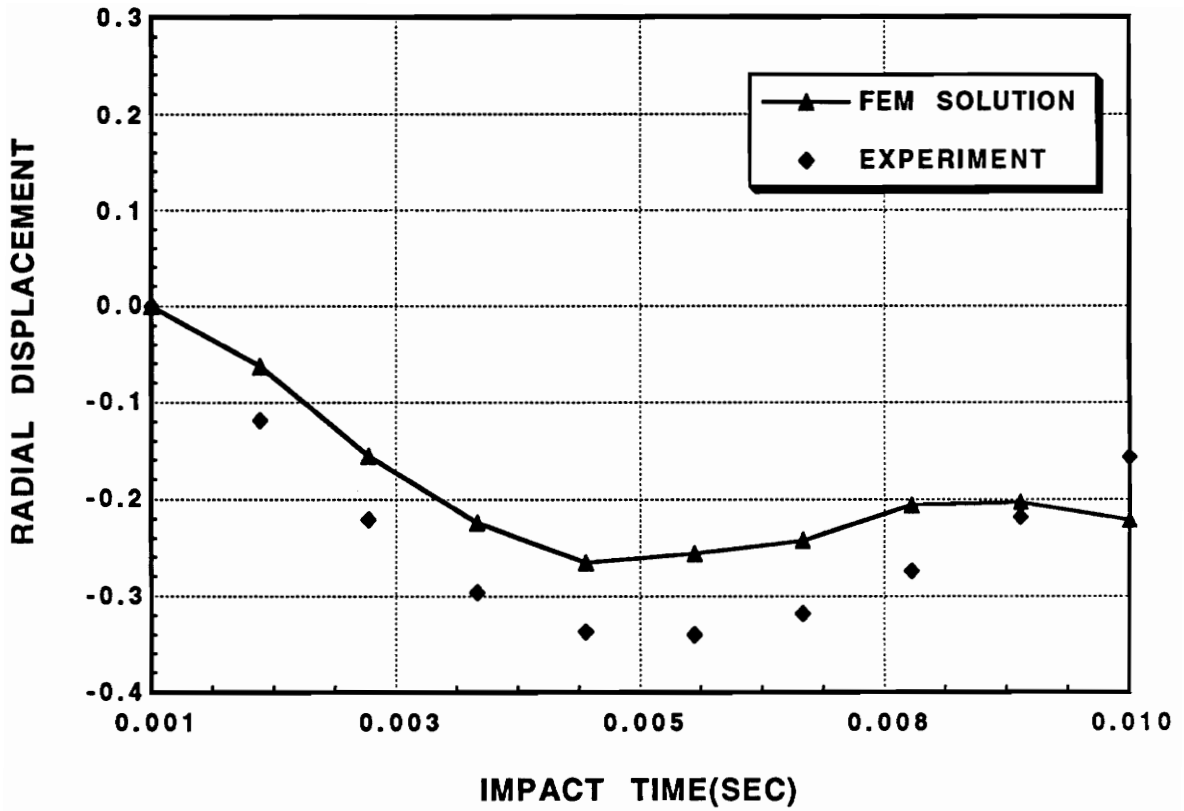


Fig. 5.22 Comparison between FEM solution and experimental results for an impact energy of 17.14 (ft-lb)

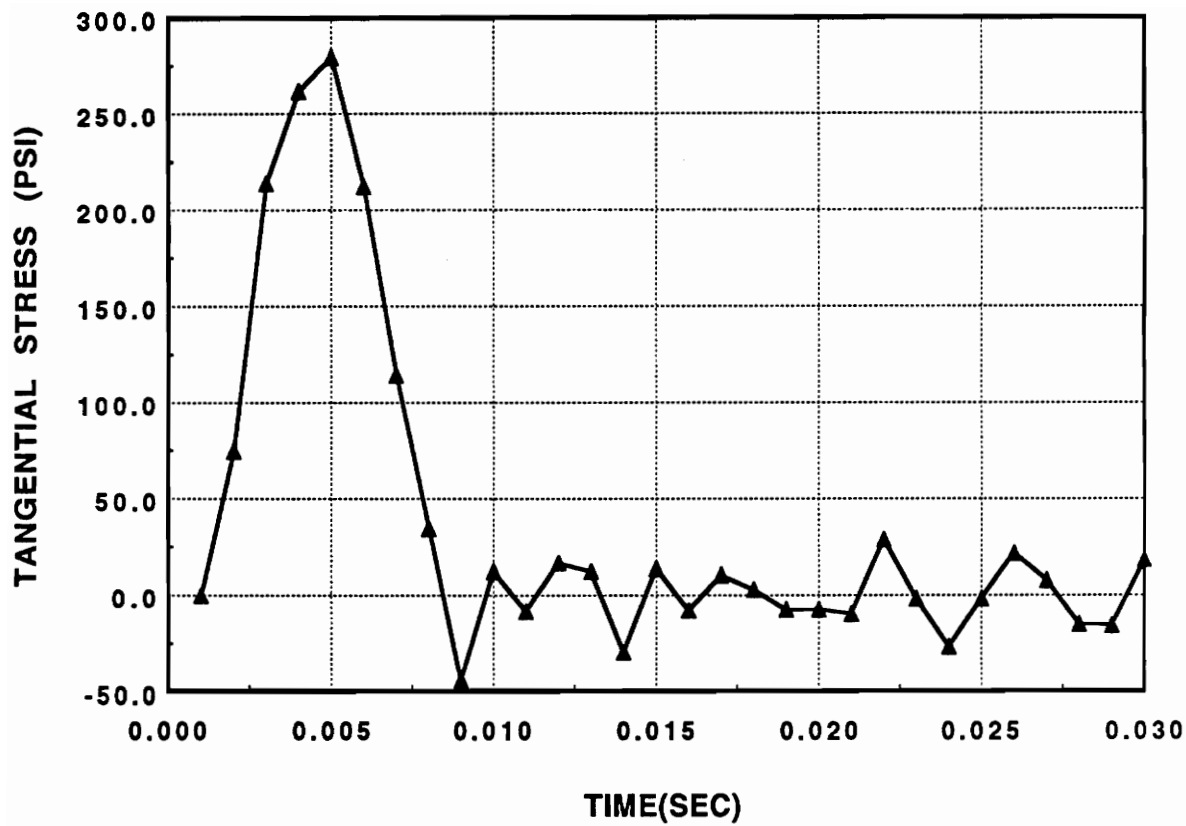


Fig. 5.23 Tangential stress under the load at the bore for an impact energy of 17.14 (ft-lb)

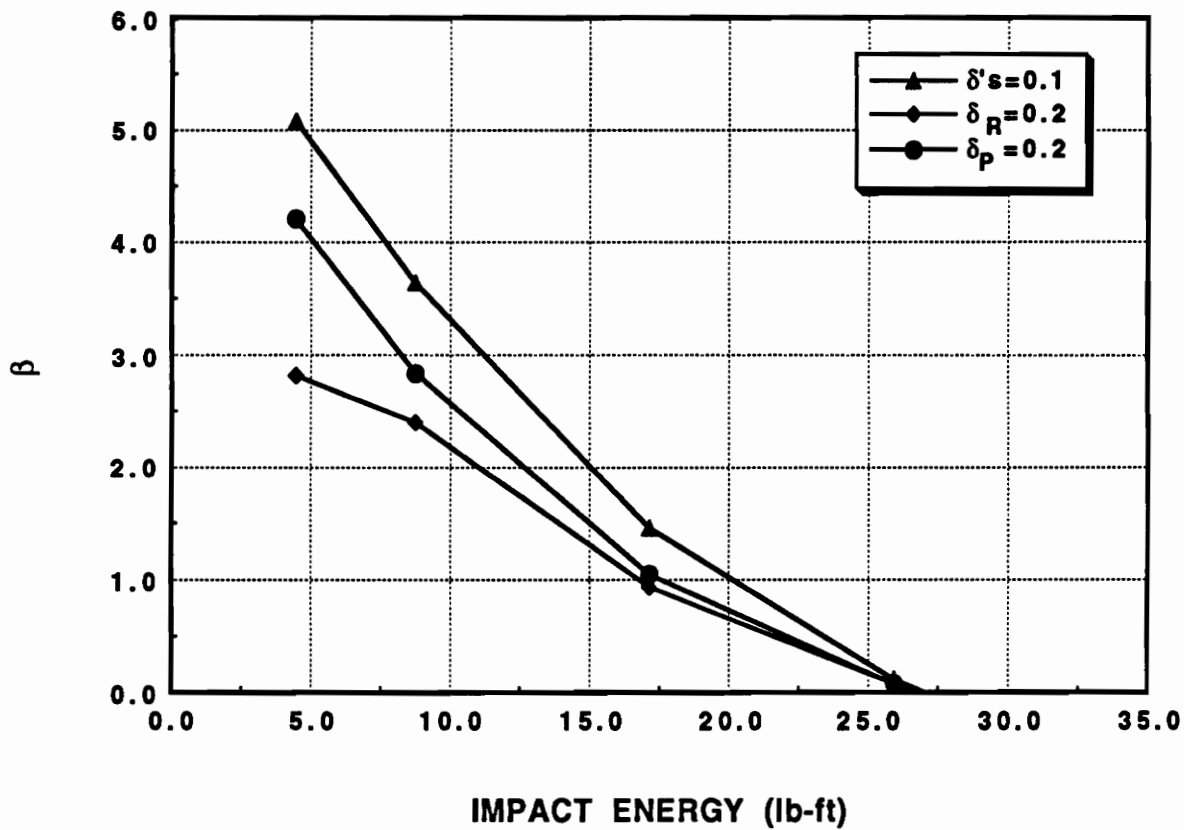


Fig. 5.24 Safety index with impact energy for different coefficients of variations

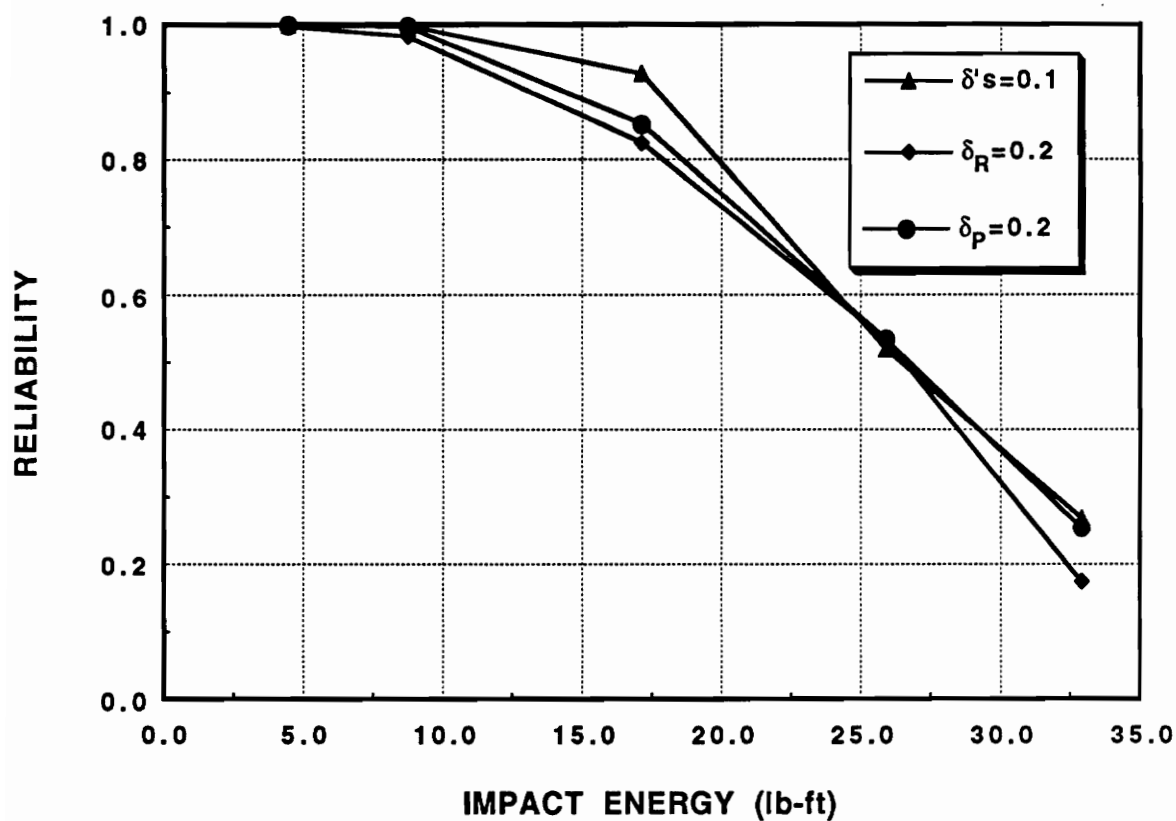


Fig. 5.25 Reliability with impact energy for different coefficients of variations

1. RADIAL DISPL. (DEFORMED)	ABS. MAX. = .4049E-3 INCH
2. CIRCUMF. DISPL. (DEFORMED)	ABS. MAX. = .1228E-3 INCH
3. RADIAL STRESS (DISTRIBUTION)	ABS. MAX. = .4613E-1 PSI
4. SHEAR STRESS (DISTRIBUTION)	ABS. MAX. = .1055E-1 PSI
5. TANGENTIAL STRESS (DISTRIB.)	ABS. MAX. = .3908E-1 PSI

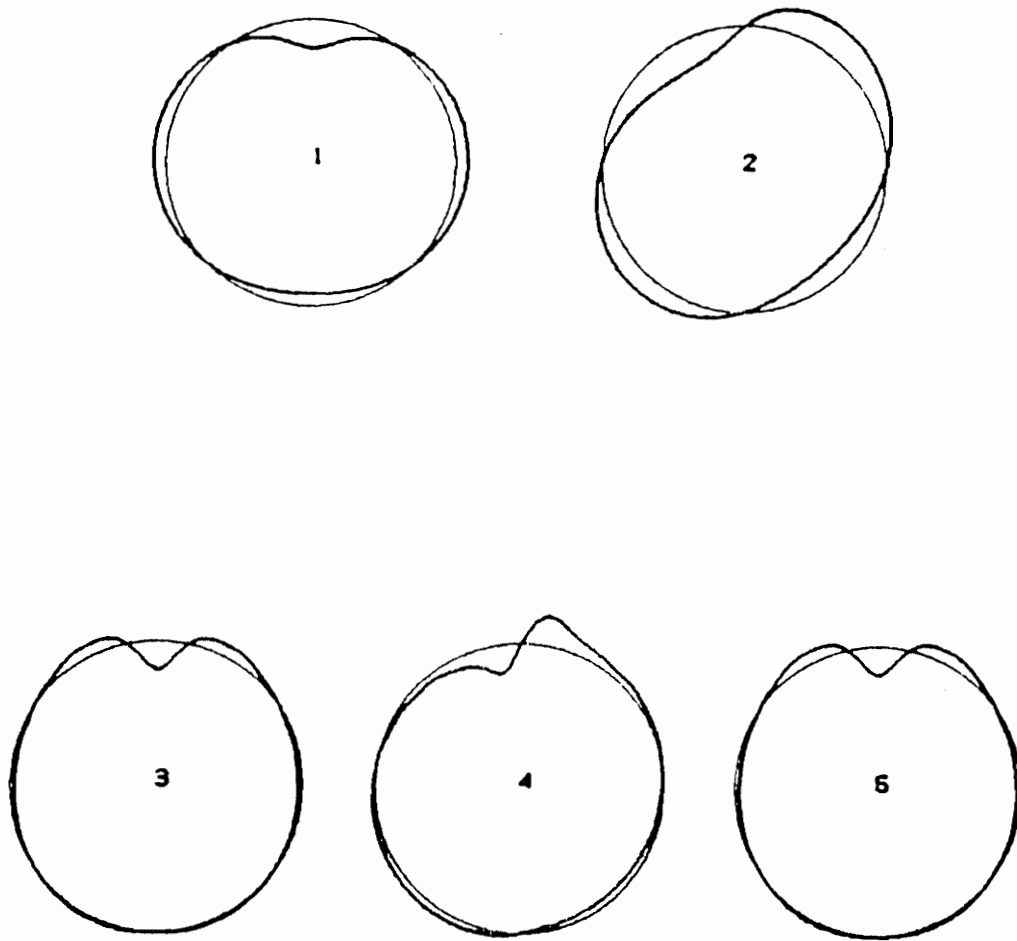


Fig. 5.26 Displacement and stress distribution (line/patch loads) along the interface under the load

Chapter VI

RELIABILITY OF LAMINATED COMPOSITE PLATES

6.1 Introduction

Laminated composite plates have been used widely in industry, especially in the last decade. Linear as well as nonlinear analyses have been carried out by many researchers for laminated composite plates under static and transient loads where all the parameters in the analysis are assumed to be deterministic, i.e., have constant values [68-71]. However, material properties, fiber orientation and loading are statistically variable quantities. Therefore, the need for probabilistic analysis exists. Moreover, since the analysis uses finite element codes, the development of probabilistic finite element codes is a "hot" research area.

In previous chapters, normally distributed and correlated design variables were considered. Probabilistic analysis was performed based on a single failure mode. In this

chapter, however, the same will be applied to a more complicated example, where geometric nonlinearity is involved. The application of non-normal variables will be considered as well as the case of multi-independent failure modes.

Probabilistic static and transient finite element analysis of a geometrically nonlinear laminated composite plate will be discussed. The probabilistic model is developed based on Response Surface Methodology (RSM) in conjunction with the First Order Second Moment (FOSM) reliability method as was discussed in chapter 3. The finite element model will be developed based on the first order shear deformation theory in conjunction with Von Karman's strain tensor. Newton-Raphson and Newmark direct integration methods are used for nonlinear and time dependent analysis, respectively. Two models are considered: a finite element model for the deterministic analysis of stresses and displacements and a probabilistic model for the reliability analysis.

6.2 Finite Element Model

6.2.1 Theory and Formulation

The first order shear deformation theory is used in conjunction with Von Karman's nonlinear strain tensor to account for large deformations. The plane strain assumption is used in this study also.

6.2.1.1 Kinematics

Based on first order shear deformation theory (Fig. 6.1), the displacement field can be written as

$$u_1 = u(x,y,t) + z\phi_x(x,y,t) \quad (6.1)$$

$$u_2 = v(x,y,t) + z\phi_y(x,y,t) \quad (6.2)$$

$$u_3 = w(x,y,t) \quad (6.3)$$

where t is the time, u_1, u_2, u_3 are the displacements in x, y, z directions, respectively, u, v, w are the associated mid-plane displacements, and ϕ_x, ϕ_y are the slopes in the xz and yz planes due to bending only.

6.2.1.2 Von Karman Nonlinear Strains

The strains in the Von Karman plate theory which account for large deflections can be expressed in the form

$$\varepsilon_{ij} = \frac{1}{2} (u_{i,j} + u_{j,i} + u_{m,i} u_{m,j}) \quad i,j = 1,2,3 \quad (6.4)$$

where the components of the strain tensor can be found in [72].

6.2.1.3 Constitutive Relations

The constitutive relations for the plate can be written as

$$\begin{Bmatrix} N \\ M \end{Bmatrix} = \begin{bmatrix} [A] & [B] \\ [B] & [D] \end{bmatrix} \begin{Bmatrix} \varepsilon^0 \\ \kappa \end{Bmatrix} \quad (6.5)$$

and

$$\begin{Bmatrix} Q_2 \\ Q_1 \end{Bmatrix} = \begin{bmatrix} A_{44} & A_{45} \\ A_{45} & A_{55} \end{bmatrix} \begin{Bmatrix} \varepsilon_4 \\ \varepsilon_5 \end{Bmatrix} \quad (6.6)$$

Where N, M and Q are called the plate generalized forces and $[A], [B], [D]$ are the plate generalized stiffnesses given in [72]. The stress strain relations can be written as

$$\begin{Bmatrix} \sigma_1 \\ \sigma_2 \\ \sigma_6 \end{Bmatrix} = [\bar{Q}] \begin{Bmatrix} \varepsilon_1 \\ \varepsilon_2 \\ \varepsilon_6 \end{Bmatrix} \quad (6.7)$$

and

$$\begin{Bmatrix} \sigma_4 \\ \sigma_5 \end{Bmatrix} = \begin{bmatrix} \bar{Q}_{44} & \bar{Q}_{45} \\ \bar{Q}_{45} & \bar{Q}_{55} \end{bmatrix} \begin{Bmatrix} \varepsilon_4 \\ \varepsilon_5 \end{Bmatrix} \quad (6.8)$$

6.2.1.4 Equations of Motion

To derive the equations of motion, Hamilton's principle is used:

$$\int_{t_0}^{t_1} \delta L dt = 0 \quad (6.9)$$

where δL is the first variation of the Lagrangian

or

$$0 = \int_{t_0}^{t_1} \left(\int_V (\sigma_{ij} \delta \varepsilon_{ij}) dv - \int_{\Omega_e} \delta w f dx dy - \oint_{\Gamma_e} (Q_n \delta w + M_n \frac{\partial \delta w}{\partial n} + M_{ns} \frac{\partial \delta w}{\partial s}) ds \right) dt \\ - \int_{t_0}^{t_1} \left(\oint_{\Gamma_e} (N_n \delta u_n + N_{ns} \delta u_s) ds + \int_{V_e} \frac{1}{2} \rho (\delta \dot{u}_1 \dot{u}_1 + \delta \dot{u}_2 \dot{u}_2 + \delta \dot{u}_3 \dot{u}_3) dv \right) dt \quad (6.10)$$

Substituting Eqs. 6.1-6.8 into Eq. 6.10 and integrating by parts, both with respect to time and spatial coordinates, results in

$$N_{1,x} + N_{6,y} = I_1 \ddot{u} + I_2 \ddot{\phi}_x \quad (6.11)$$

$$N_{6,x} + N_{2,y} = I_1 \ddot{v} + I_2 \ddot{\phi}_y \quad (6.12)$$

$$Q_{1,x} + Q_{2,y} + N(w) = I_1 \ddot{w} - f(x,y,t) \quad (6.13)$$

$$M_{1,x} + M_{6,y} - Q_1 = I_3 \ddot{\phi}_x + I_2 \ddot{u} \quad (6.14)$$

$$M_{6,x} + M_{2,y} - Q_2 = I_3 \ddot{\phi}_y + I_2 \ddot{v} \quad (6.15)$$

where

$$N(w) = \frac{\partial}{\partial x} (N_1 \frac{\partial w}{\partial x} + N_6 \frac{\partial w}{\partial y}) + \frac{\partial}{\partial y} (N_6 \frac{\partial w}{\partial x} + N_2 \frac{\partial w}{\partial y}) \quad (6.16)$$

is the contribution due to nonlinear terms, and

$$(I_1, I_2, I_3) = \sum_{m=1}^n \int_{z_m}^{z_{m+1}} \rho_m(1, z, z^2) dz \quad (6.17)$$

with ρ_m the material density of the m^{th} layer.

6.2.1.5 Variational formulation

Multiply Eqs. 6.11 to 6.15 by a weight function ($w_j(x,y)$, $j = 1,5$) and integrate by parts. The variational form can be written as

$$0 = \int_{\Omega_e} (w_1(I_1 \ddot{u} + I_2 \ddot{\phi}_x) + w_{1,x} N_1 + w_{1,y} N_6) dxdy - \oint_{\Gamma_e} N_n w_1 ds \quad (6.18)$$

$$0 = \int_{\Omega_e} (w_2(I_1 \ddot{v} + I_2 \ddot{\phi}_y) + w_{2,x} N_6 + w_{2,y} N_2) dxdy - \oint_{\Gamma_e} N_{nt} w_2 ds \quad (6.19)$$

$$0 = \int_{\Omega_e} (w_3 I_1 \ddot{w} + w_{3,x} Q_1 + w_{3,y} Q_2 + w_{3,x} (N_1 w_x + N_6 w_y)) dxdy \\ + \int_{\Omega_e} (w_{3,y} (N_6 w_x + N_2 w_y) - w_3 f) dxdy - \oint_{\Gamma_e} Q_n w_3 ds \quad (6.20)$$

$$0 = \int_{\Omega_e} (w_4(I_3 \ddot{\phi}_x + I_2 \ddot{u}) + w_{4,x} M_1 + w_{4,y} M_6 + w_4 Q_1) dxdy \\ - \oint_{\Gamma_e} M_n w_4 ds \quad (6.21)$$

$$0 = \int_{\Omega_e} (w_5(I_3 \ddot{\phi}_y + I_2 \ddot{v}) + w_{5,x} M_6 + w_{5,y} M_2 + w_5 Q_2) dxdy \\ - \oint_{\Gamma_e} M_{nt} w_5 ds \quad (6.22)$$

6.2.2 Finite Element Formulation

6.2.2.1 Polynomial Approximation

Approximating u , v , w , ϕ_x , and ϕ_y in polynomial functions and substituting into Eqs. 6.18 to 6.22, the governing equations can be written in terms of the polynomial function as given in [72], or in matrix form as

$$\begin{bmatrix} [M^{11}] & [0] & [0] & [M^{14}] & [0] \\ [0] & [M^{22}] & [0] & [0] & [M^{25}] \\ [0] & [0] & [M^{33}] & [0] & [0] \\ [M^{14}] & [0] & [0] & [M^{44}] & [0] \\ [0] & [M^{52}] & [0] & [0] & [M^{55}] \end{bmatrix} \begin{bmatrix} \{\ddot{u}\} \\ \{\ddot{v}\} \\ \{\ddot{w}\} \\ \{\ddot{x}\} \\ \{\ddot{y}\} \end{bmatrix} + \begin{bmatrix} [K^{11}] & [K^{12}] & [K^{13}] & [K^{14}] & [K^{15}] \\ [K^{21}] & [K^{22}] & [K^{23}] & [K^{24}] & [K^{25}] \\ [K^{31}] & [K^{32}] & [K^{33}] & [K^{34}] & [K^{35}] \\ [K^{41}] & [K^{42}] & [K^{43}] & [K^{44}] & [K^{45}] \\ [K^{51}] & [K^{52}] & [K^{53}] & [K^{54}] & [K^{55}] \end{bmatrix} \begin{bmatrix} \{u\} \\ \{v\} \\ \{w\} \\ \{X\} \\ \{Y\} \end{bmatrix} = \begin{bmatrix} \{F^1\} \\ \{F^2\} \\ \{F^3\} \\ \{F^4\} \\ \{F^5\} \end{bmatrix} \quad (6.23)$$

where $[M]$ is the mass matrix, $[K]$ is the stiffness matrix and $\{F\}$ the column vector which contains the boundary conditions and the transverse force. The elements of $[M]$, $[K]$ and $\{F\}$ are given in [72]. The element stiffness matrix $[K]$ is nonlinear and unsymmetric in the present formulation, the nonlinearity being due to nonlinear terms appearing in the variational form.

6.2.2.2 Newmark's Direct Integration Method for Transient Analysis

The time-dependent displacements and accelerations in Eq. 6.23 are approximated using Newmark's integration scheme [70], with $\alpha = 0.5$ and $\beta = 0.25$. Eq. 6.23 can be written as

$$[\hat{K}]\{\Delta\}_{n+1} = \{\hat{F}\}_{n,n+1} \quad (6.24)$$

where

$$[\hat{K}] = [K] + a_0[M] \quad (6.25)$$

and

$$\{\hat{F}\} = \{F\}_{n+1} + [M](a_0\{\Delta\}_n + a_1\{\dot{\Delta}\}_n + a_2\{\ddot{\Delta}\}_n) \quad (6.26)$$

and

$$a_0 = \frac{1}{\beta\Delta t^2}, \quad a_1 = a_0\Delta t, \quad a_2 = \frac{1}{2\beta} - 1 \quad (6.27)$$

Once the solution $\{\Delta\}$ is known at $t_{n+1} = (n+1)\Delta t$, the first and second derivatives (velocity and acceleration) of $\{\Delta\}$ at t_{n+1} can be computed from

$$\{\Delta\}_{n+1} = a_0(\{\Delta\}_{n+1} - \{\Delta\}_n) - a_1\{\dot{\Delta}\}_n - a_2\{\ddot{\Delta}\}_n \quad (6.28)$$

$$\{\dot{\Delta}\}_{n+1} = (\{\dot{\Delta}\}_n + a_3\{\ddot{\Delta}\}_n) + a_4\{\ddot{\Delta}\}_{n+1} \quad (6.29)$$

$$a_3 = (1 - \alpha)\Delta t, \quad a_4 = \alpha\Delta t \quad (6.30)$$

All of the operations previously indicated can be performed at the element level and the assembled form of Eq. 6.23 can be obtained for the whole problem.

6.2.2.3 Newton Raphson Method for Nonlinear Analysis

This technique is used to solve the nonlinear equations. It is based on computing what is called the tangent stiffness matrix [73] as follows:

$$[K^T] = \frac{\partial \{R\}}{\partial \{\Delta\}} \quad (6.31)$$

where

$$\{R\} = [\hat{K}]\{\Delta\} - \{\hat{F}\} \quad (6.32)$$

and $[\hat{K}]$ is a function of $\{\Delta\}$

The assembled form of Eq. 6.32 can be obtained. Applying the boundary conditions, the assembled equations may be solved. Then the solution vector can be updated as

$$\{\Delta\}_{n+1} = \{\Delta\}_n + \{\delta\Delta\} \quad (6.33)$$

In order to insure the accuracy of the solution, a check for convergence is made. The elements of the tangent stiffness matrix are given in [72].

6.3 Probabilistic Model

The probabilistic model is constructed based on the technique described in chapter III and the flow chart presented in Fig. 5.1.

6.4 Applications and Results

A computer program is written based on the finite element formulation and is used as a subroutine in the probabilistic model code. Before the probabilistic analysis is performed, the computer program is tested against some of the results that are available in the literature. Fig. 6.2 shows a comparison with reference [71] for a $[90/0]$ simply supported plate subjected to uniformly distributed load, and a good agreement is obtained for linear and nonlinear analyses. In Fig. 6.3 a comparison is made with reference [70] for a $[+45/-45]$ simply supported plate subjected to time-dependent load, and a good agreement is obtained also. Material properties as well as loading information can be found in these references.

The program is then tested for the following example: a 100" x 100" plate with $[+45/-45]_{25/s}$ subjected to uniformly distributed static and transient loads. Material properties, fiber orientations and loads are assumed to be random variables, as shown in Table 6.1.

6.4.1 Probabilistic Static Analysis (Linear and Nonlinear)

In this and the next two sections, a single failure mode is considered based on the maximum allowable deflection, W_{all} , and will be referred to as the strength of the plate, [74]. The maximum deflection, W_{max} , is located at the center of the plate according to Fig. 6.4; therefore the G function will be defined as $W_{all} - W_{max}$

Using the FOSM the mean and the standard deviation of the central deflection with load for linear and nonlinear analyses is presented in Fig. 6.5. The linear analysis results in more deflection than the nonlinear one; in fact, the difference between the two analyses increases as the load increases. This observation applies to the standard deviation too. To compare the probability of failure between linear and nonlinear analyses, the performance function, G , is designed based on a maximum allowable deflection of 1.5' with 10% coefficient of variation. The analysis is performed and the results are presented in Fig. 6.6 for the safety index, β , with load and in Fig. 6.7 for the probability of failure with load. In Fig. 6.6 high values for β correspond to nonlinear analysis while in Fig. 6.7 high values for the probability of failure they correspond to linear analysis.

In order to investigate the effects of the strength in the analysis, three different values for the maximum allowable deflection are assumed (0.8,1.0,1.5'). The results are shown in Fig. 6.8 for β with load and Fig. 6.9 for the probability of failure with load. In these two figures, by increasing the maximum allowable deflection, high values for β and low values for the probability of failure are obtained.

To study the sensitivity of the plate to design parameters, the probability of failure is computed based on different coefficients of variation as shown in Fig. 6.10. The probability of failure increases by increasing the coefficient of variation for the strength.

By increasing the coefficient of variation for the load by the same amount, the probability of failure increases but does not reach the same level.

6.4.2 Probabilistic Transient Analysis (Linear and Nonlinear)

A load factor ($f = 25$ or $p = 0.65$ psi) is assumed to be time dependent (step function applied at $t = 0$) when applied to the plate. The linear and nonlinear mean and standard deviation for the central deflection is presented in Fig. 6.11 as a function of time. In this figure the linear deflection has higher peaks for μ and σ than the nonlinear one. On the other hand, the nonlinear deflection has a shorter period than the linear one.

In Fig. 6.12, the safety index is presented for a maximum allowable deflection of 1.5 (in) and coefficients of variation of 10%. The values for linear and nonlinear analyses are plotted and show high values for β in the nonlinear analysis. Fig. 6.13 represents the progressive probability of failure for both analyses as defined in section 3.5. High values are obtained because the response keeps repeating itself.

The effect of the strength in the analysis is presented in Fig. 6.14 for the safety index and Fig. 6.15 for the progressive probability of failure. In Fig. 6.16 the effect of different coefficients of variation is considered. The progressive probability of failure increases by increasing the coefficient of variation for the strength. However, by increasing the coefficient of variation for the load by the same value, the progressive probability of failure increases but does not reach the same level.

6.4.3 Application to Non-Normal Variables

To examine the developed technique for non-normal variables, three different distributions are assumed for the strength of the plate, normal, lognormal and Weibull. The technique described in section 3.4 is used and the analysis is performed for a mean strength of 1.5" and 10% coefficient of variation for different load values. Results are shown in Fig. 6.17 for the safety index, Fig. 6.18 for the reliability and Fig 6.19 for the probability of failure as functions of load.

A close look at Fig. 6.18 shows that the lognormal distribution gives the most conservative assumption and the Weibull gives the least one, while the normal one is in between. These results, however, are not absolute and they may change from one example to another. They are produced here to show that the developed technique can handle non-normal variables.

6.4.4 Application to Multi-Failure Modes

In this section, multi-failure modes are considered and different meshes are tested. Failure is considered based on the maximum bending stress through the thickness of the plate where several locations can be obtained and compared with the allowable strength. Because fibers are weak in compression compared to tension, the maximum compressive stress is computed in each element. The results are shown in Fig. 6.20 and Fig. 6.21 for 1.95 psi uniform load in a 3-D plot and contour lines, respectively. It is clear from these two figures that there are many critical regions.

To demonstrate the effect of considering single and multi-failure modes, the probabilistic analysis is performed based on the maximum compressive stress through the

thickness for the whole plate. A comparison is made in terms of the safety index for different failure and the results are shown in Fig. 6.22 for the 64 elements mesh and Fig. 6.23 for the 256 elements mesh. It is clear from these two figures that a single failure mode is a nonconservative assumption because it produces higher values for the plate reliability. The analysis is also performed based on the maximum compressive stress at the center of the plate computed for a 64 and a 256 element mesh. Results are shown in Fig. 6.24 for the safety index, Fig. 6.25 for the reliability and Fig. 6.26 for the probability of failure for different compressive strength values. The reason a small difference appears between the two analyses is due to the fact that a fine mesh produces higher values for the stresses than a coarse mesh.

However, if the stress distribution over the whole plate is considered, it is clear that there is more than one critical region where the stress is equal or greater than the stress at the center of the plate. This means that for such a case, it is not justified to consider a single failure mode for the probabilistic analysis. The question now is how to handle such a case: if the failure of one element represents the failure of the plate, e.g., brittle failure, then the reliability of each element is to be computed and the total reliability of the plate is computed as the product of these individual reliabilities. But by doing this, the more elements in the mesh, the plate becomes less reliable, as shown in Fig. 6.27 for the safety index, Fig. 6.28 for the reliability and Fig. 6.29 for the probability of failure. It is shown in Fig. 6.27 and Fig. 6.28 that lower safety index and reliability are obtained for the 256 element mesh than for the 64 element mesh. In Fig. 6.29 higher probability of failure is obtained for the 256 element mesh than for the 64 element mesh.

To overcome this difficulty, the size of the element is introduced into the element strength as described in section 3.6. The results are shown in Fig. 6.30 for the safety index, Fig. 6.31 for the reliability and Fig. 6.32 for the probability of failure. It is seen that the same results are obtained regardless of the mesh size. The small difference be-

tween the two meshes is due to the fact that the fine mesh produces higher stresses than the coarse one. A comparison between different meshes with and without size effect is shown in Fig. 6.33 for the safety index, Fig. 6.34 for the reliability and Fig. 6.35 for the probability of failure. It is seen that by including the size of element in the probabilistic model, reasonable values for the safety index, the reliability and the probability of failure are obtained and they are independent of the number of elements in the domain.

A comparison is also made for the safety index which includes different meshes, all elements with and without size effect, and critical modes. The result is shown in Fig. 6.36. It shows that when the size of the element is included in the probabilistic mode, the values of β obtained by size effect are independent of the number of elements in the mesh. They are also close to the one obtained when critical modes are considered only. This result is good because it can be used for problems where the critical or failure modes are not clear.

6.5 Conclusions

Results have shown the sensitivity of the response (deflection) to the variation in the design parameters. For example, in Fig. 6.5 a 10% variation in each of the design variables produces more than 13% variation in the central deflection. In fact the linear analysis produces more variation than the nonlinear one. For this reason the standard deviation of the deflection for linear analysis is much higher than for the nonlinear one in Fig. 6.11.

Results have also shown that the variation in the strength produces higher probability of failure than the variation in the load (Fig. 6.10 and Fig. 6.16). Therefore, in a certain design it is more efficient to control the strength than control the load.

It is noticed that the period for the nonlinear analysis is less than that for the linear one. This happens because the nonlinear analysis assumes a stiffer plate. However, when computing the progressive probability of failure for a short period of time the linear analysis has produced higher values than the nonlinear one (Fig. 6.6 and Fig. 6.7). On the other hand, if the analysis is performed for longer periods of time, the nonlinear analysis will produce greater probability of failure than the linear one.

In Fig. 6.20 some of the bending stress values are close to zero away from the corners of the plate and high at the corners. This is because the two simply supported sides at each corner make the corner act as a fixed end, which produces high bending stress at each corner and causes a change in curvature of the vertical displacement as shown in Fig. 6.4. The points where the curvature changes sign are called inflection points that correspond to zero moment and consequently zero bending stresses.

Table 6.1 Design variables for laminated composite plate

Variable	Mean	standard deviation	Coefficient of variation δ
E_{11} (psi)	7.8 E + 06	7.8 E + 05	0.10
E_{22} (psi)	2.6 E + 06	2.6 E + 05	0.10
$G_{12} = G_{13} = G_{23}$ (psi)	1.3 E + 06	1.3 E + 05	0.10
ν_{12}	0.25	0.025	0.10
θ_1	+ 45	4.5	0.10
θ_2	- 45	4.5	0.10
P (psi)	0.13 to 1.3	0.013 to 0.13	0.10
	0.13 to 1.3	0.026 to 0.26	0.20
R (in)	0.8, 1.0, 1.5	0.08, 0.1,0.15	0.10
	0.8, 1.0, 1.5	0.16, 0.2,0.30	0.20
R (psi)	7.5E3 to 22.5E3	7.5E2 to 22.5E2	0.10
h_i (in)	0.01	---	---
a (in)	100	---	---

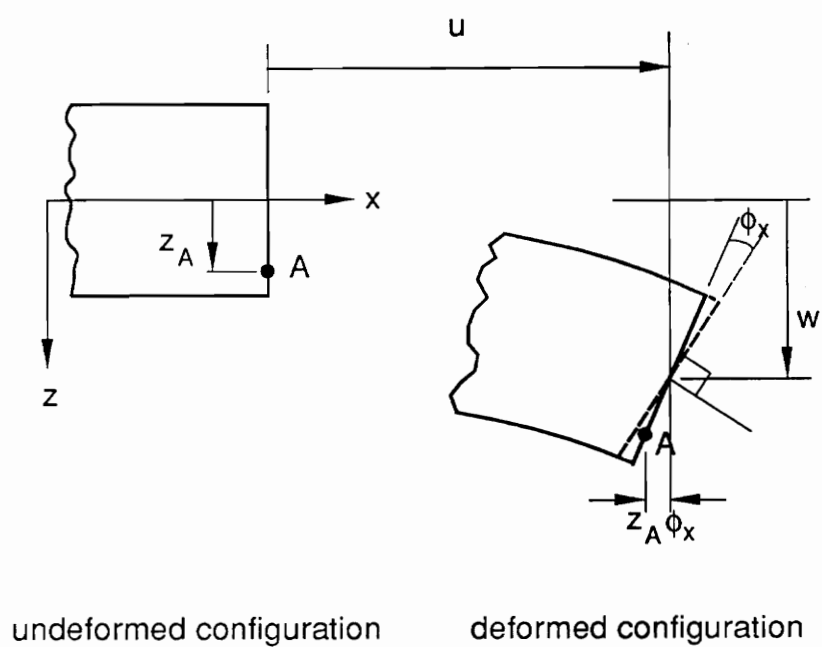


Fig. 6.1 Geometry of the undeformed and deformed xz plane

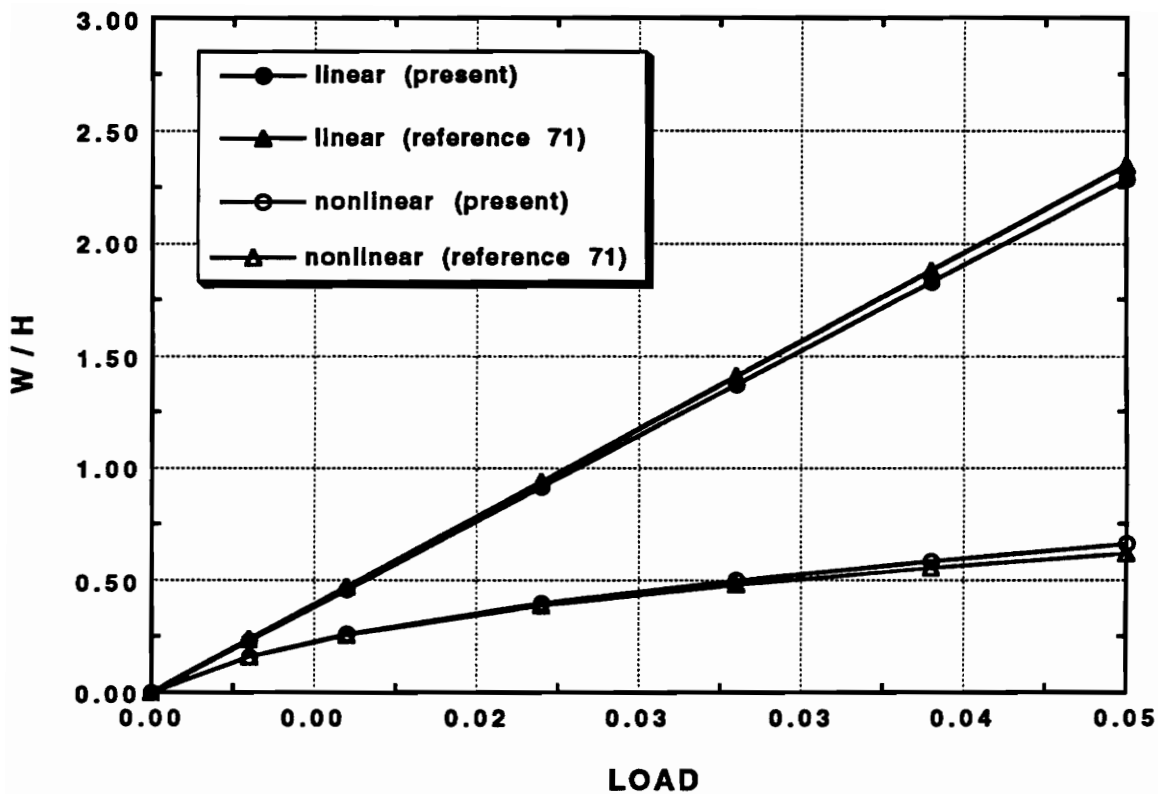


Fig 6.2 Center deflection for $[90/0]_T$ S.S. plate under uniform load, comparison between present study and reference [71]

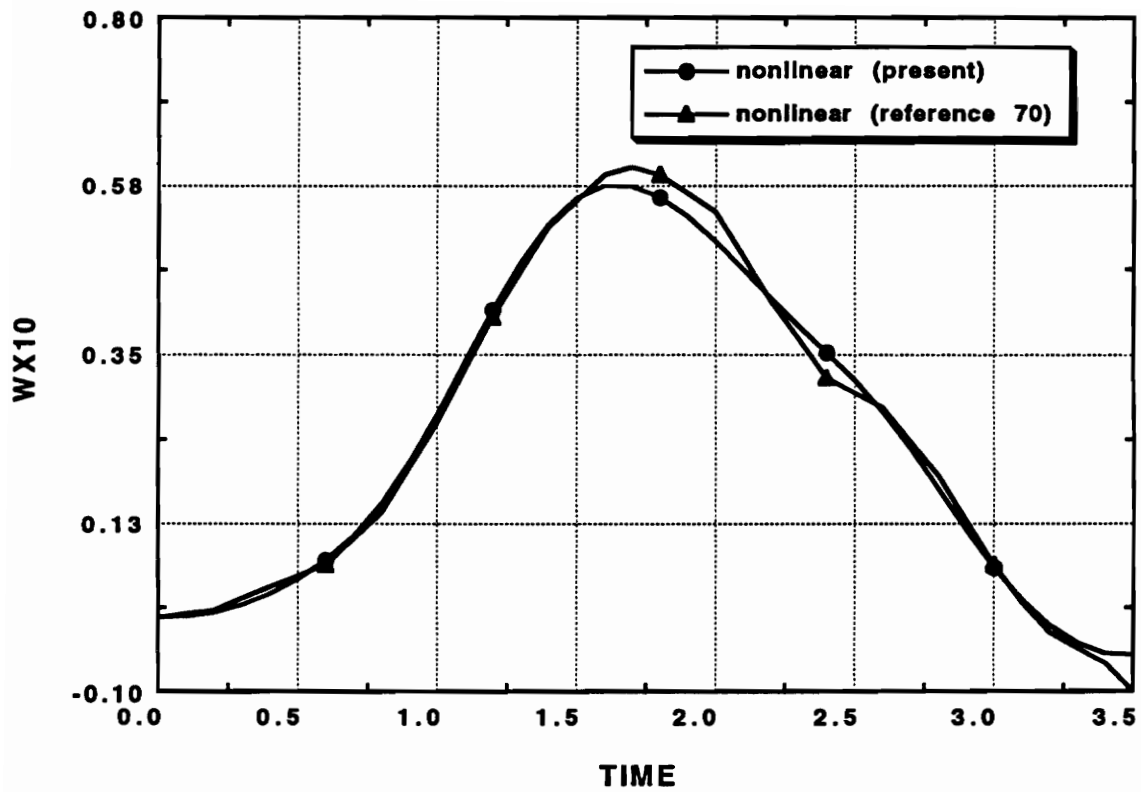


Fig. 6.3 Center deflection for $[45/-45]_T$ S.S. plate under time dependent load; comparison between present solution and reference [70]

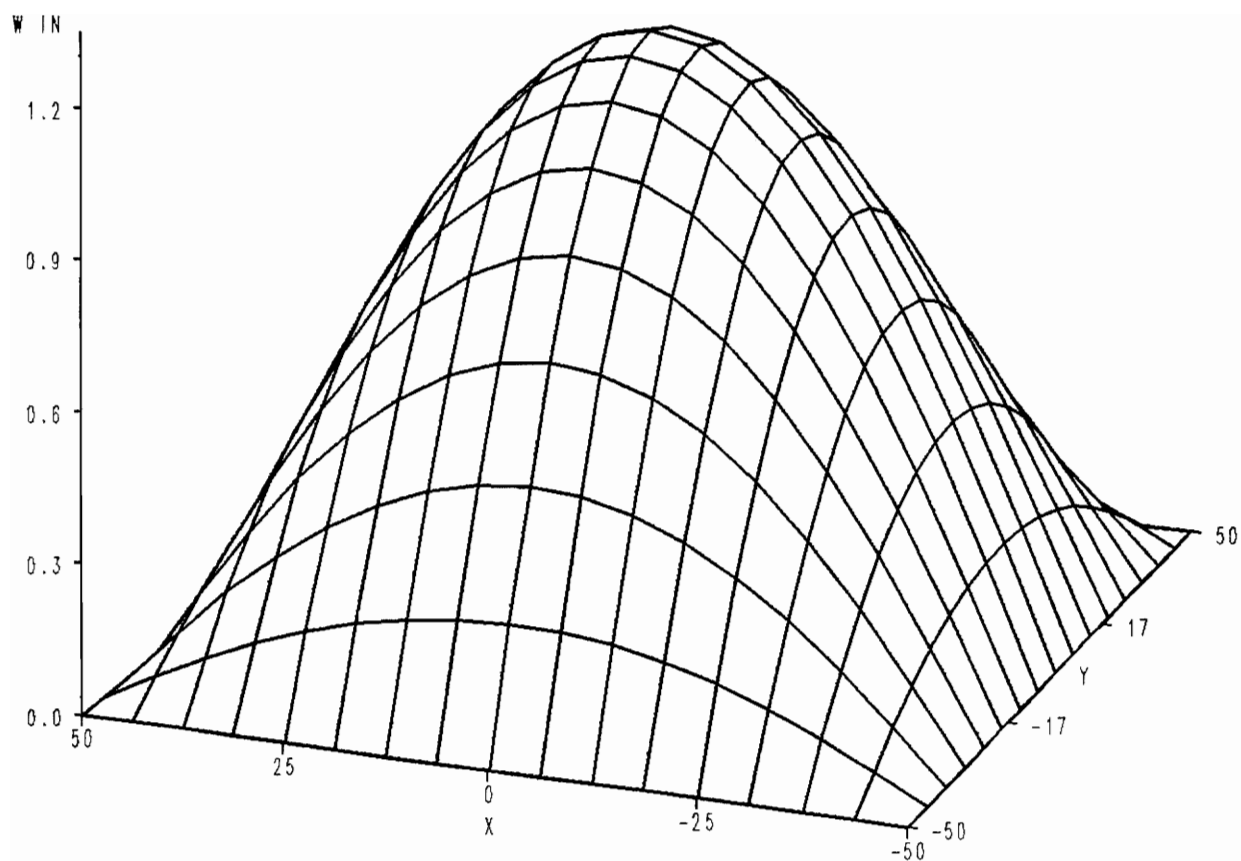


Fig. 6.4 The vertical deflection of $[\pm 45/25]_s$ simply supported plate under a uniform load of 1.3 psi or load factor of 50

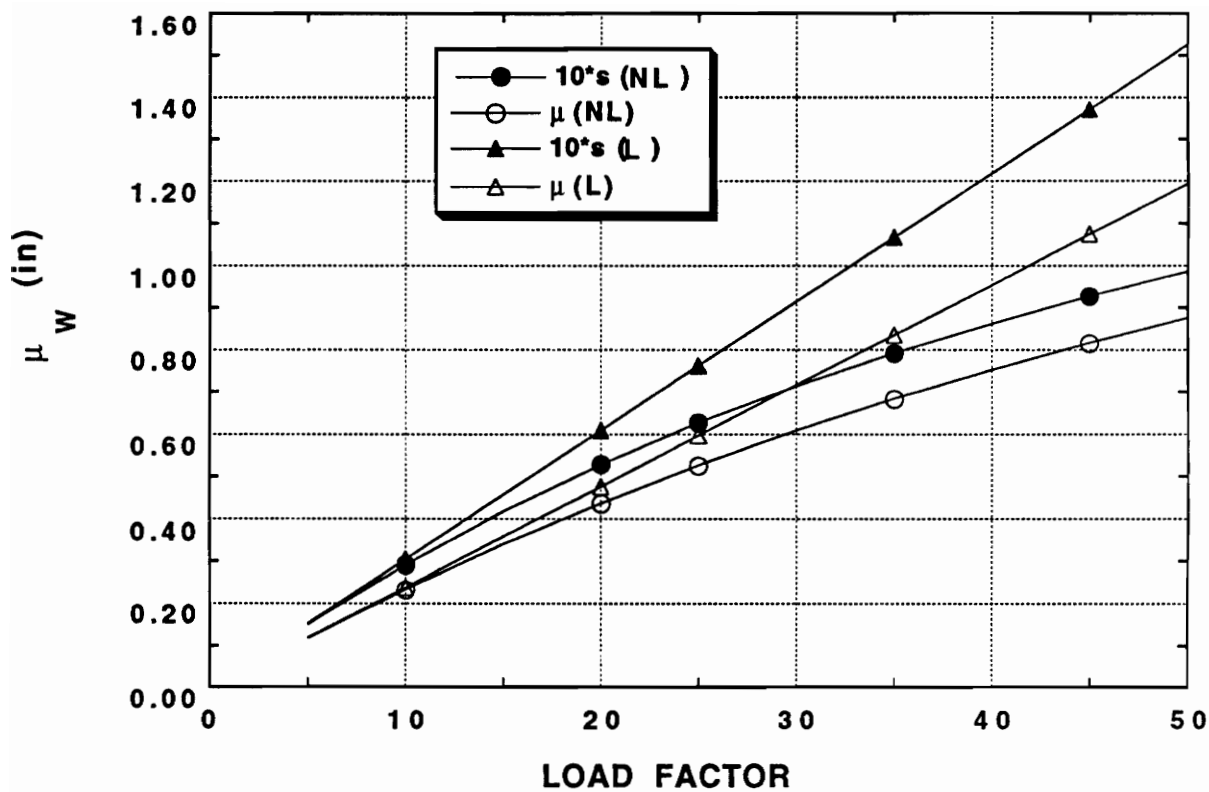


Fig. 6.5 Mean and standard deviation of W for linear and nonlinear analyses, $\delta = 0.1$

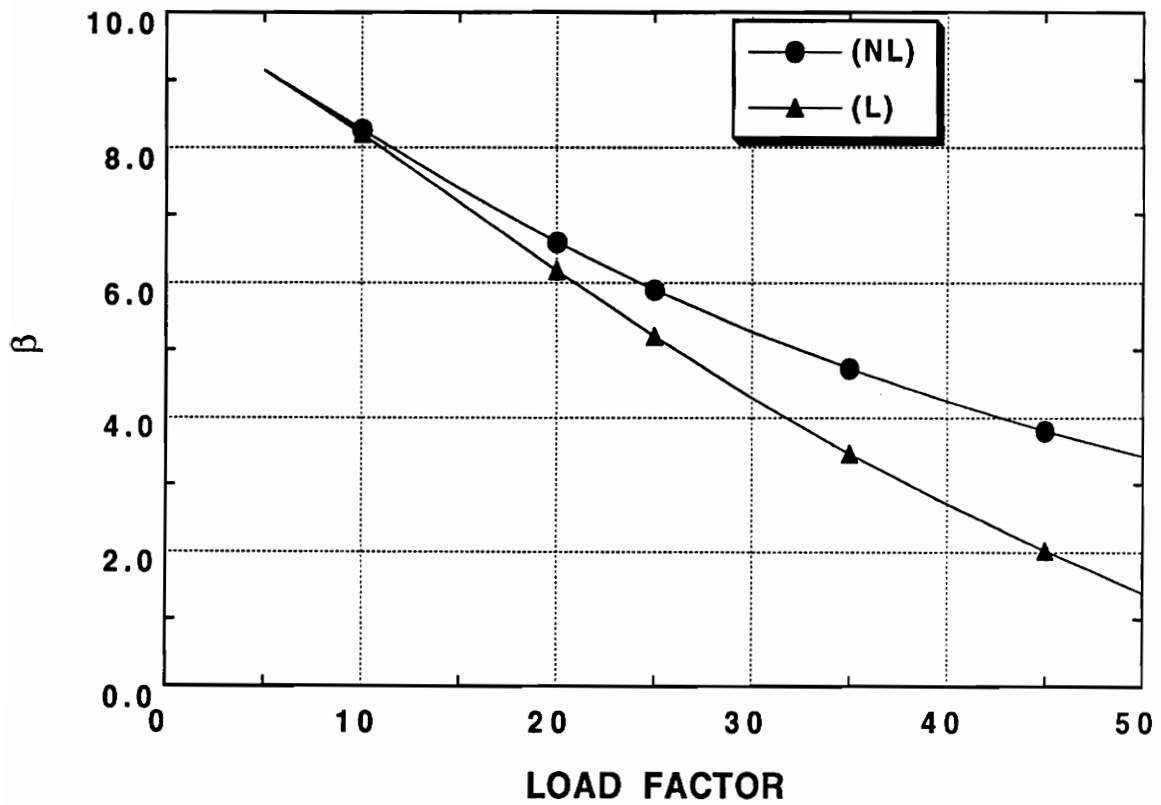


Fig. 6.6 Safety index with load for linear and nonlinear analyses, $R = 1.5''$ and $\delta = 0.1$

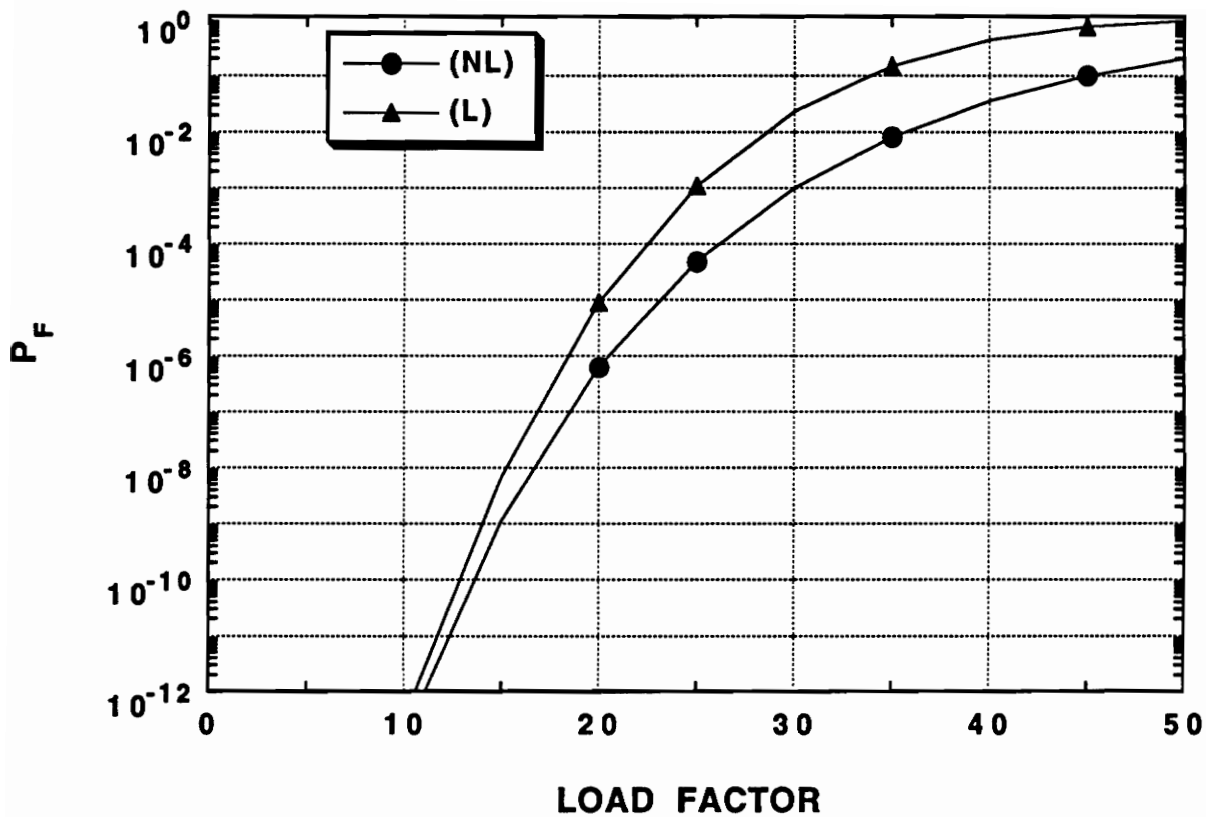


Fig. 6.7 Probability of failure with load for linear and nonlinear analyses ($R=1.5''$ and $\delta=0.1$)

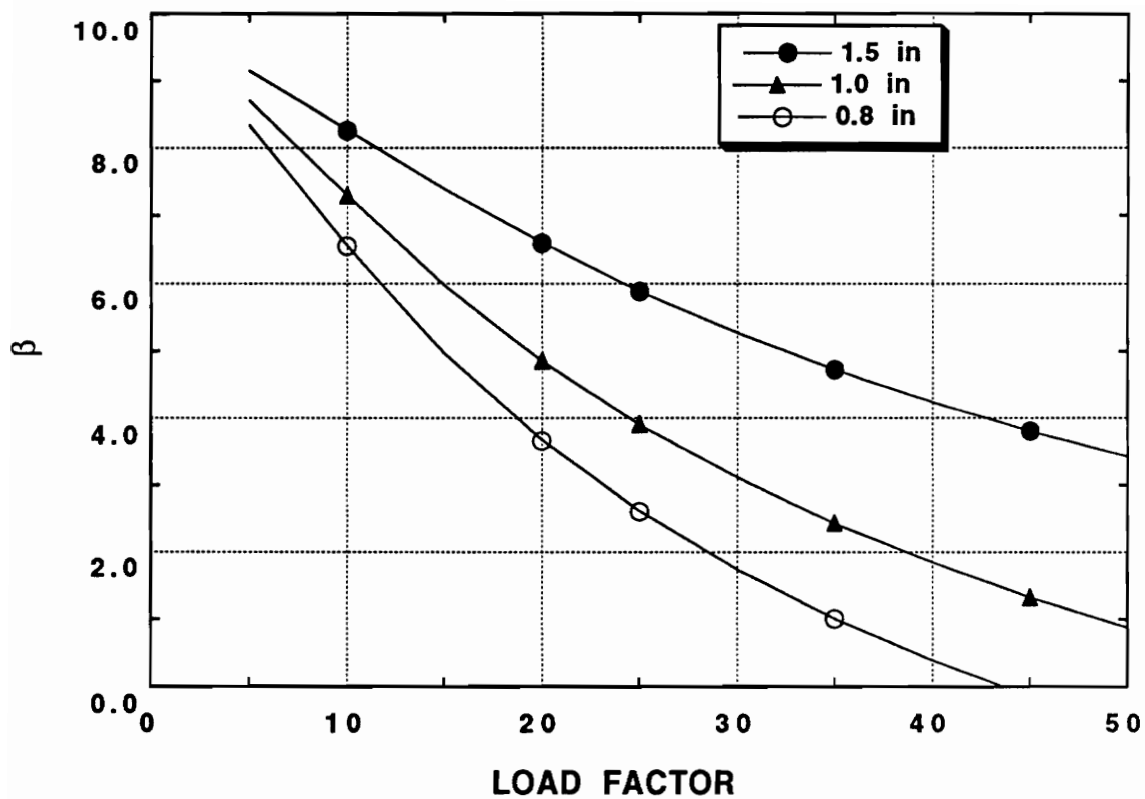


Fig. 6.8 Safety index with load for different values of R and nonlinear analysis, $\delta = 0.1$

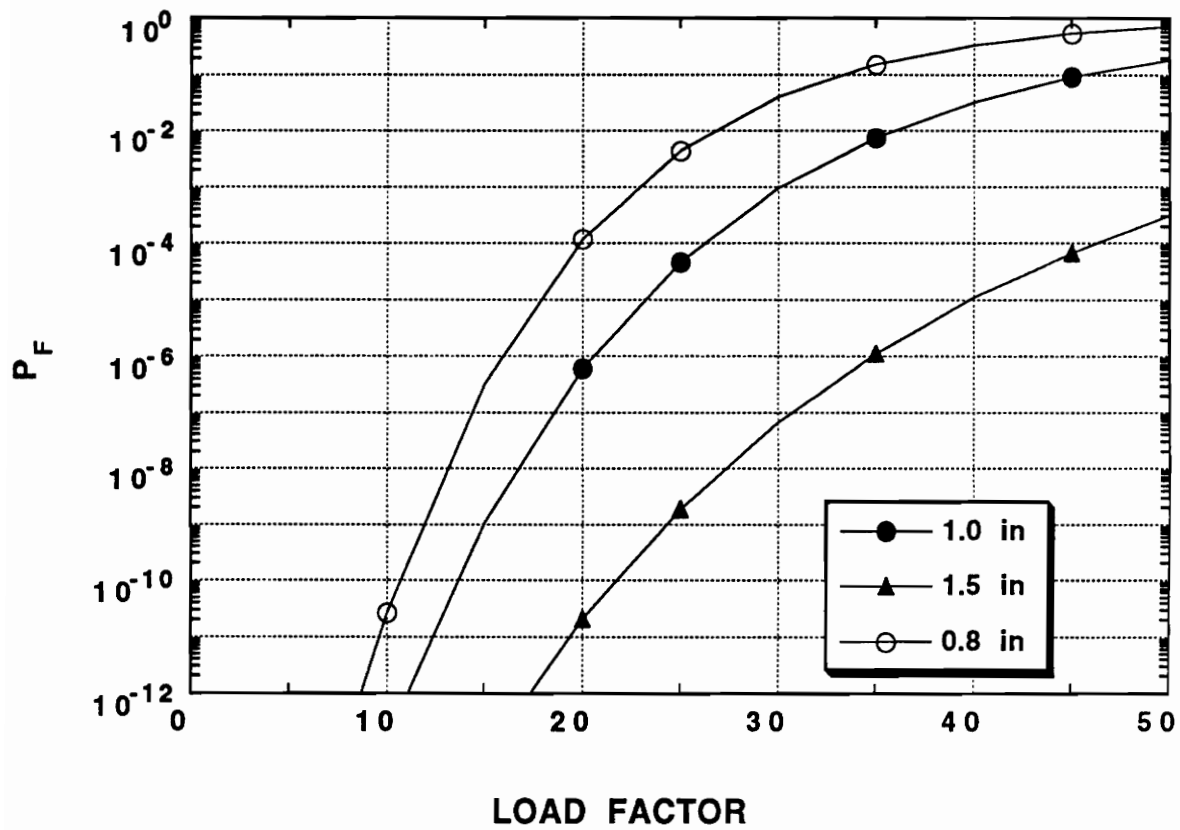


Fig. 6.9 Probability of failure with load for different values of R and nonlinear analysis ($\delta = 0.1$)

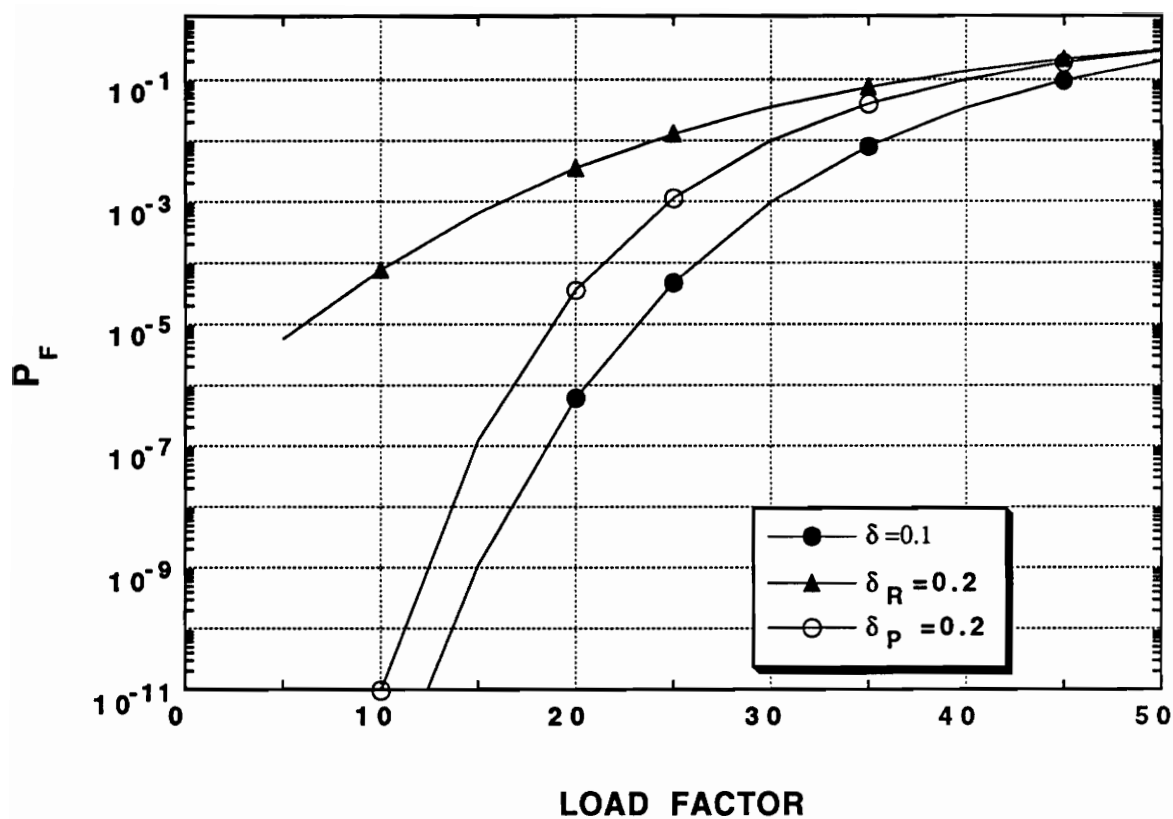


Fig. 6.10 Probability of failure for different coefficients of variation and nonlinear analysis ($R=1.0$ in)

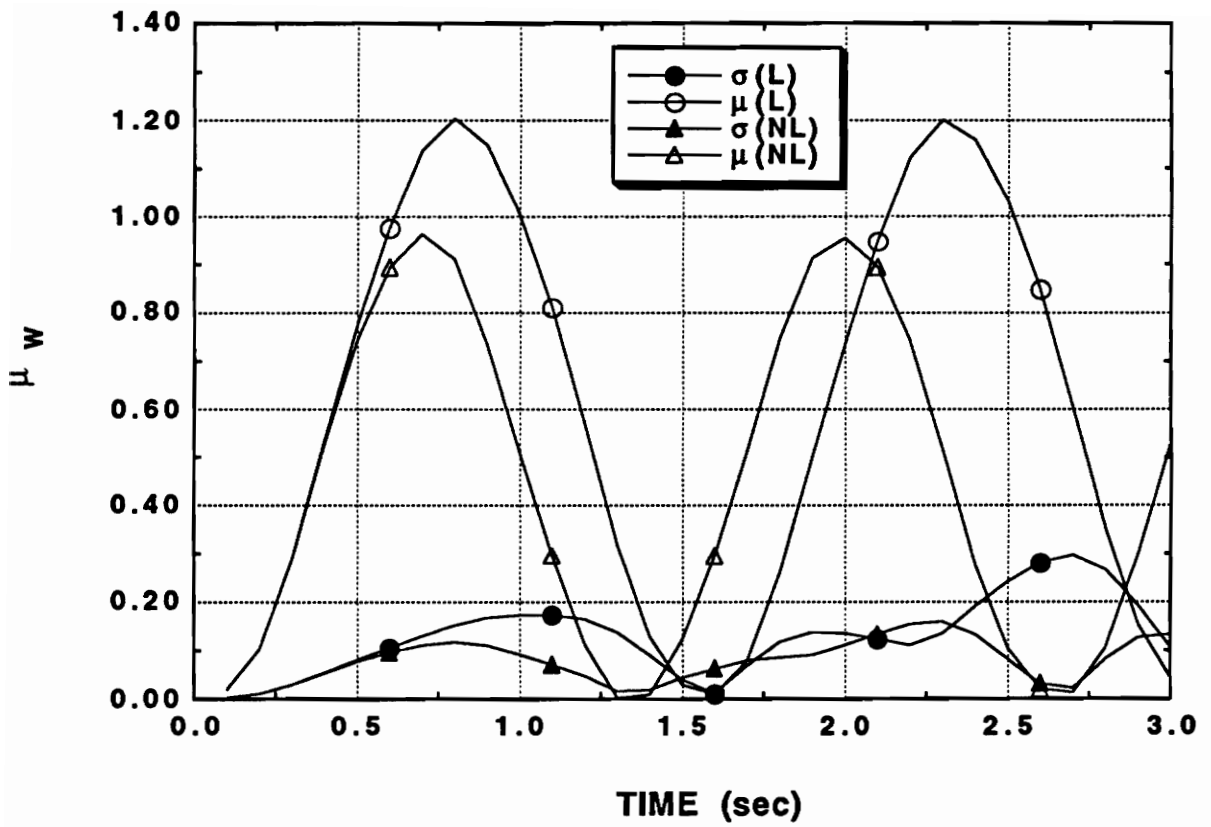


Fig. 6.11 Mean and standard deviation of W with time for linear and nonlinear analyses, $\delta = 0.1$ and load factor of 25

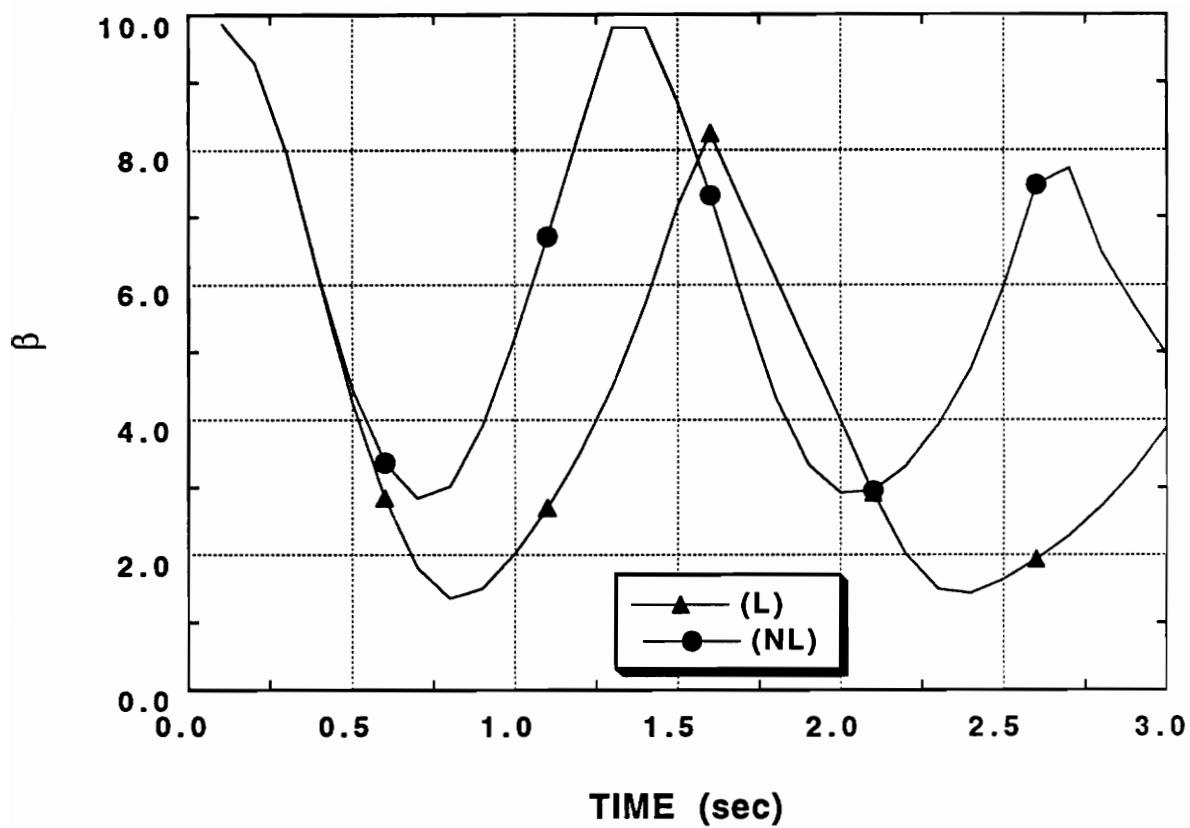


Fig. 6.12 Safety index with time for linear and nonlinear analysis
 $\delta=0.1$, $R=1.5$ in and load factor of 2.5

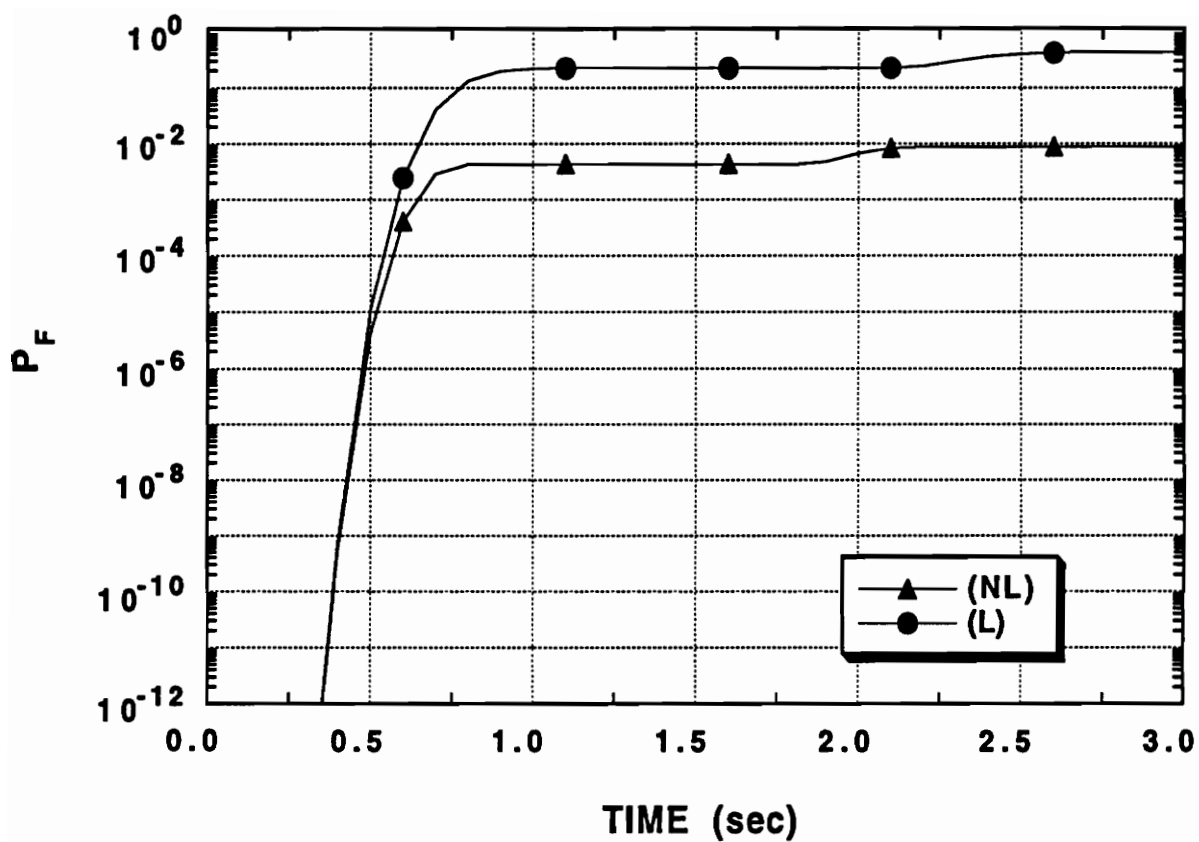


Fig. 6.13 Progressive probability of failure with time for linear and nonlinear analyses, $\delta=0.1$, $R=1.5$ in. and load factor of 25

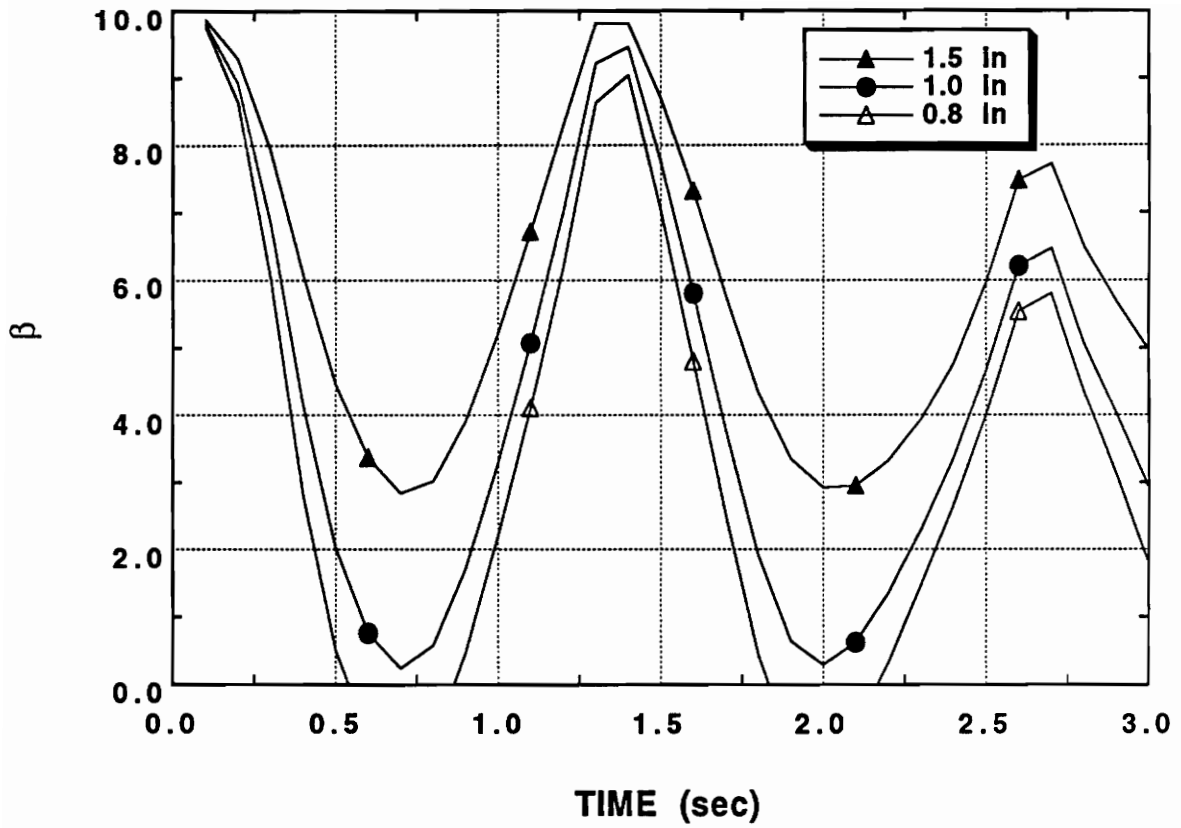


Fig. 6.14 Safety index with time for different values of R and nonlinear analysis, $\delta=0.1$ and load factor of 25

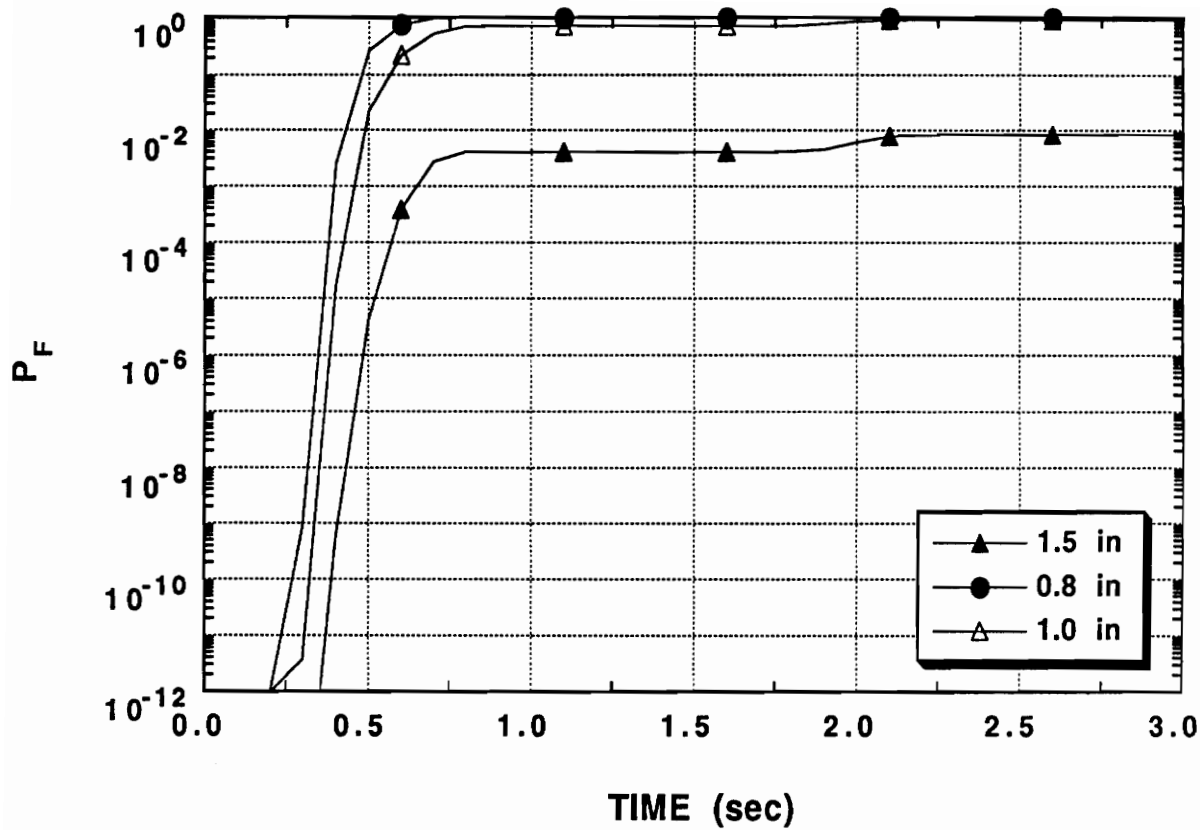


Fig. 6.15 Progressive probability of failure with time for different values of R and nonlinear analysis, $\delta=0.1$ and load factor of 25

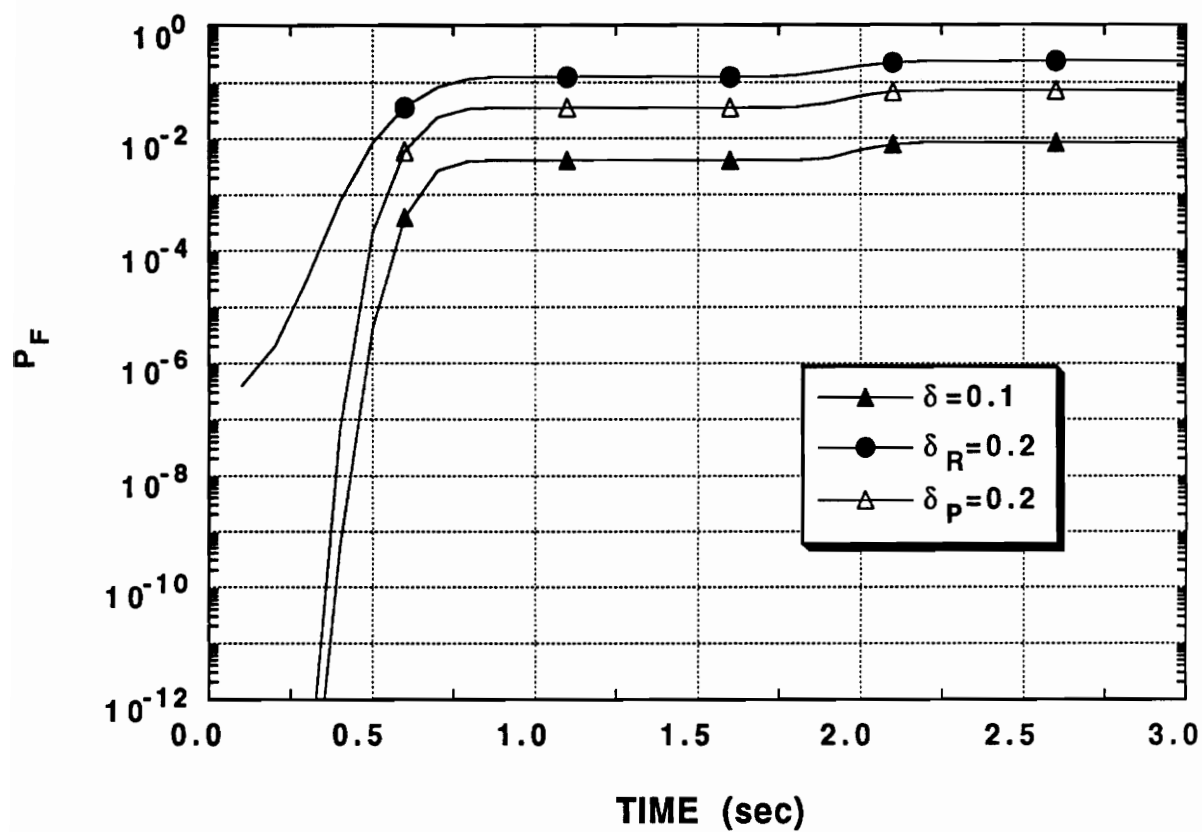


Fig. 6.16 Progressive probability of failure with time for different values of δ and nonlinear analysis, $R=1.5$ and load factor of 25

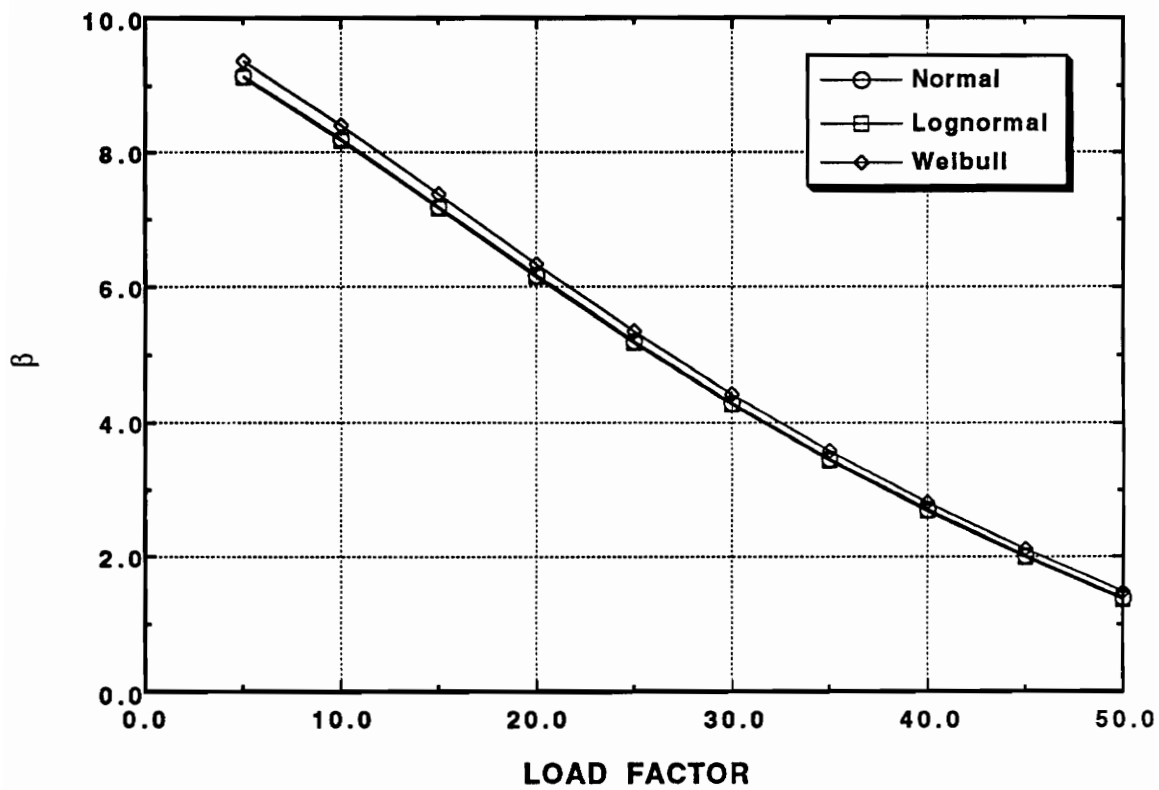


Fig. 6.17 Safety index with load for different strength distributions, $R=1.5$ and $\delta=0.1$

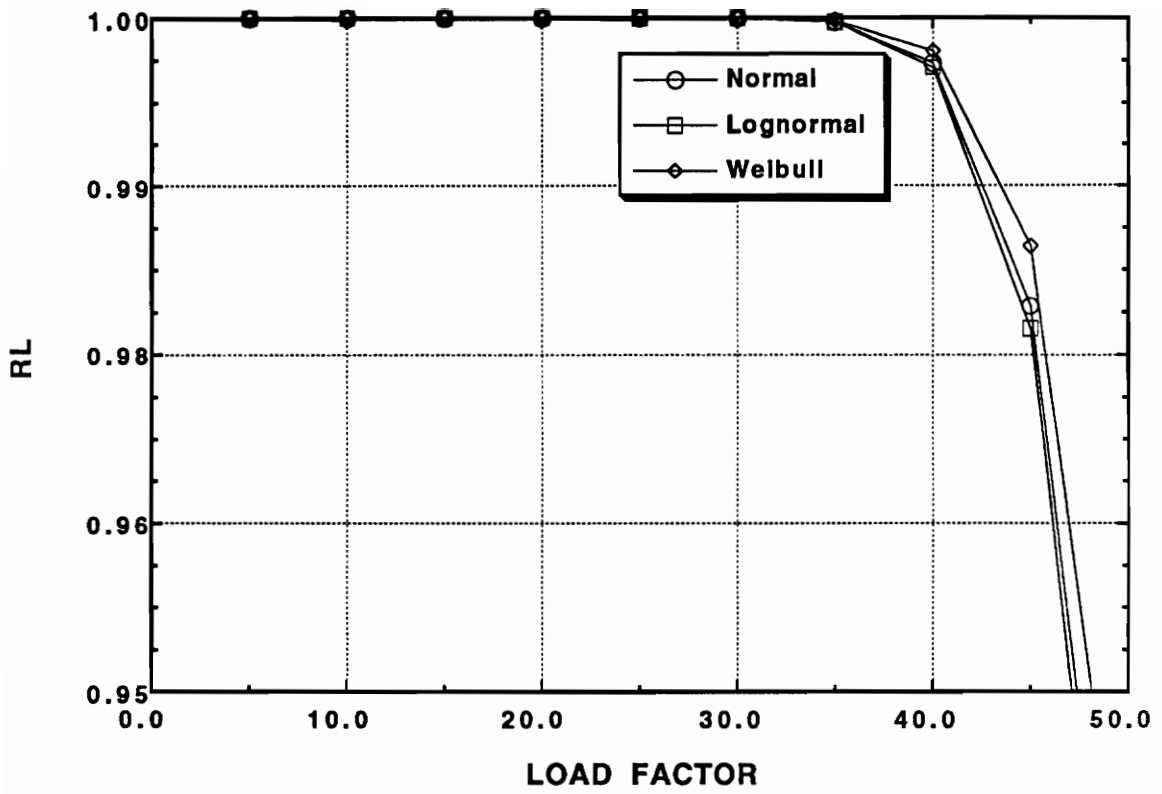


Fig. 6.18 Reliability with load for different strength distributions, $R=1.5$ in and $\delta = 0.1$

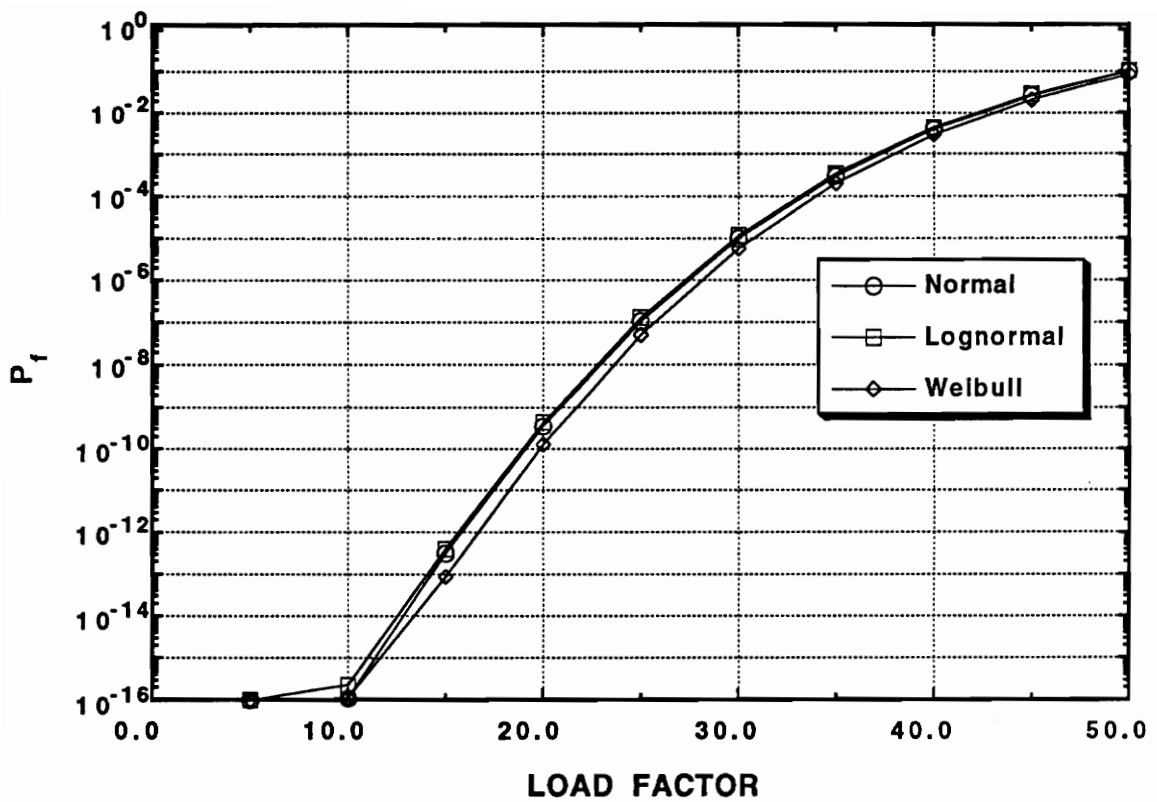


Fig. 6.19 Probability of failure with load for different strength distributions, $R=1.5$ in and $\delta=0.1$

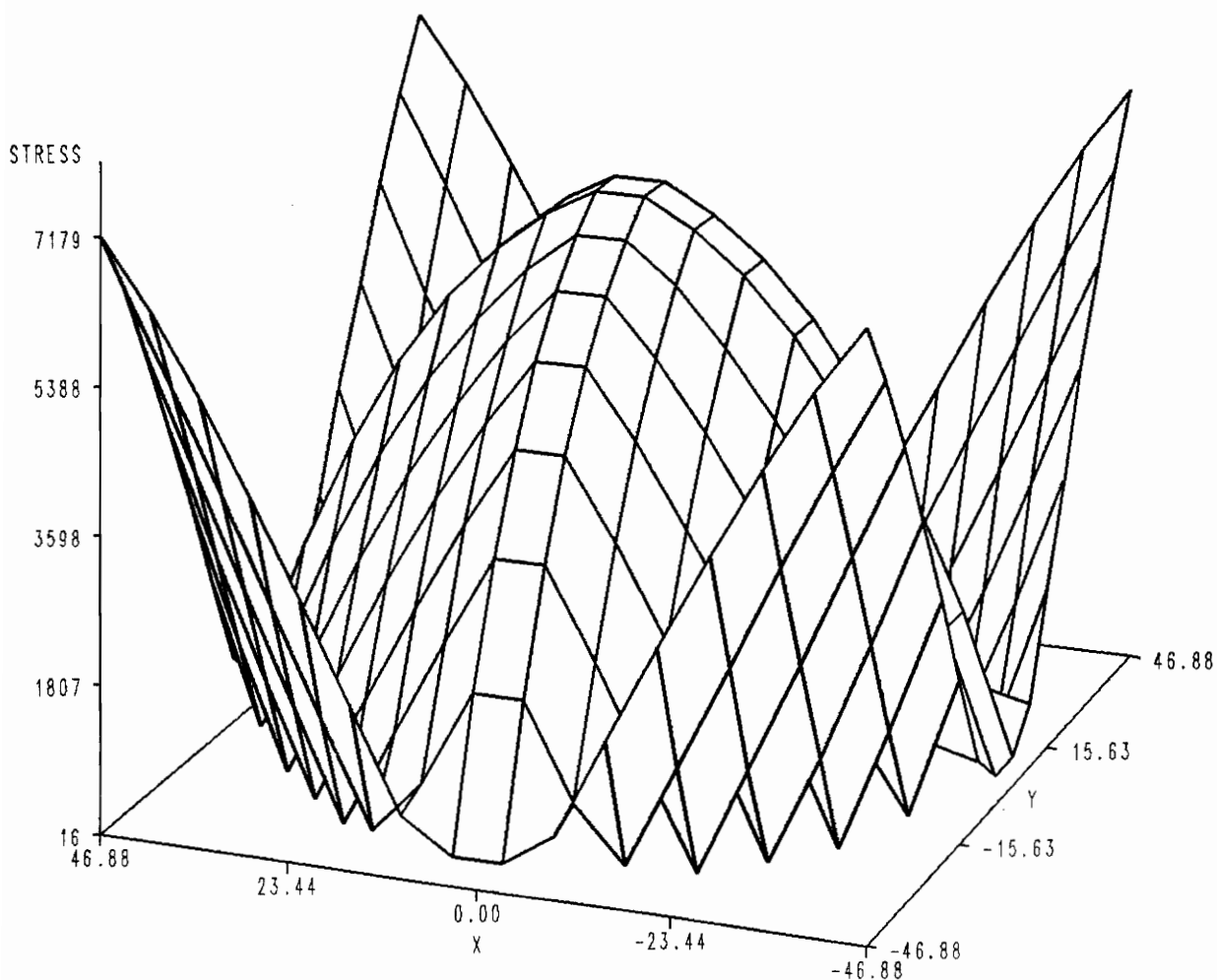


Fig. 6.20 Compressive stress over the plate due to a 1.95 psi uniform load or 75 load factor and linear analysis (256 elements mesh)

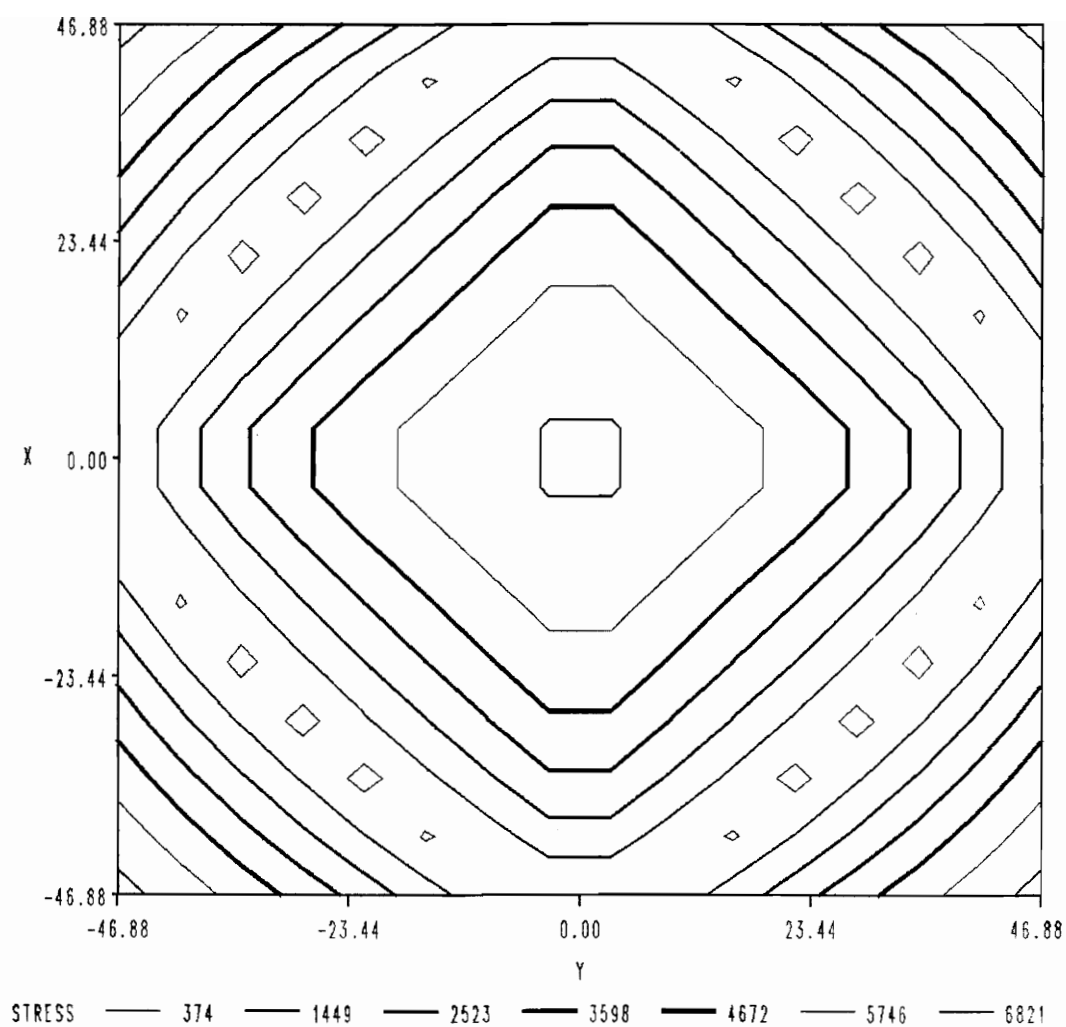


Fig. 6.21 Compressive stress contours over the plate due to a 1.95 psi uniform load or 75 load factor and linear analysis (256 elements mesh)

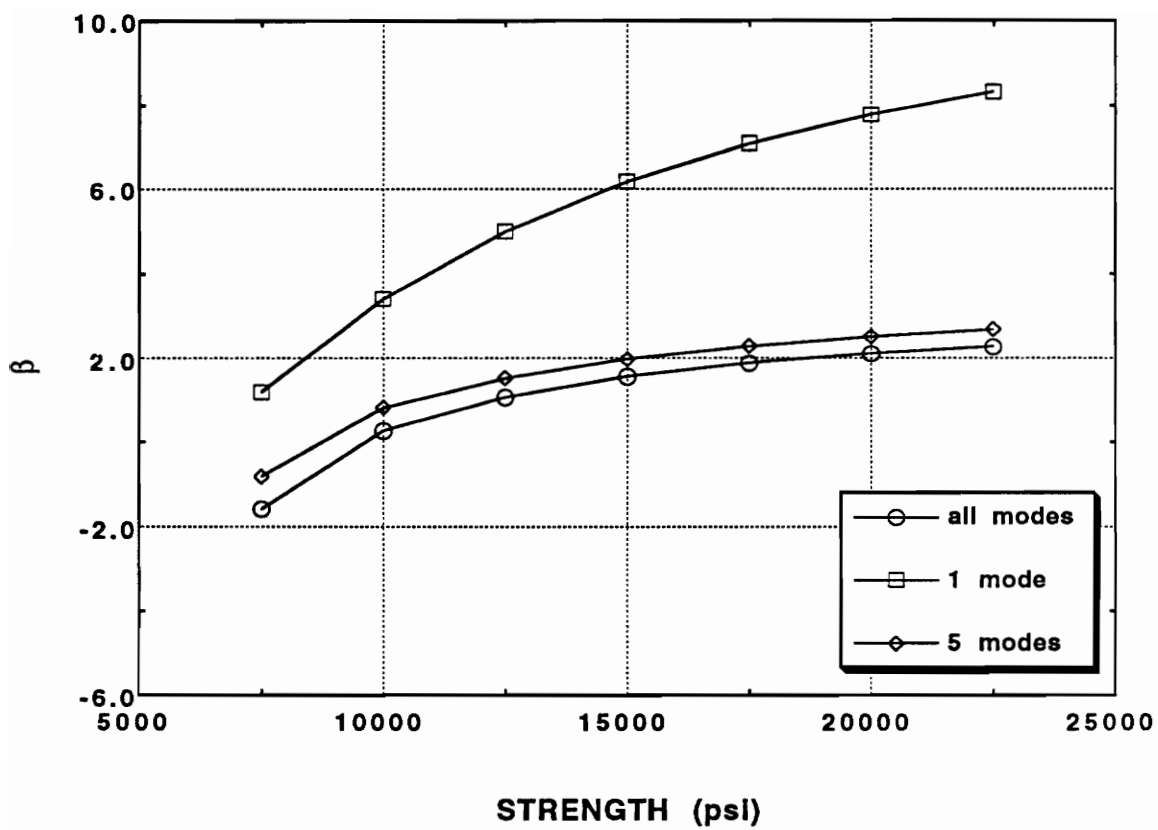


Fig 6.22 Safety index with strength for a 64 elements mesh and different failure modes

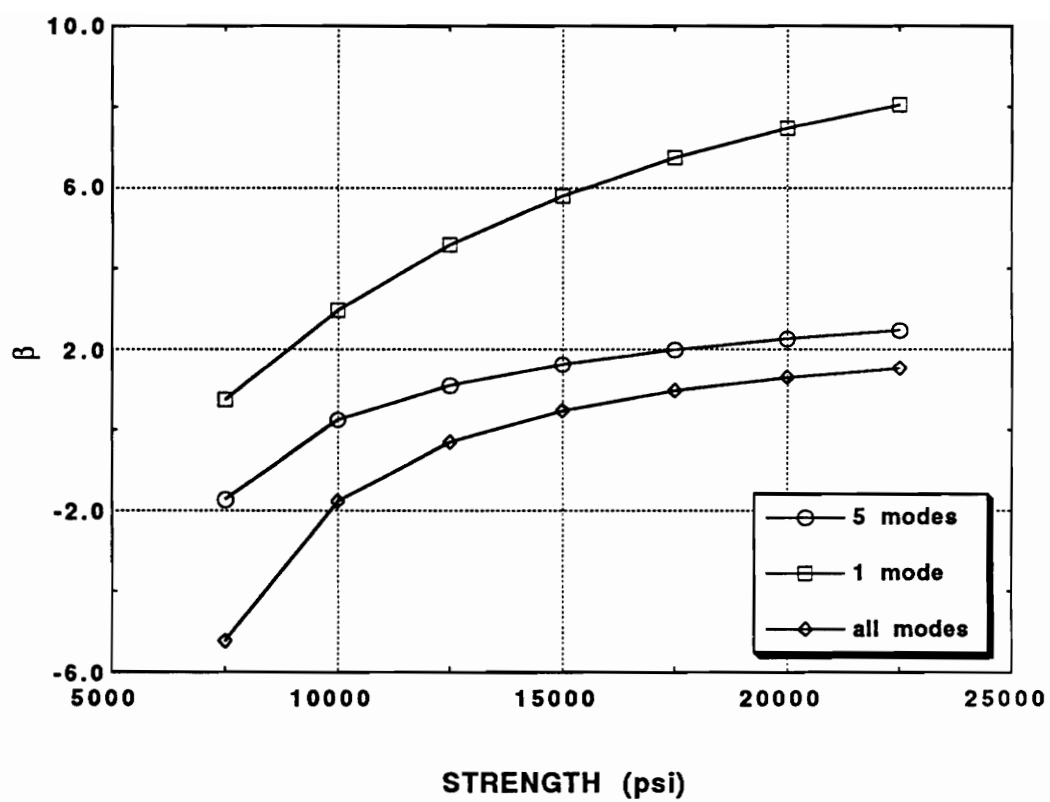


Fig. 6.23 Safety index with strength for a 256 elements mesh and different failure modes

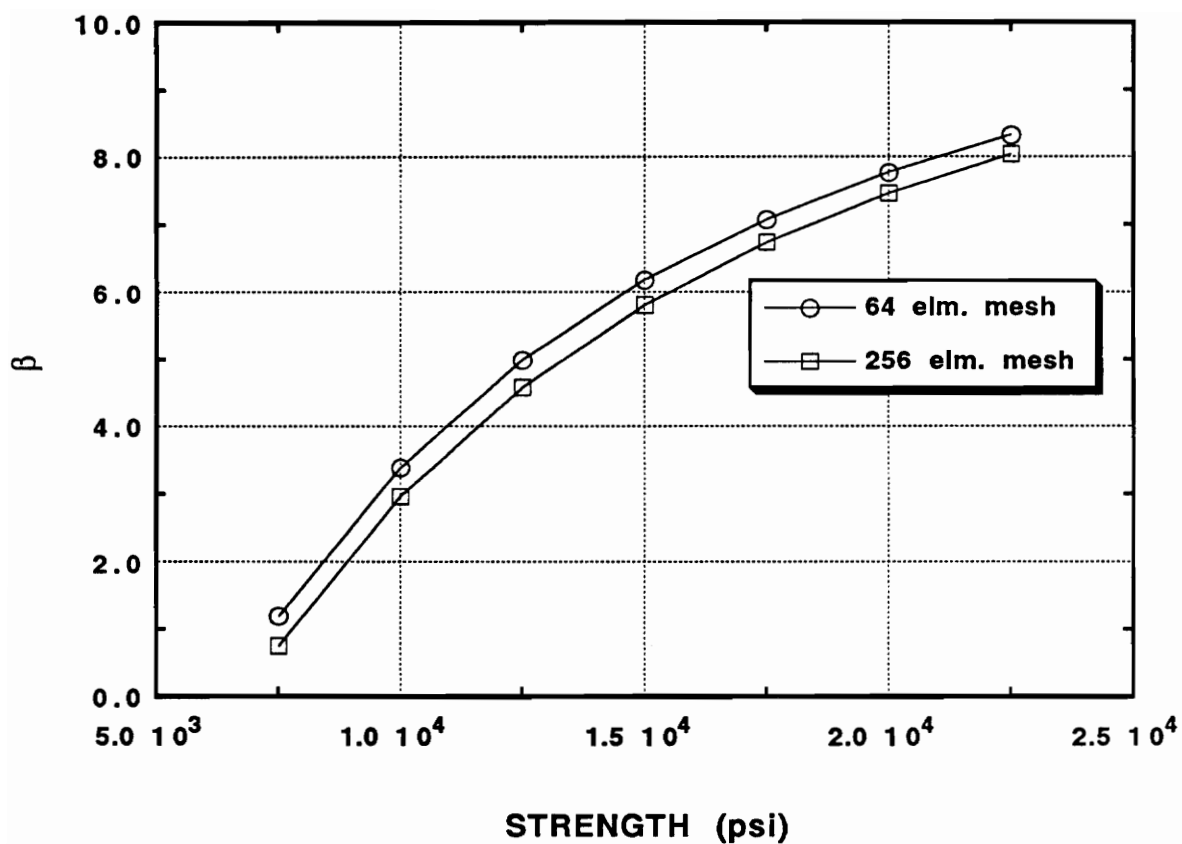


Fig. 6.24 Safety index with strength based on the maximum compressive stress at the center of the plate for different meshes

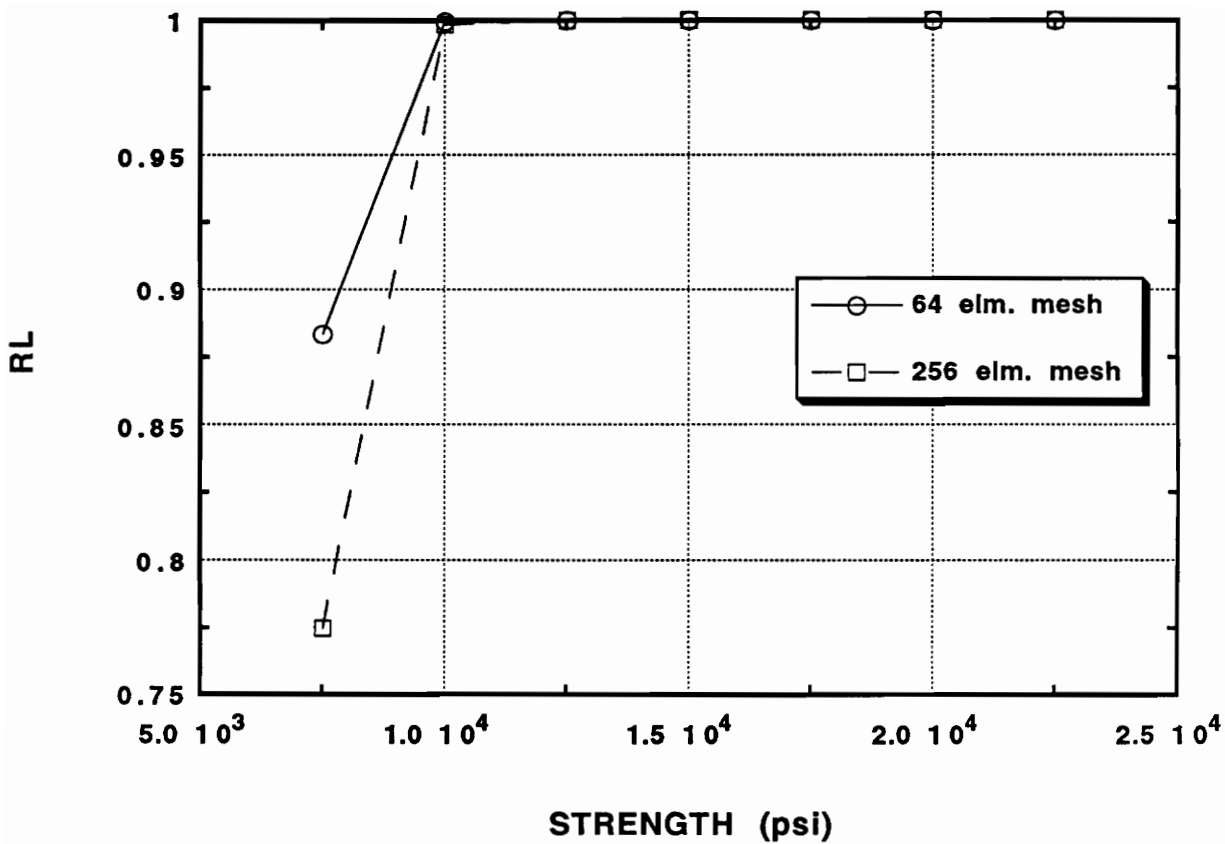


Fig. 6.25 Reliability with strength based on the maximum compressive stress at the center of the plate for different meshes

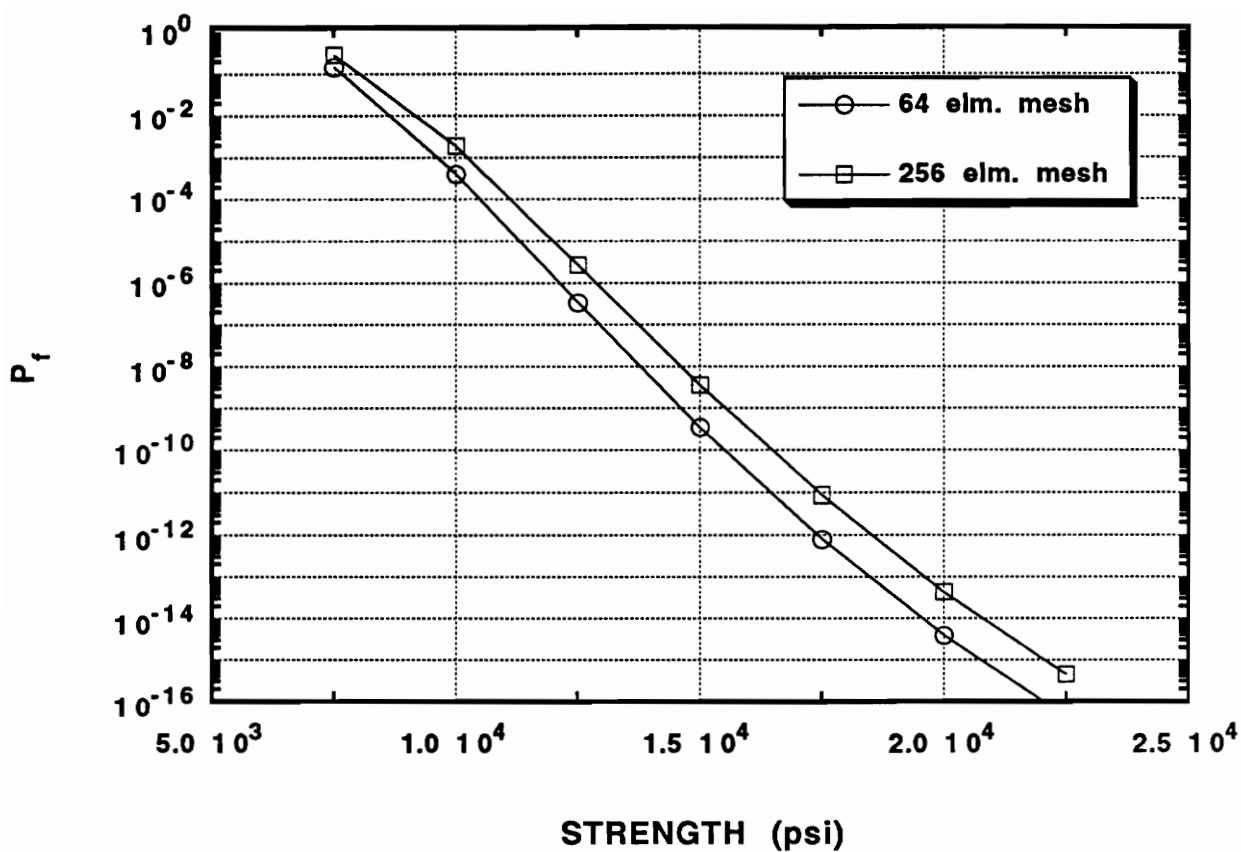


Fig. 6.26 Probability of failure with strength based on the maximum compressive stress at the center of the plate for different meshes

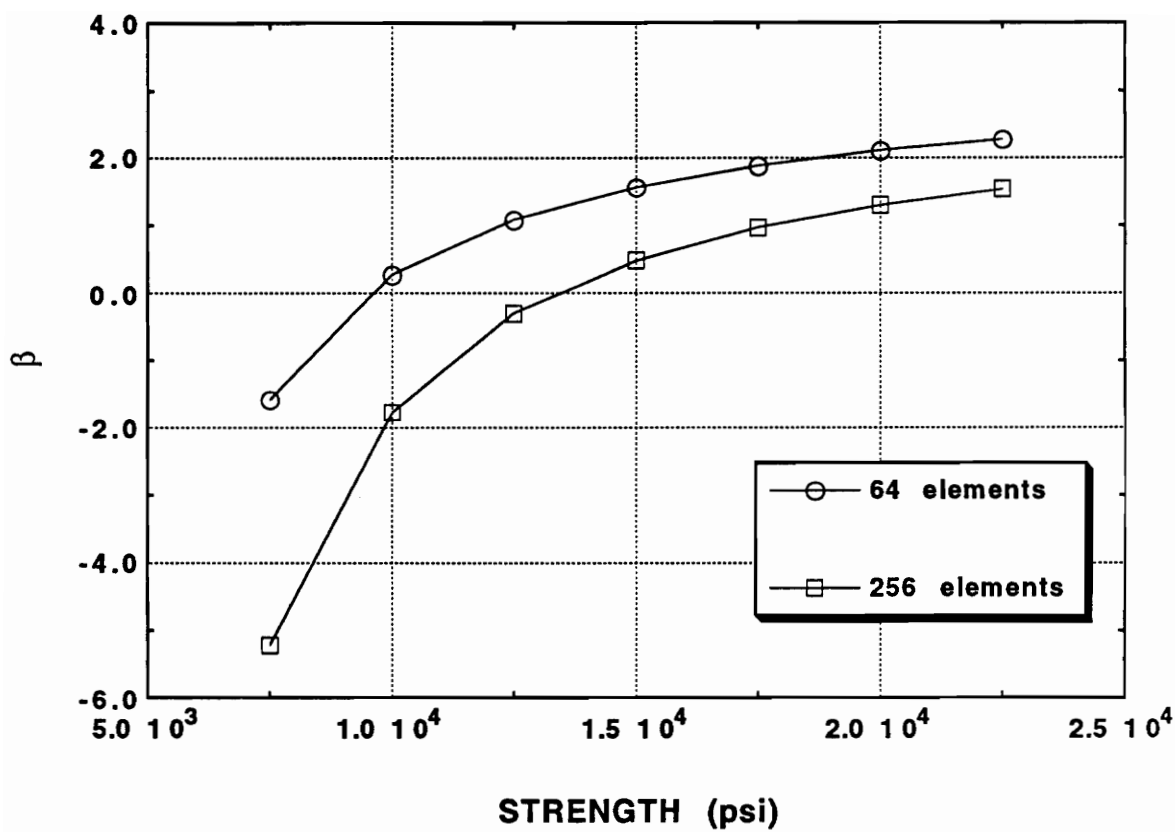


Fig. 6.27 Safety index with strength based on the maximum compressive stress for different meshes (no size effect included)

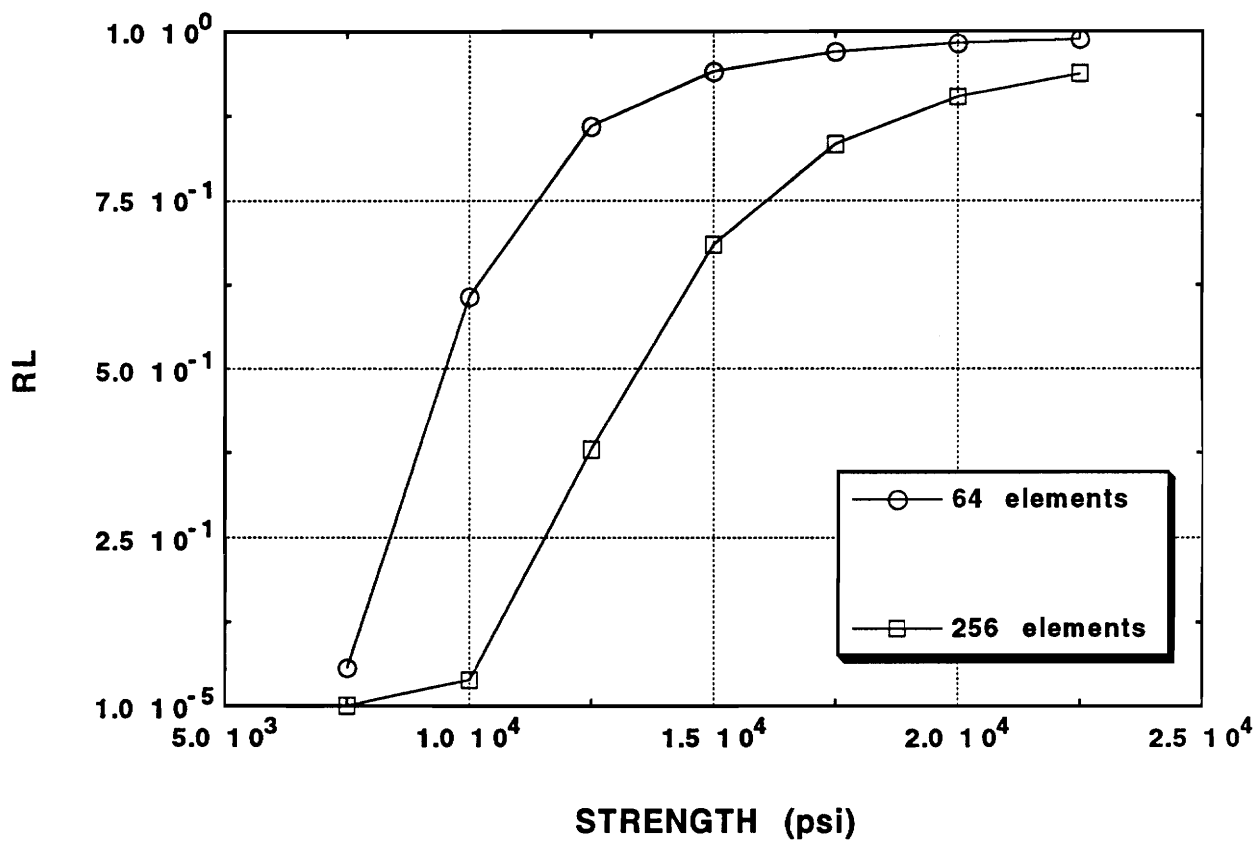


Fig. 6.28 Reliability with strength based on the maximum compressive stress for different meshes (no size effect included)

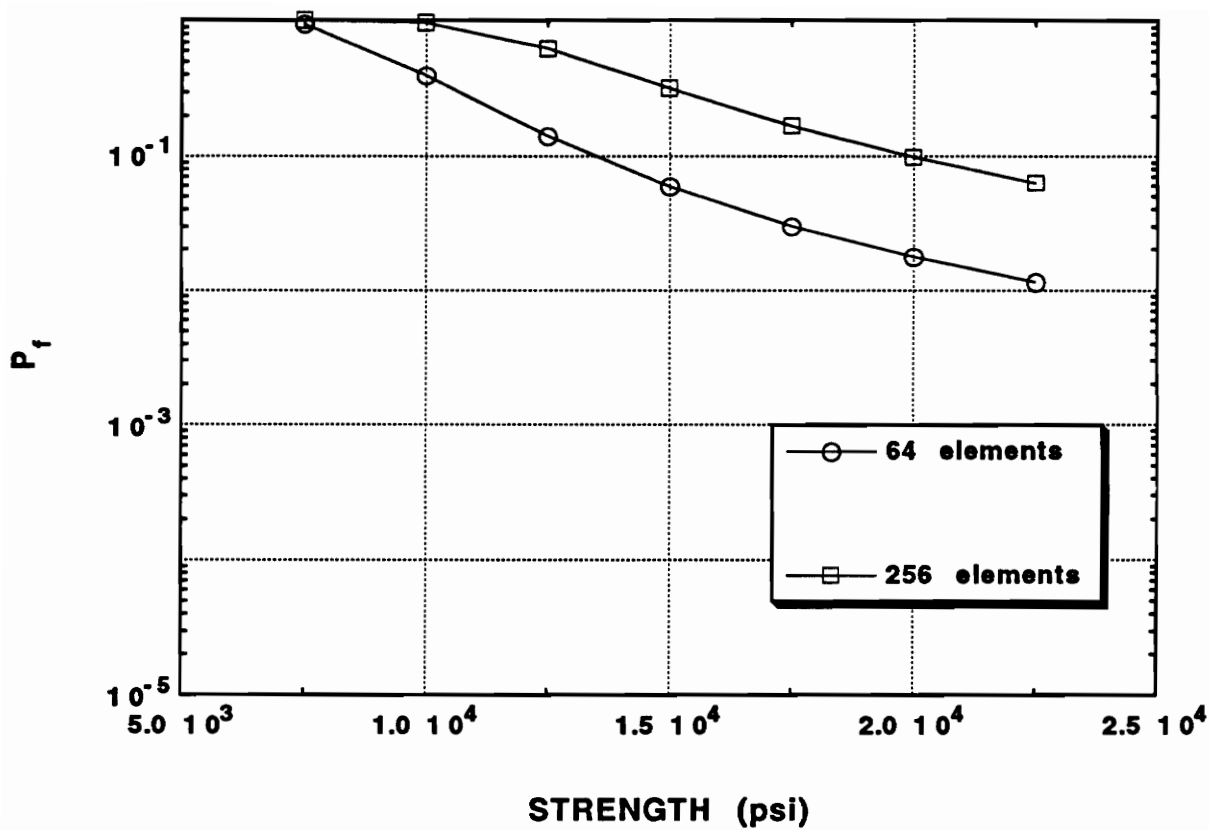


Fig. 6.29 probability of failure with strength based on the maximum compressive stress for different meshes (no size effect included)

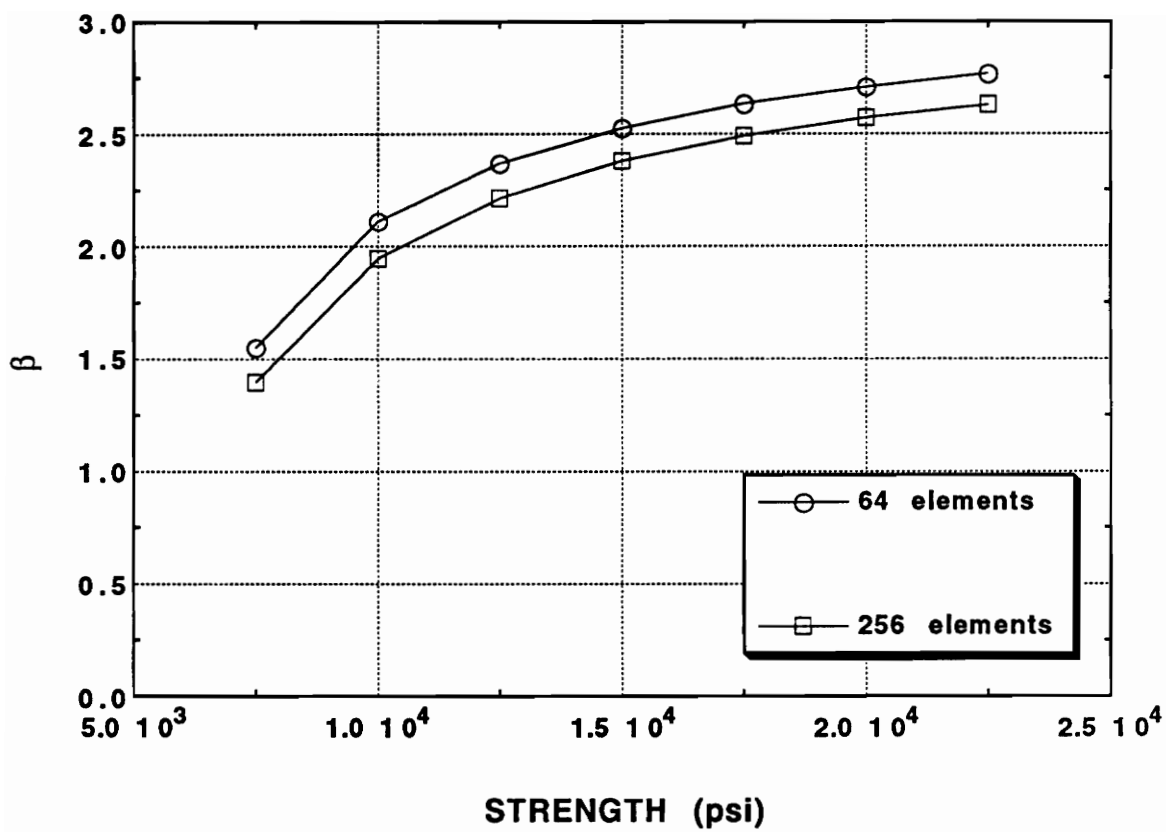


Fig. 6.30 Safety index with strength based on the maximum compressive stress for different meshes (size effect included)

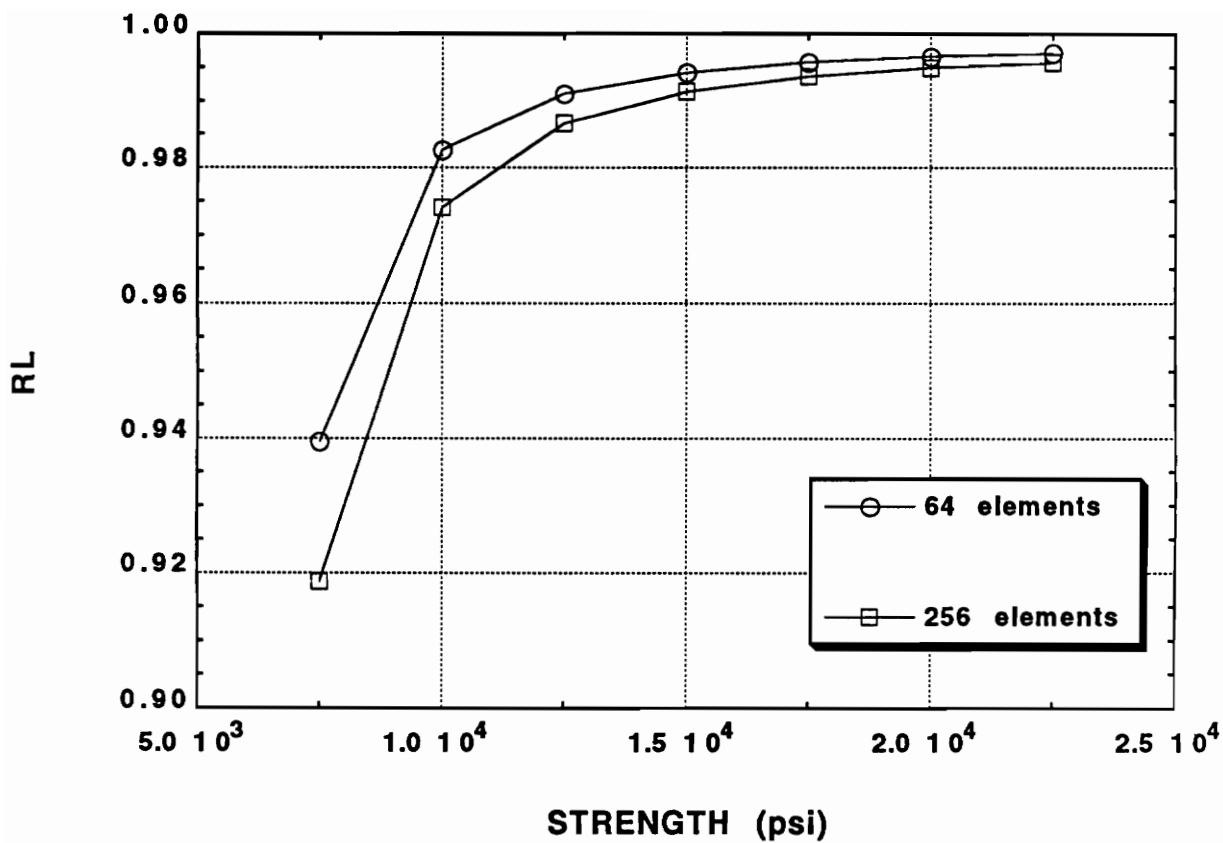


Fig. 6.31 Reliability with strength based on the maximum compressive stress for different meshes (size effect included)

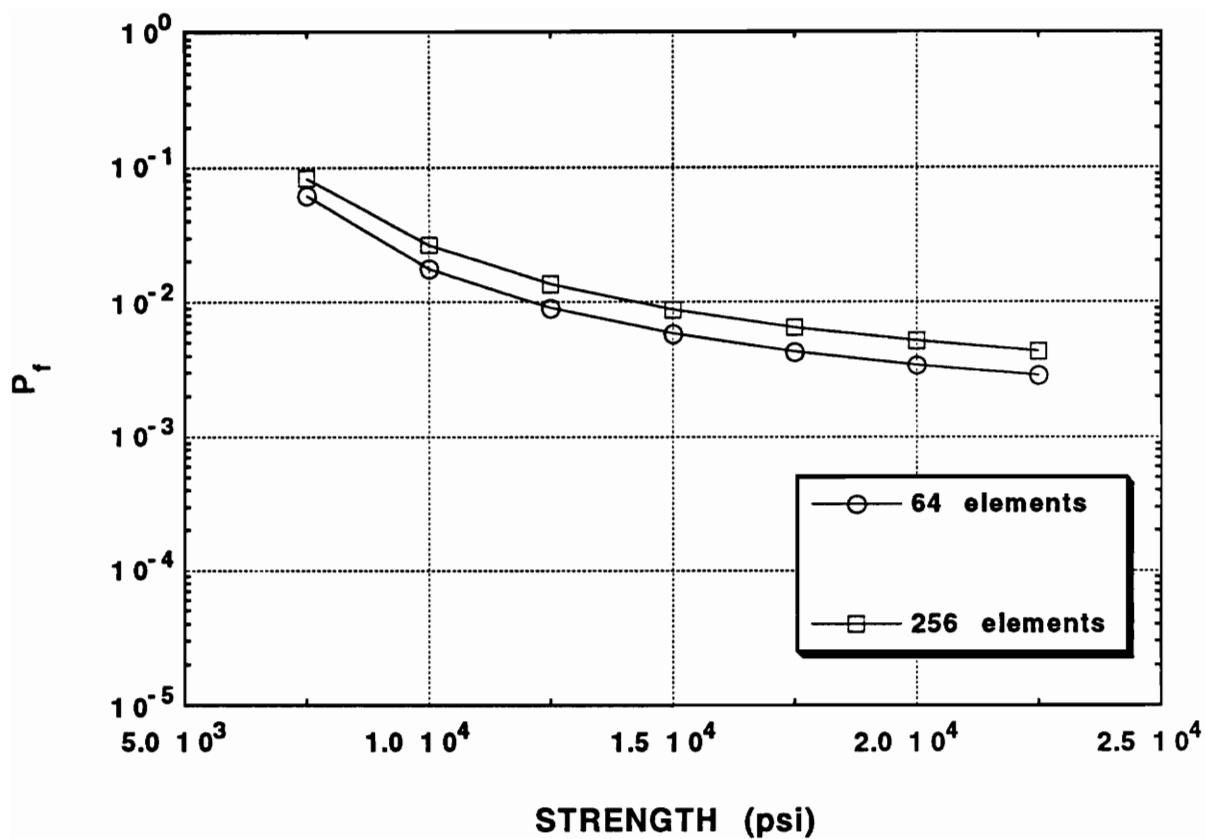


Fig. 6.32 probability of failure with strength based on the maximum compressive stress for different meshes (size effect included)

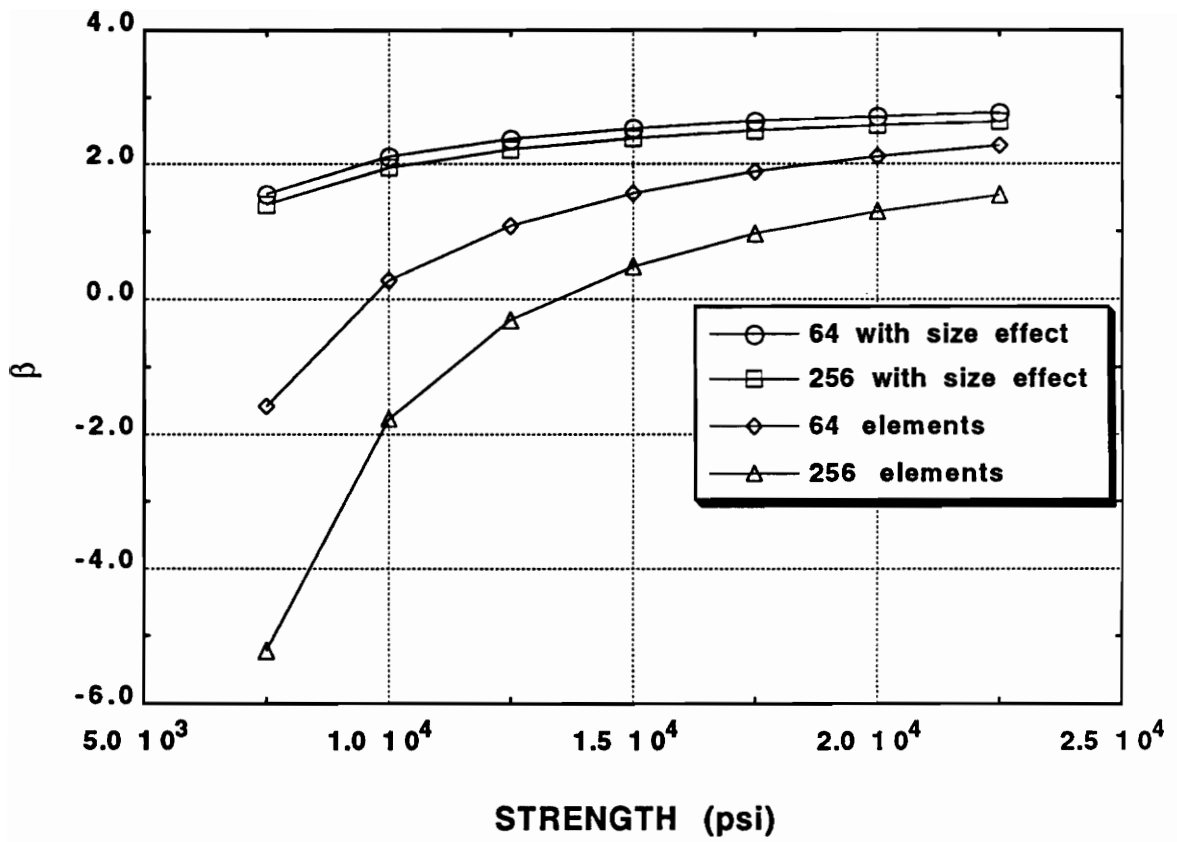


Fig. 6.33 Safety index with strength based on the maximum compressive stress for different meshes

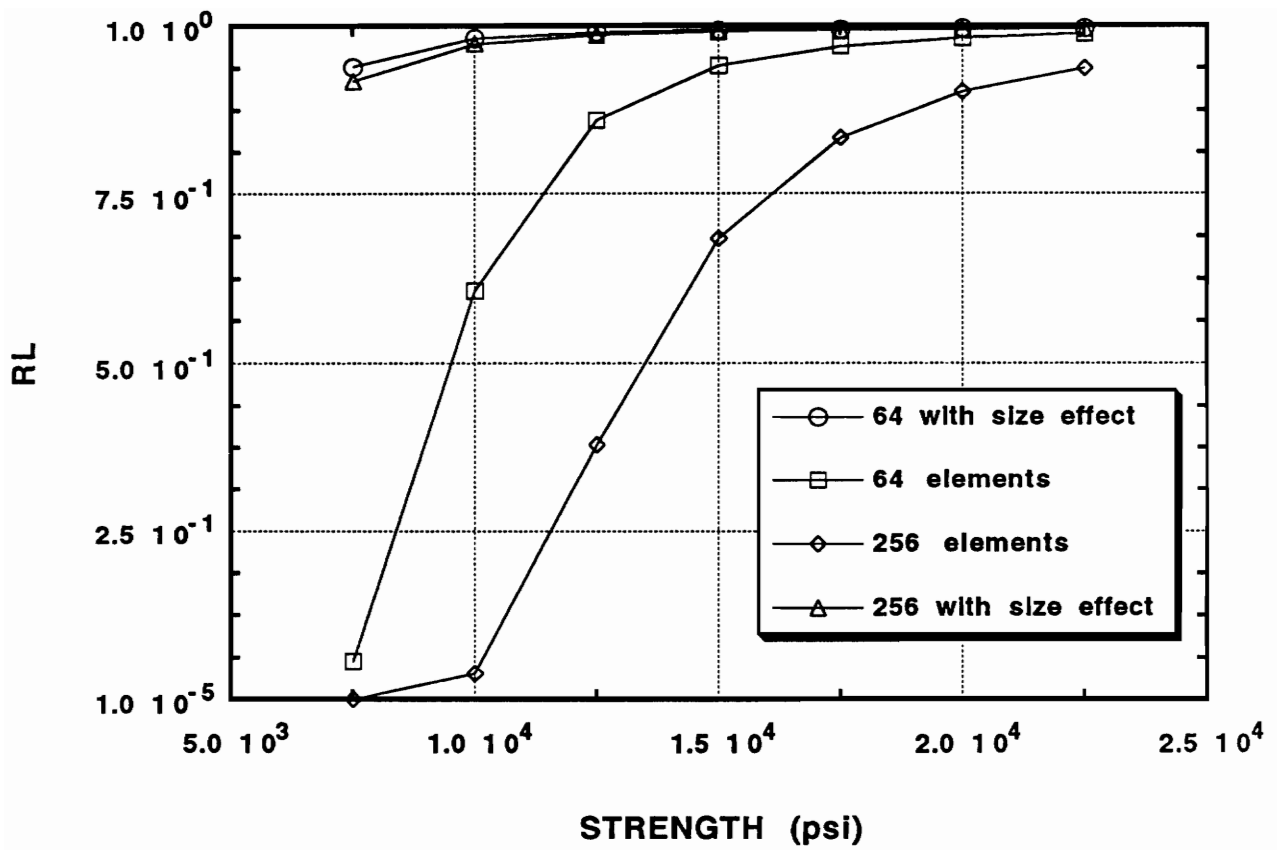


Fig. 6.34 Reliability with strength based on the maximum compressive stress for different meshes

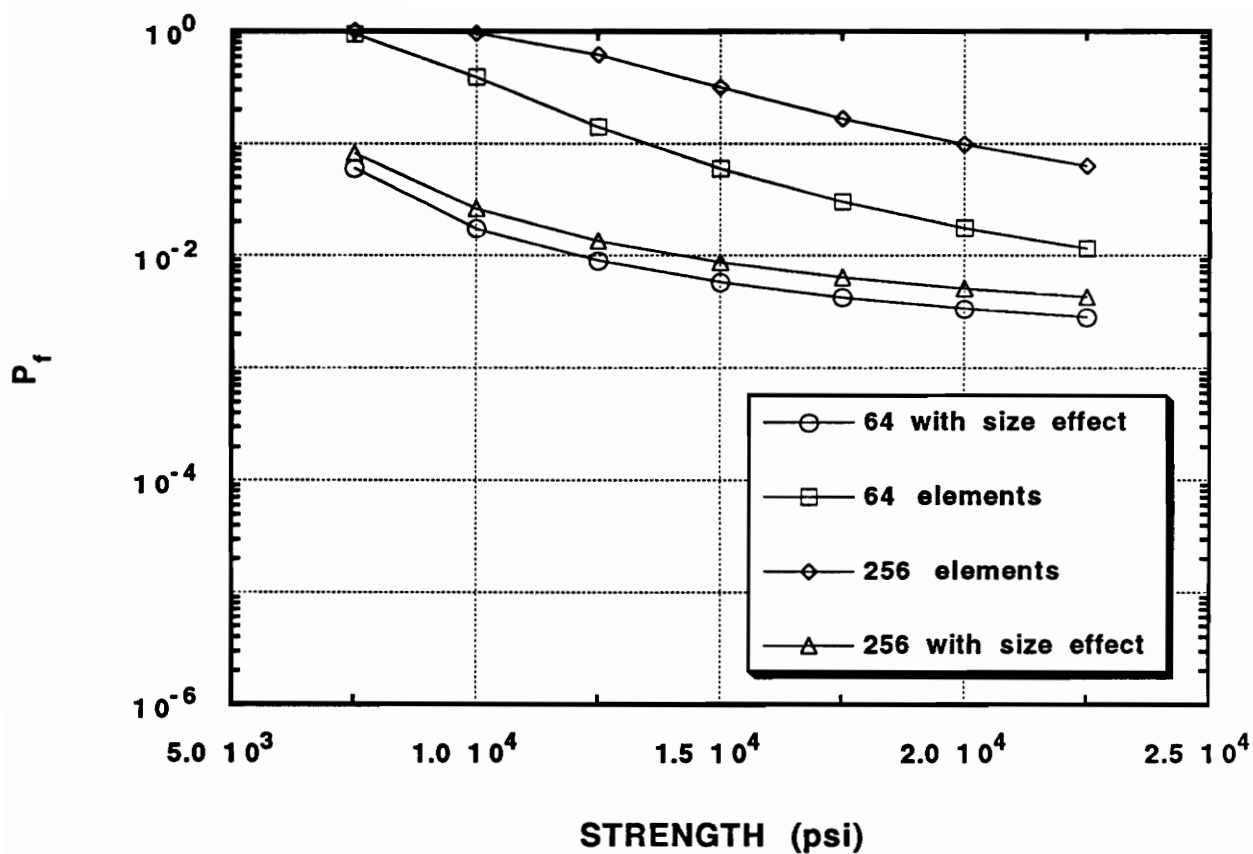


Fig. 6.35 Probability of failure with strength based on the maximum compressive stress for different meshes

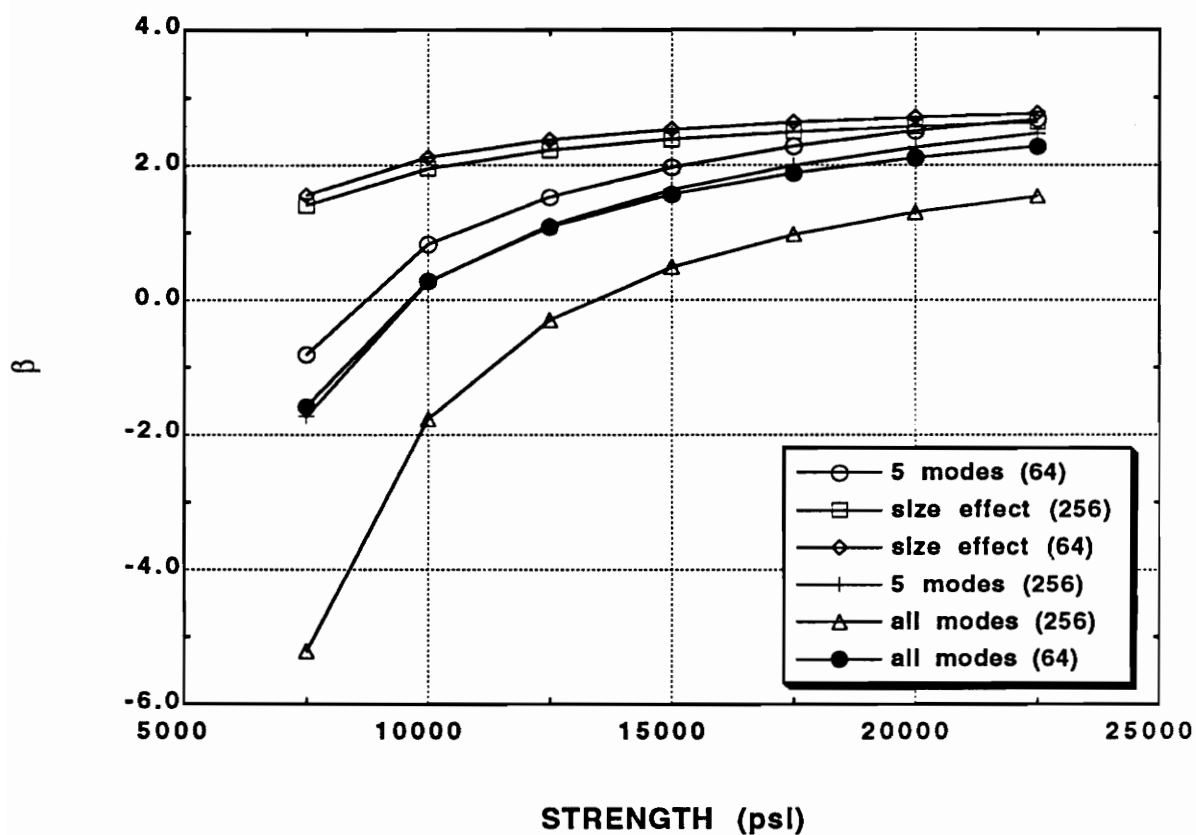


Fig 6.36 Safety index with strength for different meshes and modes, comparison between size effect and nonsize effect analyses

Chapter VII

SUMMARY AND CONCLUSIONS

7.1 Introduction

In this chapter the efficiency as well as the accuracy of the developed technique will be discussed. A comparison with a numerical technique that uses FOSM utilizing numerical differentiations will be made as well as comparison with the Monte Carlo simulation technique. The comparison will be made in terms of the safety index obtained by each technique. The extension of the commercial finite element code ABAQUS to allow for probabilistic analysis will be made also.

A summary of the results obtained in each chapter will be presented. The use of probabilistic analysis to improve the structural performance will be explained too. Recommendations for future works will be stated and the shortcomings of the developed technique will be discussed also.

7.2 Efficiency and Accuracy of the Developed Technique

In this section an example is chosen from Ang and Tang [9]. The solution is obtained using different methods, the developed technique (RSM), a computer algorithm that uses the FOSM utilizing numerical differentiation, developed by Dr. Thangjitham and his group [10], which is available on the main frame system of Virginia Tech, and the Monte Carlo simulation technique. The Monte Carlo technique is used when uncorrelated variables are considered. The safety index β is obtained using the three methods and a comparison is shown in Table 7.1.

The results presented in Table 7.1 show a good agreement between the developed technique and the other techniques. This adds more evidence to the accuracy of the developed technique, with a similar accuracy being obtained in chapter IV.

To add more evidence to the efficiency of the developed technique, an example is solved using ABAQUS where the reliability analysis is required. The example is taken from Heller et al. [75]. It is a rocket motor with orthotropic shell under point load; material properties as well as loadings are assumed random variables. The stress analysis is performed using ABAQUS for three dimensional analysis. To make ABAQUS handle probabilistic analysis, a design matrix is generated based on six random variables and transformed in terms of non-normalized variables. The order of the matrix is 45x6. Then each row in the transformed matrix is used as a set of input data for ABAQUS. The algorithm described in section 2 of chapter V is used to obtain the safety index and the reliability of the motor as a function of the applied load. Results are shown in Fig. 7.1 and Fig. 7.2 for the safety index and the reliability of the motor, respectively. It is important to mention here that without the developed technique such results are impossible to obtain. This proves the efficiency of the developed technique.

7.3 Summary of Results and Conclusions

The use of RSM in conjunction with the FOSM reliability method produced an efficient reliability technique. It can be used for complicated structures where stress analysis is performed using numerical techniques such as the finite element method and no explicit solutions are available, because it uses an available deterministic finite element code as a subroutine. This will cause the extension of most available finite element codes (source codes or executions codes) to allow for probabilistic analysis by adding uncertainty to any design variable. It handles variables with normally as well as non-normally distributed probability density functions. Correlated as well as uncorrelated variables can also be handled using this technique.

The use of a sensitivity analysis scheme that has been developed was proven to be efficient. It can save tremendously in terms of computation time with a power of 2 for each variable that can be excluded from the probabilistic model. It takes the gradient of the performance function and directs the analysis towards the failure region. This analysis becomes very useful for cases where large numbers of design variables are included in the stress analysis. It is also very useful in cases where the user is having difficulty determining if a variable needs to be treated as random or not.

The sensitivity analysis can be useful in a design problem or in increasing the reliability of a certain structure. This can be done by looking at the results of sensitivity analysis and determining the variables with the lowest PRF value. Then by changing these variables the reliability of the structure can be improved.

It was shown in chapter III that the 2nd order surface, used to approximate the performance function, is the 2nd order Taylor's series expansion of this function around the mean value of the design variables. But the design variables used in the RSM are

normalized with respect to the mean and the standard deviation of each variable; therefore, the mean value and the standard deviation of each design variable in the RSM are 0 and 1, respectively. The main advantage of this normalization is the linear system that is produced for the calculation of the coefficients of the second order surface. It will contain a homogenous matrix and no ill conditioning will be associated with this matrix.

In chapter IV, the service life of solid propellant rocket motors subjected to thermal stresses was predicted. Design variables as well as temperature parameters were treated as random variables. Correlated variables with different probability density functions were considered as well. Results have shown that the service life can be under or over estimated at the same probability of failure level when variables with different density functions are considered. This shows the importance of using the real probability density function for each variable when it is possible.

Since the strength and the modulus of the propellant are both time and temperature dependent, it was noticed that the assumption of correlation between them increases the service life of the motor. It was noticed, also, that when the correlation coefficient increases, the service life increases as well for the same value of the probability of failure. This example was solved analytically using the FOSM. When tested using the developed technique, results have shown an excellent agreement.

In chapter V, the developed technique was used to study the reliability of rocket motors under mechanical loadings. Stress analysis for such a case was performed using finite element analysis, program MCYL1 developed by Heller and Lin [65]. It was extended in this study to allow for probabilistic analysis under the name ROCKT3. All design variables are assumed random with correlation among some of them. The use of the sensitivity analysis scheme that has been developed in this study was seen to be powerful in reducing the number of computations and in showing the significant variables in the design. For example, the same reliability value was obtained when 11 and

6 random variables were considered, which reduced the computation by a factor of 6. It was also shown that the assumption of correlation between strength and modulus of the propellant layer increases the reliability of the motor. Moreover, results have shown that the increase in the strength variation increases the probability of failure much more than if the same increase in variation is applied to the load.

Experiments were performed to determine the critical region on the motor where failure might occur. It was found that there are two failure regions, one at the bore and the other at the interface between propellant and case. Results have shown, however, that the failure at the bore may occur before the failure at the interface. This was observed for well designed motors, i.e., no cracks in the propellant before testing. On the other hand, if cracks do exist, especially at the interface, failure might occur at this location due to stress concentration.

An application of the size effect technique that has been developed in chapter III was shown in chapter VI. In this chapter the developed technique was applied to obtain the reliability of a laminated composite plate under static and dynamic loadings. Linear as well as nonlinear analysis were considered to allow for large deformations. Results have shown that when the size of each element in the mesh is included in the probabilistic model, the same reliability value is obtained regardless of the mesh size. This type of analysis is very helpful for cases where the failure region is unidentified and stress analysis must be performed at every point. Single as well as multi-failure modes were considered and results have shown that a probabilistic analysis based on a single failure mode produces higher reliability value than a multi-failure mode.

Results have also shown that the variation in the strength affects the reliability much more than the variation in the load. Therefore, in such design it is more significant to control the strength than the load. This result was observed for the motor in chapter V as well.

7.4 Recommendations for Future Work

An efficient technique for structural reliability was developed for problems where explicit or exact solutions are not available, analysis is performed using finite element codes, large numbers of design variables are involved, correlated normal as well as non-normal random variables are included and failure regions are unknown. The shortcomings of this technique, however, can be used for a future investigation of this study; these are:

1. When correlated variables are considered, the user must be careful in matching the standard deviation for each variable with its eigenvalue. Therefore, the technique should be extended to overcome this difficulty.
2. When multi-failure modes are considered, it is hard to reevaluate the performance function because different design points are produced from each failure mode. Therefore, the solution might not be accurate for large values of β .
3. This study was developed for reliability assessment of structures and it needs to be extended to handle design problems where a target reliability is required.

Table 7.1 Comparison between different methods

This example is taken from Ang and Tang [9], example 6.11.

The G function is given as:

$$G = R - N \frac{C_c}{1 + e_0} H \log \frac{p_0 + \Delta p}{p_0}$$

The mean, coefficient of variation and standard deviation for each variable are given as follows:

variable	mean	coeff. of variation	standard deviation
R	2.5,5.0,7.5	0.0	0.0
N	1.000	0.200	0.200
C_c	0.396	0.25	0.099
e_0	1.190	0.150	0.1785
H	168.0	0.050	8.400
p_0	3.720	0.050	0.186
Δp	0.500	0.200	0.100

Case 1, $R = 2.5$:

method	β
MC	1.2107
RSM	1.1326
Thangjitham	1.1214

Case 2, $R = 5.0$:

method	β
MC	3.4136
RSM	3.3420
Thangjitham	3.3440

Case 3, $R = 7.5$:

method	β
MC	4.8916
RSM	4.8400
Thangjitham	4.8230

Case 4, $R = 2.5$; $\delta_N=0.1$ and correlated variables; $\rho_{N,\Delta p}=0.4$

method	β
RSM	1.1875
Thangjitham	1.1900

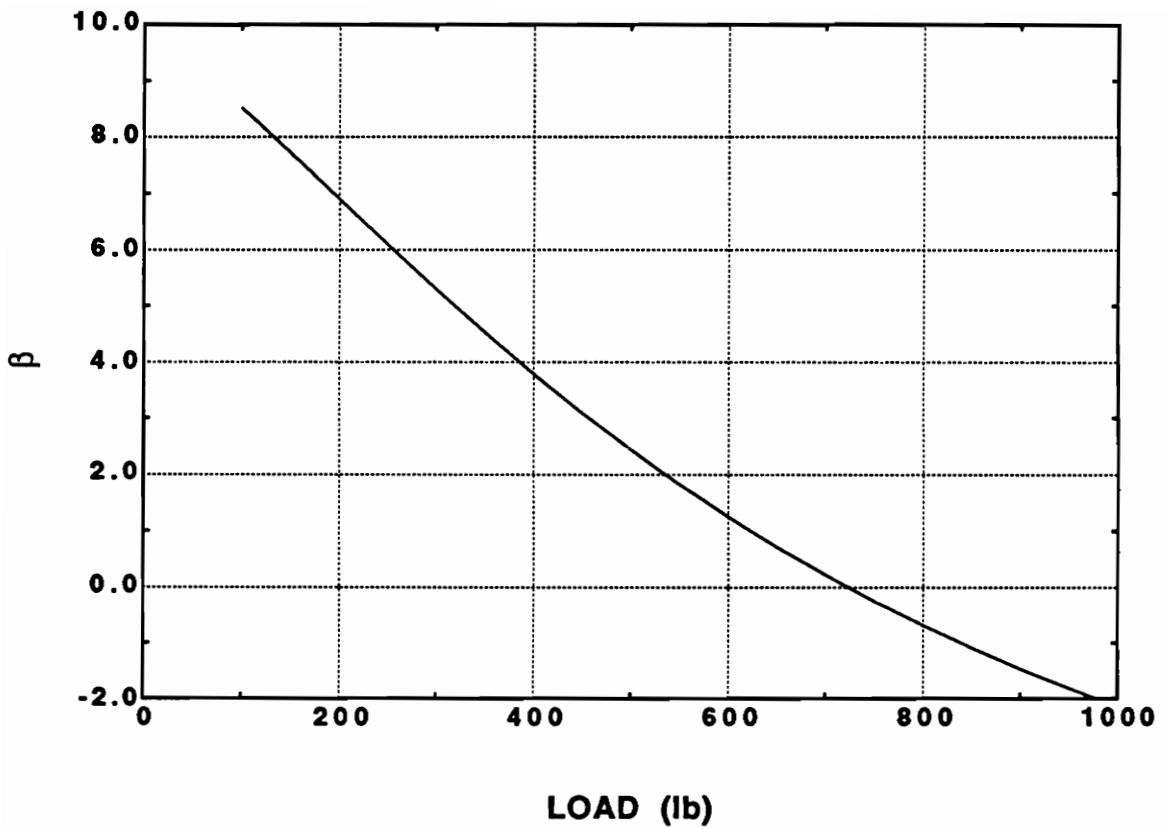


**Fig. 7.1 Safety index with load for a motor with orthotropic case
(analysis is performed using ABAQUS)**

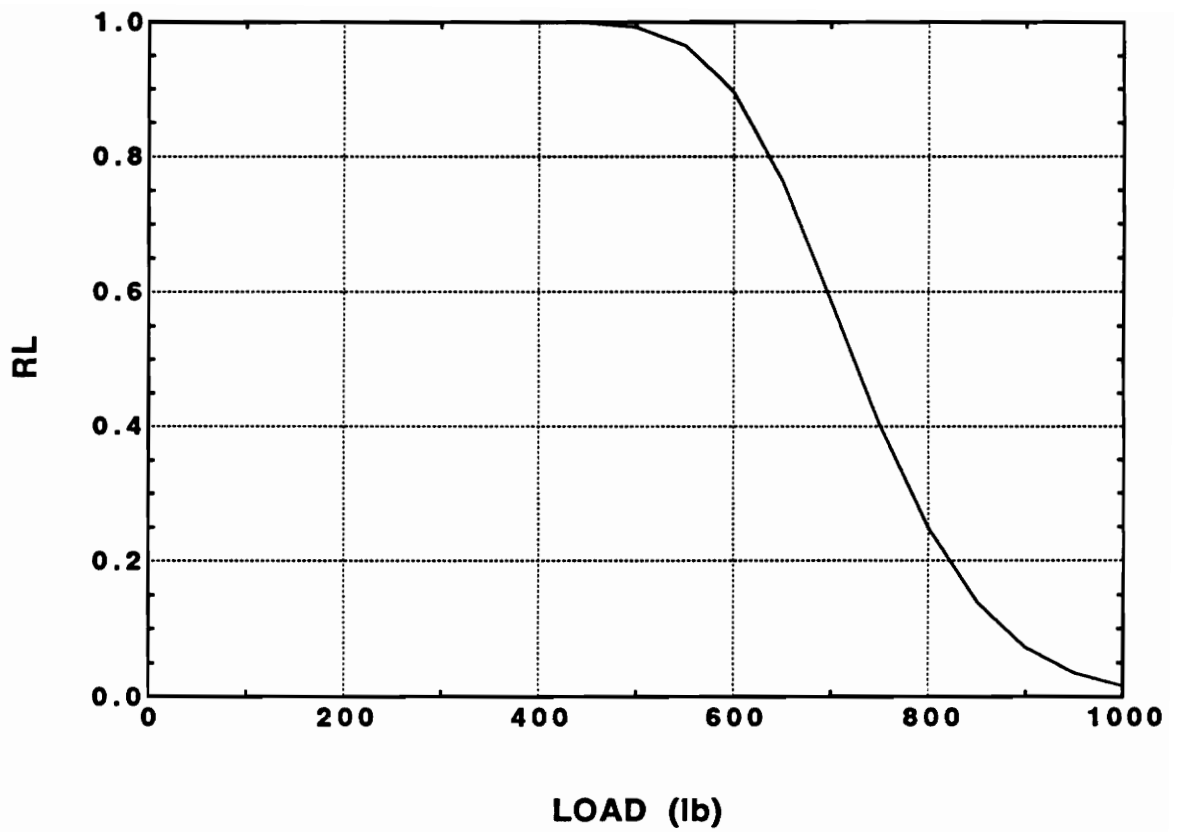


**Fig. 7.2 Reliability with load for a motor with orthotropic case
(analysis is performed using ABAQUS)**

REFERENCES

1. Freudenthal, A. M., " Safety of Structures ", Transactions, *ASCE* , Vol. 112, 1947, pp. 125-180.
2. Freudenthal, A. M., Garrelts, J. M., and Shinozuka, M., " The Analysis of Structural Safety ", *Journal of the Structural Division*, ASCE, Vol. 92, No. ST1, February 1966, pp. 267-325.
3. Cornel, C. A., " A Probability-Based Structural Code,;" *Journal of the American Concrete Institute*, Vol. 66, No. 12, December 1969.
4. Hosfer, A. M. and Lind, N. C., " Exact and Invariant Second-Moment Code Format, " *Journal of Engineering Mechanics Division*, ASCE, Vol. 100, No. EM1, February 1974, pp. 111-121.
5. Rackwitz, R. and Fiessler, B., " Structural Reliability Under Combined Random Load Sequences, " *Computers and Structures*, Vol. 9, 1978, pp. 489-494.
6. Wirsching, P. H., Ortiz, K. and Lee, S. J. " An Overview of Reliability Methods in Mechanical and Structural Design, " Proceeding, *AIAA*, 87-0765.
7. Chen, X. and Lind, N. C. " Fast Probability Integration by the Three Parameter Normal Tail Approximation, " *Structural Safety*, Vol. 1, 1983, pp. 269-276.
8. Shinozuka, M., "Basic Analysis of Structural Safety ", *Journal of Structural Engineering*, ASCE Vol. 109, No. 3, March, pp. 721-740.
9. Ang, A.H.S. and Tang, W.H., *Probability Concepts in Engineering Planning and Design*, Vol. II, Wiley, New York, 1984.
10. Thangjitham, S., *A Computer Program for the Reliability Calculation of Structures*, Probabilistic Mechanics Group, Department of Engineering Science and Mechanics, Virginia Tech, Blacksburg, Virginia.
11. Law, A. M. and Kelton, W. D., *Simulation Modeling and Analysis*, McGraw-Hill Book Co. N.Y., 1982.
12. Wu, Y. T., " Efficient Method for Mechanical and Structural Reliability Analysis and Design," *Ph.D Dissertation*, The University of Arizona, April, 1984.

13. Wu, Y. T., " Demonstration of a New, Fast Probability Integration Method for Reliability Analysis," *Proceedings of Symposium on Probabilistic Structural Design and Analysis*, ASME, 1985, pp. 63-73.
14. Wu, Y. T. and Wirsching, P. H., " A New Algorithm for Structural Reliability Estimation, " *Journal of Engineering Mechanics*, ASCE, Vol. 13, No. 9, September, 1987, pp. 1319-1336.
15. Wirsching, P. H. and Wu, Y. T. " Advanced Reliability Methods for Structural Evaluation, " *Journal of Engineering for Industry*, ASME, Vol. 109, No. 1, 1987, pp. 19-23.
16. Bucher, C. G., Chen, Y. M. and Schüeller, G. I., " Time Variant Reliability Analysis Utilizing Response Surface Approach, ", *Proceeding of the 2nd IFIP WG7.5 Conference*, London, UK, September 26-28, 1988.
17. Schüeller, G. I., Bucher, C. G., Bourgund, U. and Ouypornprasert, W., " On Efficient Computational Schemes to Calculate Structural Failure Probabilities", *Probabilistic Engineering Mechanics* , Vol. 4, No. 1, 1989, pp. 10-18.
18. Nagpal, V. K., Rubinstein, R. and Chamis, C. C., " Probabilistic Structural Analysis to Quantify Uncertainties Associated with Turbopump Blades ", *AIAA Journal* , Vol. 27, No. 6, June 1989, pp. 809-813.
19. Bucher, C.G. and Bourgund, U., "A Fast and Efficient Response Surface Approach for Structural Reliability Problems", *Structural Safety*, 7-1990, pp. 57-66.
20. Tong, T. Y. and Wu, Y. T., " Development of a Probabilistic Analysis Methodology for Structural Reliability Estimation" *AIAA/ASME/ASCE/AHS/ASC 32nd Structures, Structural Dynamics and Materials Conference*, Part 2, April 8-10, 1991.
21. Ibrahim, Y., " General Strategy for Structural Systems Reliability Analysis, " *Journal of Structural Engineering*, ASCE, Vol. 117, No. 3, March, 1991, pp. 789-807.
22. Handa, K. and Anderson, K., " Application of Finite Element Methods in Statistical Analysis of Structures, " *Proceedings ICOSSAR 81, 3rd International Conference on Structural Safety and Reliability*, Trondheim, Norway, 1981.
23. Hisada, T. and Nakagiri, S., " Stochastic Finite Element Methods Developed for Structural Safety and Reliability, " *Proceedings ICOSSAR 81, 3rd International Conference on Structural Safety and Reliability*, Trondheim, Norway, 1981.
24. Nakagiri, S., Takabatake, H. and Tani, S., " Uncertain Eigenvalue Analysis of Composite Laminated Plates by the Stochastic Finite Element Method, " *Journal of Engineering for Industry*, Vol. 109, No. 1, February, 1987, pp. 9-12.
25. Tani, S., Nakagiri, S., and Higashino, T., " Assessment of the Reliability Indices of CFRP Laminated Plate, " *Computational Probabilistic Methods*, Presented at the Joint ASME/SES Applied Mechanics and Engineering Science Conference, Berkeley, CA, June 20-22, 1988.

26. Tani, S., Nakagiri, S., " Reliability Synthesis of CFRP Laminated Plate, " *Proceedings ICOSSAR 89, 5rd International Conference on Structural Safety and Reliability*, San Francisco, CA, 1989.
27. Sato, Y., Watanabe, K. and Nakagiri, S., " Stochastic Finite Element Analysis of Stresses in FRP Pressure Vessels, " *ASME Pressure Vessels and Piping Division*, PVP Vol. 177, 1989.
28. Liu, W. K., Belytschko, T. and Mani, A., " Random Field Finite Elements, " *International Journal for Numerical Methods in Engineering*, Vol. 23, No. 10, 1986, pp. 1831-1845.
29. Liu, W. K., Belytschko, T. and Mani, A., " Probabilistic Finite Elements for Non-linear Structural Dynamics, " *Computer Methods in Applied Mechanics and Engineering*, Vol. 56, No. 1, 1986, pp. 61-81.
30. Liu, W. K., Besterfield, G. and Belytschko, T., " Transient Probabilistic Systems, " *Computer Methods in Applied Mechanics and Engineering*, Vol. 67, 1988, pp. 27-54.
31. Liu, W. K., Besterfield, G. and Belytschko, T., " Variational Approach to Probabilistic Finite Elements, " *Journal of Engineering Mechanics*, Vol. 114, No. 12, December, 1988, pp. 2115-2133.
32. Tokada, T. and Shinozuka, M., " Local Integration Method in Stochastic Finite Element Analysis, " *Proceedings ICOSSAR 89, 5rd International Conference on Structural Safety and Reliability*, San Francisco, CA, 1989.
33. Engelstad, S. P. and Reddy, J. N., " Nonlinear Probabilistic Finite Element Models of Laminated Composite Shells, " *CCMS-91-02 Report*, Virginia Polytechnic Institute and State University, Blacksburg, VA., January, 1991.
34. Weibull, W., " Investigation into Strength Properties of Brittle Materials, " *Proceedings of the Royal Swedish Institute for Engineering Research*, No. 149, 1938, pp. 1-27.
35. Weibull, W., " A Statistical Distribution Function of Wide Applicability, " *Journal of Applied Mechanics*, Vol. 18, No. 3, 1951, pp. 293-297.
36. Margeston, J., " A Statistical Theory of Brittle Failure for an Anisotropic Structure Subjected to a Multiaxial Stress State, " *Rocket Propulsion Establishment*, TR. No. 48, Westcott, England.
37. Stanley, P. and Margeston, J., " Failure Probability Analysis of an Elastic Orthotropic Brittle Cylinder Subjected to Axisymmetric Thermal and Pressure Loading, " *International Journal of Fracture*, Vol. 13, No. 6, Dec. 1977, pp. 787-806.
38. Heller, R. A., " Guide to the Use of the Weibull Distribution, " *HRB-Bericht Nr. BF 0684*, December 1, 1981.

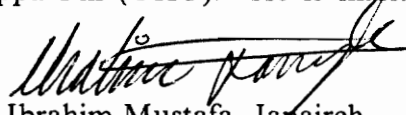
39. Heller, R. A., "Reliability Analysis of Brittle Componentets," *HRB-Bericht Nr. BF 0687*, December 12, 1981.
40. Heller, R. A., Schmidt, A., Deninghoff, R., "The Weakest Link Concept after Proof Testing," *Proceedings of the IUTAM Symposium on Probabilistic Methods in the Mechanics of Solids and Structures*, S. Eggwertz Ed., Springer, Berlin, June, 1984, pp. 241-251.
41. Heller, R. A., Thangjitham, S. and Wall, L. L., "Probability of Failure of a Proof Loaded Composite Plate with a Circular Hole," *Proceedings of International Symposium on Composite Materials and Structures*, T. T. Loo and C. T. Sun, Eds., Beijing, China, June 10-13, 1986.
42. Thangjitham, S. and Heller, R. A., "Reliability of a Proof-Loaded Fiber-Composite Plate under Randomly Oriented Loads," *AIAA/ASME/ASCE/AHS 28th Structures, Structural Dynamics and Materials Conference*, Part 1, April 6-8, 1987, pp. 257-281.
43. Heller, R. A., Thangjitham, S. and Yeo, I., "Size Effects in Brittle Ceramics," *AIAA/ASME/ASCE/AHS 31st Structures, Structural Dynamics and Materials Conference*, Long Beach, CA, April 2-4, 1990, pp. 69-73.
44. Yeo, I., "Reliability and Failure Analysis of Composite Beams and Plates Containing Stress Concentration," *Ph.D Dissertation*, Virginia Polytechnic Institute and State University, Blacksburg, VA., August, 1991.
45. Heller, R. A., "Life Prediction of Dump Stored Motors with Statistically Varying Strength and Temperature," *U. S. Army Missile Command*, TR. RK-76-12, April 1976.
46. Cost, T. L., "Probabilistic Service Life Prediction of Solid Rocket Motors Subjected to Thermal Load Using Computer Simulation," *Chemical Propulsion Information Agency, 14th JANNAF Structures and Mechanical Working-Group Meeting*, Laurel, Md., CPIA Report No. 283, February 15-17, 1977.
47. Heller, R. A., Kmat, M. P. and Singh, M. P., "Probability of Solid Propellant Motor Failure Due to Environmental Temperatures," *Journal of Spacecraft and Rockets*, Vol. 16, No. 3, 1979, pp. 140-146.
48. Heller, R. A. and Singh, M. P., "Thermal Storage Life of Solid Propellant Motors," *Journal of Spacecraft and Rockets*, Vol. 20, No. 2, 1983, pp. 144-149.
49. Zibdeh, H. S. and Heller, R. A., "The Use of the First Passage Method in Service Life Prediction of Rocket Motors," *AIAA/ASME/SAE/ASEE 22nd Joint Propulsion Conference*, Huntsville, Alabama, June 16-18, 1986.
50. Montgomery, D.C. and Elizabeth, A.P., *Introduction to Linear Regression Analysis*, Wiley, New York, 1982.
51. Myers, R.H., *Response Surface Methodology*, Allyn and Bacon Inc., Boston 1971.

52. Box, G.E.P. and Draper, N.R., *Empirical Model Building and Response Surfaces*, Wiley, New York, 1987.
53. Myers, R.H., *Class Notes on Response Surface Methodology* , Virginia Polytechnic Institute and State University, Blacksburg, VA, Fall 1991.
54. Myers, R.H., *Classical and Modern Regression with Applications*, Second Edition, PWS-KENT, Boston, 1990.
55. Walpole, R. E. and Myers, R. H., *Probability and Statistics for Engineers and Scientists*, Macmillan, New York, 1978.
56. Abramowitz, M. and Stegun, I. A., *Handbook of Mathematical Functions with Formulas, Graphs and Mathematical Tables*, National Bureau of Standards, Applied Mathematics Series .55, Tenth Printing, December 1972.
57. Heller, R. A., "Class Notes on Reliability Methods in Structures and Mechanics", *Virginia Polytechnic Institute and State University*, Blacksburg, VA, Spring 1990
58. Thangjitham, S. and Heller, R.A., "Test and Evaluation of Dynamic Properties of Solid-Propellant Rocket Motor Materials", Volume I-Random Environmental Thermal Load Models and their Effects on the Service Life of Rocket Motors, Technical Report CR-RD-86-8, USAMICOM, Redstone Arsenal, Alabama, Oct. 1986.
59. Zibdeh, H.S. and Heller, R.A., "Environmental Thermal Stress as a First Passage Problem" in *Random Vibration-Status and Present Developments*, Elishakoff and Lyon, (Eds.), Elsevier, New York, 1986, pp. 537-553.
60. Zibdeh, H.S. and Heller, R.A., "Rocket Motor Service Life Calculations Based on the First Passage Method", *Journal of Spacecraft and Rockets*, Vol. 26, No. 4, 1989, pp. 279-284.
61. Little, R.R. and Woods, H. G., "Comparison of Inert and Live Propellant Bondlines: Bondline Fabrication and Testing", Final Report, RD-PR-92-5, U.S. Army Missile Command, Huntsville, AL. Dec. 1991.
62. Bills, K.W., Jr., and Wiegand, J.H., "The Application of an Integrated Structural Analysis to the Prediction of Reliability", *Annals of Reliability and Maintainability*, Feb. 1970, pp. 514-526.
63. Layton, L.H., "Chemical Aging Studies on ANB-3066 and TP-H1011 Propellants", Final Technical Report, Air Force Rocket Propulsion Lab. AFRPL-TR-74-16, EDWARDS, CA. Dec. 1974.
64. Heller, R. A. Thangjitham, S. and Janajreh, I. M., "User's Guide to the Safety Index Calculation Program ROCKT2" ,*U. S. Army Missile Command* Technical Report CR-RD-PR-91-2, Sep. 1991.

65. Heller, R. A. and Lin, Y. T., "User's Guide to the Static-Elastic and Dynamic Program MCYLI", *U. S. Army Missile Command Technical Report CR-RD-PR-87-2*, June 1989.
66. Lin, Y. T., "Stress Analysis of Rocket Motors with Viscoelastic Propellant by a Mixed Finite Element Model", *Ph.D Dissertation*, Virginia Polytechnic Institute and State University, Blacksburg, VA, July, 1989.
67. Heller, R. A. and Janajreh, I. M., "User's Guide to the Reliability Program ROCKT3", *U. S. Army Missile Command Technical Report CR-RD-PR-92*, July 1992.
68. Reddy, J.N., "A Simple Higher-Order Theory for Laminated Composite plates", *Journal of Applied Mechanics*, Vol. 51, Dec 1984, pp. 745-752.
69. Reddy, J.N., "Dynamic (Transient) Analysis of Layered Anisotropic Composite Material Plates", *International Journal for Numerical Methods in Engineering*, Vol. 19, 1983, pp. 237-255.
70. Reddy, J.N., "Geometrically Nonlinear Transient Analysis of Composite Plates", *AIAA Journal*, Vol. 21, 1983, pp. 621-629.
71. Reddy, J.N., "On Refined Computational Models of Composite Laminates", *International Journal for Numerical Methods in Engineering*, Vol. 27, 1989, pp. 361-382
72. Janajreh, I.M., "Static and Transient Finite Element Analysis of Geometrically Nonlinear Laminated Composite Plates", Term paper for Finite Element II "Class", Department of Engineering Science and Mechanics, *Virginia Polytechnic Institute and State University*, Blacksburg, VA, Spring 1991.
73. Reddy, J.N., "Class Notes on Finite Element Method II", *Virginia Polytechnic Institute and State University*, Blacksburg, VA, 1991
74. Janajreh, I. M. and Heller, R. A., "Probabilistic Static and Transient Finite Element Analysis of Geometrically Nonlinear Laminated Composite Plates", Presented at the CCMS&CAS Joint Conference, *Virginia Polytechnic Institute and State University*, Blacksburg, VA, March 24, 1992.
75. Heller, R. A., Thangjitham, S. and Wang, X., "Stress and Reliability Analysis of Composite Cased Rocket Motor Under Asymmetric Loads", *U. S. Army Missile Command, Technical Report CR-RD-PR-92-10*, October 1992.

Vita

The author was born on November 2nd 1962 at Zarka-Jordan. In 1981 he attended Yarmouk University to pursue a B.S. degree in civil engineering. In 1985 he joined the department of mechanical engineering at Jordan University of Science and Technology and worked towards his master degree. In 1988 he obtained his M.S. degree in the area of structural reliability under the supervision of professor Hazim Zebdeh. While working towards his degrees the author was working as a part time engineer at Janajreh Construction Company in Jordan from which he gained an extensive practical experience. He was awarded an assistantship from the Department of Mechanical Engineering while pursuing his Master's. In the spring of 1989 he joined the Department of Engineering Science and Mechanics at Virginia Tech and started his doctoral degree under the supervision of professor Robert Heller in the area of probabilistic mechanics. Since then, he has been working on a sponsored research project in his area of expertise. The author's areas of interest include solid mechanics, structural reliability, random vibrations and probabilistic finite element analysis. He is a member of the Jordanian Engineering Association (JEA), the American Society of Mechanical Engineering (ASME) and the honor society of Phi Kappa Phi ($\Phi\text{K}\Phi$). He is married and enjoys soccer, hunting and outdoor camping.



Ibrahim Mustafa Janajreh
November, 1992